7.2 SIMULATION OF PLUG-FLOW REACTOR EXPERIMENT

A tuff dissolution experiment was used to test geochemical models that were developed for the DST THC and the Tptpmn and Tptpll THC seepage models. The tuff dissolution experiment was performed under isothermal elevated temperature conditions with well-constrained initial water and rock compositions. Measured water compositions of samples obtained during the duration of the experiment also allowed the evaluation of kinetically controlled reactions with time. A number of simulations were run to evaluate the sensitivity of the geochemical models to the mineral surface area, rock composition, mineral thermodynamic data, and changes to the TOUGHREACT code.

A plug-flow reactor experiment was performed as part of a study investigating mineral dissolution and precipitation (Figure 7.2-1). Topopah Spring tuff (Tptpmn) obtained from overcores from borehole ESF-TMA-TC-H-1 was crushed, sieved, and washed. Material was combined from the 75–150 μm (89%) and 150–212 μm (11%) fractions (DTN: LB0011THCDISSX.001 [153380]). Scanning electron microscope images of the tuff (Fig. 7.2-2) indicate that the actual grain sizes are smaller than the nominal sieve-size fractions, with values ranging from 30 to 180 μm (DTN: LB0011THCDISSX.001 [153380]). The crushed tuff was added to a 29.8 cm long by 7.5 cm diameter polypropylene tube. The filled tube had a measured porosity of 37.5%.

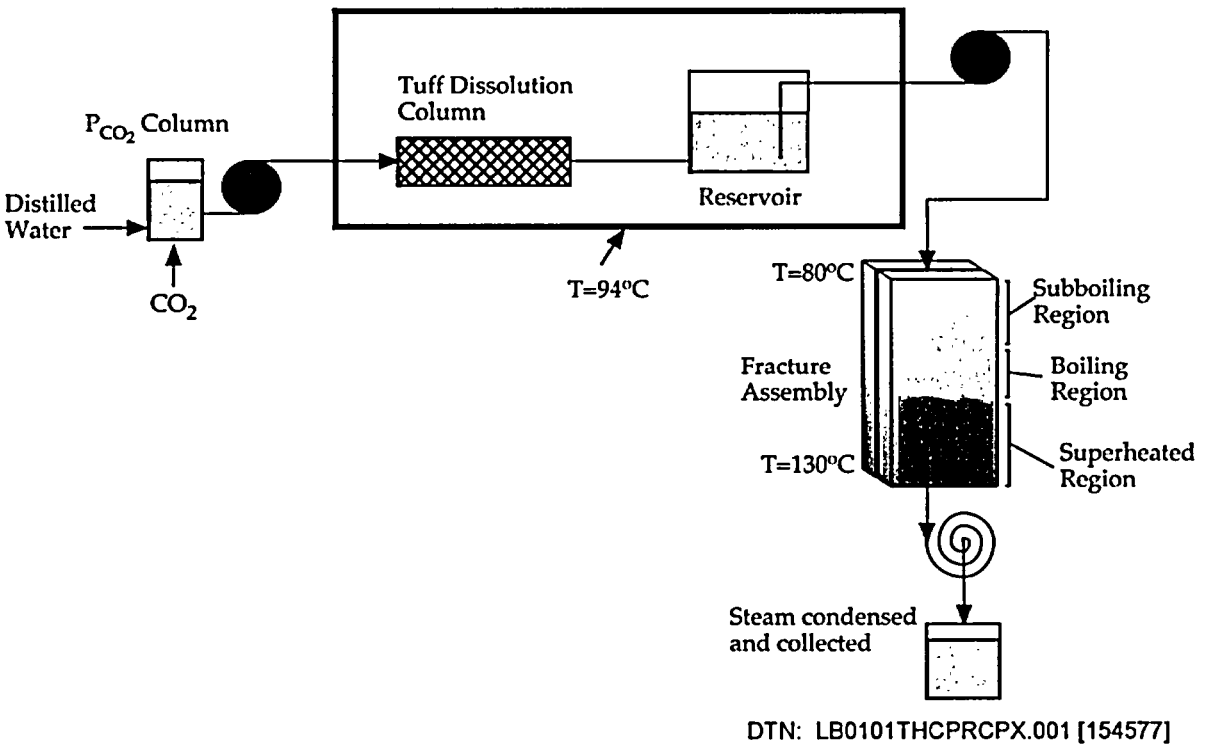

DTN: LB0101THCPRCPX.001 [154577]

Figure 7.2-1. Schematic Diagram of the Tuff Plug-Flow and Fracture Sealing Experiments

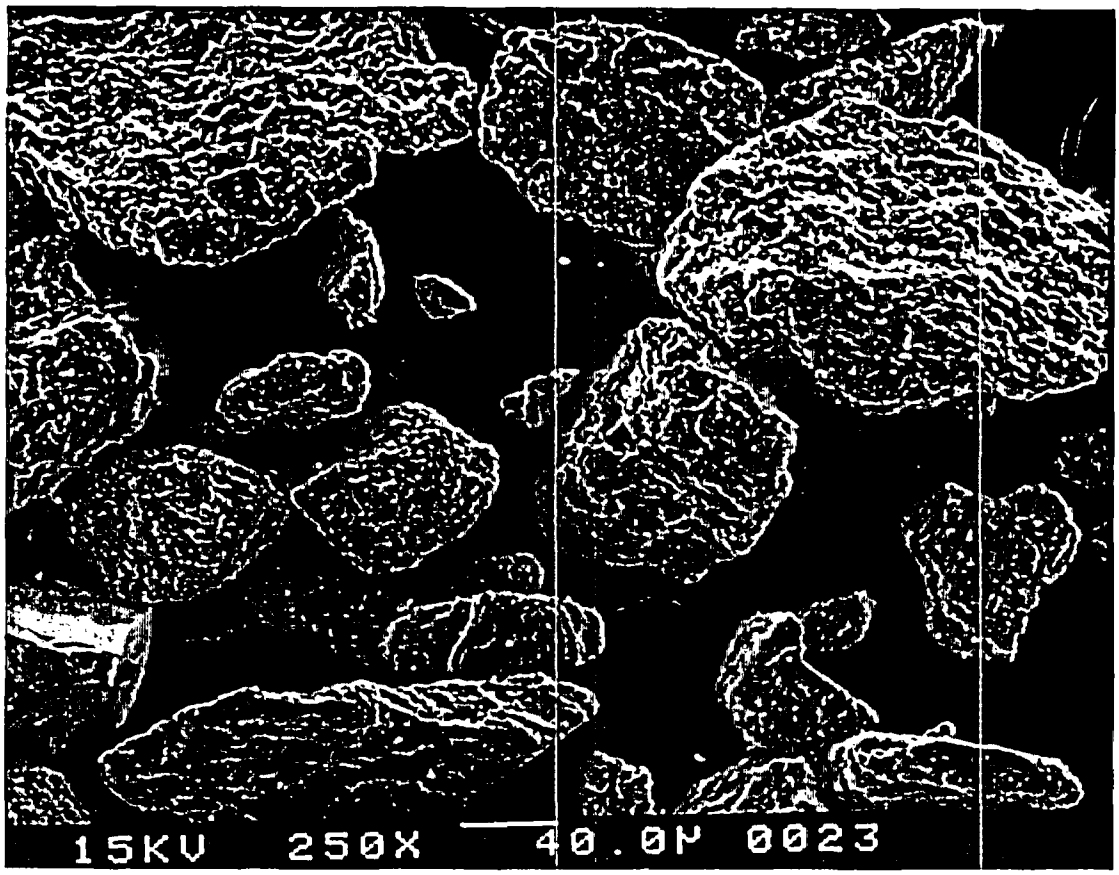

DTN: LB0011THCDISSX.001 [153380]

NOTE: The grains have a fairly wide range in diameter (30–180 µm), with irregular shapes and rough surfaces, contributing to a larger surface area per unit weight value.

Figure 7.2-2. SEM Image of Topopah Spring Tuff Grains Used for Plug-Flow Experiment

The inlet fluid consisted of deionized water initially equilibrated using a CO_2/N_2 gas mixture with 50,200 ppm CO_2 at 17°C. The resulting water had a measured pH of 4.58 (DTN: LB0011THCDISSX.001 [153380]). This water was heated to 94°C and then introduced into the tuff column (also at 94°C) at a rate of 25 mL/h. Water exiting the tuff column was collected in a reservoir and sampled periodically for chemical analysis over the length of the experiment (63.8 days). A fraction of the water exiting the tuff column was directly used in an experiment evaluating the effects of boiling on mineral dissolution and precipitation and fluid flow in a fracture. The sampled waters for the plug-flow reactor experiment were allowed to cool and equilibrate with the atmosphere at room temperature. These sampling conditions resulted in changes to the pH and bicarbonate values, because of the loss of CO_2 gas.

A series of isothermal 1-D TOUGHREACT V2.2 (LBNL 1999 [153219]) and V2.3 (LBNL 2001 [153101]) simulations were performed to model this dissolution, using a 149-element mesh, with dimensions and interface areas identical to those of the plug-flow experiment, plus one additional boundary element to obtain the appropriate outlet conditions (Dobson 2001 [160252], p. 9). The goals of these simulations were to validate the geochemical model developed for the THC

models presented in this Model Report and test the sensitivity of the simulations to changes in input parameters, such as reactive surface area and mineralogy.

Initial mineralogy used for plug-flow simulations was obtained from the Tptpmn (tsw34) matrix composition reported in Attachment I (tswm4) (DTN: LB991200DSTTHC.003 [161276]). K-smectite was not considered in simulations run using TOUGHREACT V2.3 (LBNL 2001 [153101]), consistent with the revised "extended" mineralogical system used for the Tptpll THC simulations in Section 6.5.5.2 (Table 6.2-2). The corresponding volume fraction of K-smectite was either added to illite or disregarded, as noted for each sensitivity run. An initial fluid composition was calculated (Table 7.2-1) using SOLVEQ/CHILLER V1.0 (LBNL 1999 [153217]) and the measured pH and CO_2 concentration (Dobson 2001 [160252], pp. 18–22, 45–51). Trace amounts of other dissolved constituents were used in the simulation to reduce computational problems caused by zero values. The column was assumed to be liquid-saturated, with no separate gas phase present.

Table 7.2-1. Initial Water Composition for Tuff Plug-Flow Simulations

Species	Concentration (moles/liter)	Concentration (mg/liter)
Na^+	1.000E-10	2.299E-06
K^+	1.000E-10	3.910E-06
Ca^{2+}	1.000E-10	4.008E-06
Mg^{2+}	1.000E-10	2.431E-06
HCO_3^-	1.943E-03	1.186E+02
$SiO_{2(aq)}$	1.000E-10	6.008E-06
Cl^-	1.000E-10	3.545E-06
SO_4^{2-}	1.000E-10	9.606E-06
F^-	1.000E-10	1.900E-06
AlO_2^-	1.000E-10	5.898E-06
$HFeO_{2(aq)}$	1.000E-10	8.885E-06
pH (20°C)	4.58	

DTN: LB0011THCDISSM.001 [153381]

NOTE: Bicarbonate (HCO_3^-) concentrations represent the sum of all carbonate species present.

A total column flow-through time of 19.75 hours was determined using the calculated pore volume of 493.7 cm^3 and the flow rate of 25 mL/h. This time corresponds to a flow-through time of 477 seconds per element block (Dobson 2001 [160252], pp. 10–11). The maximum time step (360 seconds) for each of the simulations was chosen to be smaller than this value. The temperature of the simulation was fixed at 94°C.

Two simulations were performed using TOUGHREACT V2.2 (LBNL 1999 [153219]), and three additional simulations were made with TOUGHREACT V2.3 (LBNL 2001 [153101]) (Table 7.2-2). Two different grain-size models were used for the TOUGHREACT V2.2 (LBNL 1999 [153219]) simulations to evaluate the sensitivity of surface-area values on kinetic mineral reactions (Dobson 2001 [160252], pp. 17–18). Because no BET (Brunauer-Emmett-Teller)

measurement data were available, simple geometric models were constructed to derive surface area to volume values for the minerals. The first simulation employed mineral surface areas calculated using spherical grains with a diameter of 60 μm, with clay minerals represented by rectangular plates having dimensions of 60 × 60 × 1.2 μm. The second simulation used spherical grains with diameters of 120 μm and clay minerals with dimensions 120 × 120 × 2.4 μm. The results of these simulations are depicted in Figures 7.2-3 (a–f).

Table 7.2-2. Summary Table of Tuff Dissolution Simulations

Run #	TOUGHREACT version	Thermodynamic database	Grain size surface area model	Thermodynamic representation of potassium feldspar	Thermodynamic representation of K-smectite
1	V2.2 [153219]	thermokapps2.05.dat *	60 μm dia.	microcline	K-smectite
2	V2.2 [153219]	thermokapps2.05.dat *	120 μm dia.	microcline	K-smectite
3	V2.3 [153101]	thermok2.07.dat †	60 μm dia.	microcline	not used
4	V2.3 [153101]	thermok2.07.dat †	60 μm dia.	K-feldspar	not used
5	V2.3 [153101]	thermok2.07.dat †	60 μm dia.	K-feldspar	illite

NOTE: * DTN: LB0101DSTTHCR1.005 [161676]
† DTN: LB0101DSTTHCR1.006 [161280]

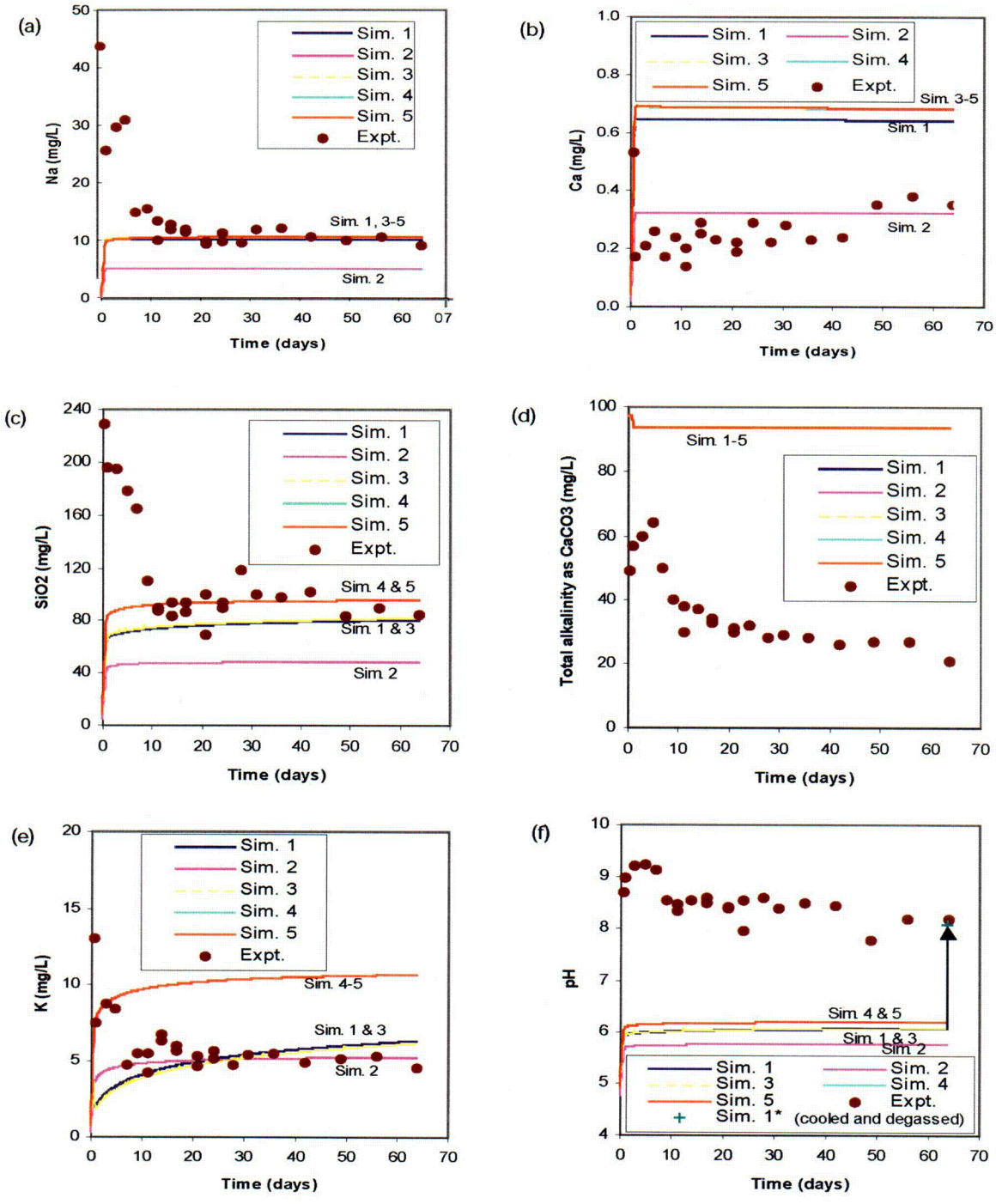

Output-DTN: LB0301PLUGFLOW.001
DTN: LB0011THCDISSX.001 [153380] (measured data)

NOTE: Plots show variations with time for Na^+ (a), Ca^{2+} (b), $SiO_{2(aq)}$ (c), total alkalinity as $CaCO_3$ (d), K^+ (e), and pH (f).

Figure 7.2-3. Comparison of Measured and Simulated Results of Tuff Dissolution Plug-Flow Experiment

C140

7.2.1 Validation Criteria

The criteria for model validation are specified in the *Technical Work Plan for: Performance Assessment Unsaturated Zone* (BSC 2002 [160819], Attachment I, Section I-3-4-1). The model validation criterion applicable to this work is that the modeled concentrations for the major (>1 mg/L) dissolved species in the effluent should be within one order of magnitude of the measured average steady-state concentrations. This range is reasonable because chemical potential is proportional to the logarithm of activity. Discussion of uncertainty associated with coupled process (THC) modeling is presented in Section 6.9.

7.2.2 Results of Simulations and Comparison to Measured Data

The measured concentrations of all dissolved components initially increased rapidly, and then declined until about 11 days, after which relatively steady concentrations were achieved (Figure 7.2-3). The high initial measured concentrations may have resulted from the dissolution of fine tuff particles not removed in the washing process, which resulted in a much higher available reactive surface area at the start of the experiment, or from the initial mineral surfaces being more reactive because of crushing and surface roughness, none of which is accounted for in the simulations.

A comparison of the simulated compositions of the major dissolved species with the average steady-state fluid composition from the tuff dissolution experiment is presented in Table 7.2-3. All of the simulation results fall within the low- and high-bound validation criteria values. Although all of the simulations met these criteria, some of the simulations exhibited closer matches with the measured results of the plug-flow experiments (Figure 7.2-3; Dobson 2001 [160252], pp. 30–34). Large (up to 100%) differences were observed between the two grain-size models for Na^+, $SiO_{2(aq)}$, and Ca^{2+} concentrations. These variations result from the two-fold difference in calculated initial surface areas that affect the kinetic mineral reactions controlling the concentrations of these species in solution. There is a close match between the measured and calculated concentrations of Na^+ and $SiO_{2(aq)}$ for the 60 μm grain-size (larger surface area/unit volume) simulation. As a result, the surface areas corresponding to this grain-size model were used for subsequent TOUGHREACT V2.3 (LBNL 2001 [153101]) simulations of the plug-flow experiment.

Table 7.2-3. Validation of Tuff Dissolution Simulations

	Run	Na^+ (mg/L)	K^+ (mg/L)	Ca^{2+} (mg/L)	$SiO_{2(aq)}$ (mg/L)	alkalinity (mg/L $CaCO_3$)
Steady-state experimental value (average composition of 17 samples, collected between day 11 and 64)		11.1	5.3	0.26	91.8	30.2
Low bound of validation criteria		1.1	0.53	0.026	9.2	3.0
High bound of validation criteria		111	53.2	2.6	918	302
Simulation values (final compositions)	1	10.4	6.3	0.64	80.6	93.6
	2	5.3	5.2	0.32	48.4	93.6
	3	10.8	6.2	0.68	82.4	93.6
	4	10.7	10.7	0.68	95.7	93.6
	5	10.7	10.7	0.68	95.7	93.6

Source: Experimental data from LB0011THCDISSX.001 [153380]. Simulation results from Output-DTN: LB0301PLUGFLOW.001.

None of the simulation results directly fits the measured values of pH and total alkalinity. The discrepancy in pH can be attributed to the exposure of the plug-flow effluent to air and the subsequent cooling and degassing of the outflow solution before analysis. The outflow pH values match the simulated results closely after they have been corrected for these processes (using SOLVEQ/CHILLER V1.0 (LBNL 1999 [153217])) (Dobson 2001 [160252], pp. 35–38). Although the model alkalinity values are lower than the measured values, they are within the order-of-magnitude validation range as specified in Section 7.2.1.

A second set of simulations was conducted using TOUGHREACT V2.3 (LBNL 2001 [153101]) (Dobson 2001 [160252], pp. 39–44, 60). Version 2.3 of the code has various improvements related to parameters used for calculating water-rock interaction. This version also utilized a thermodynamic database (thermok2.07.dat; Attachment V) that differs in several respects from the database (thermokapps2.05.dat; BSC 2002 [158375], Attachment V) used in the TOUGHREACT V2.2 (LBNL 1999 [153219]) simulations. Other changes included modified activity coefficients, the removal of K-smectite as a mineral phase, and the incorporation of a smectite solid-solution model. Several changes were made for the TOUGHREACT V2.3 (LBNL 2001 [153101]) simulations. For all runs, smectite end members were considered as a solid solution. Different initial surface areas for minerals not initially present were used for the V2.3 (LBNL 2001 [153101]) runs as a sensitivity study on this parameter (Dobson 2001 [160252], pp. 16, 39). For two of the runs, thermodynamic data for microcline were substituted by K-spar for the potassium feldspar. The simulations also evaluated the removal of the K-smectite component from the new thermodynamic database. One simulation added the K-smectite mineral fraction to the illite component. In the other two simulations, the K-smectite fraction was simply removed from the initial composition. The 60 μm grain size model was used for all of the TOUGHREACT V2.3 (LBNL 2001 [153101]) simulations.

Several important observations can be obtained from the TOUGHREACT V2.3 (LBNL 2001 [153101]) simulations. First, TOUGHREACT V2.3 (LBNL 2001 [153101]) and its thermodynamic database produced results similar to those generated using V2.2 (LBNL 1999 [153219]). Most of the concentration profiles have steady-state compositions slightly higher than the corresponding values obtained from the TOUGHREACT V2.2 (LBNL 1999 [153219]) runs. These higher compositions result from the incorporation of the change in water density to the mineral surface area calculations in V2.3. Some of the fluid concentration profiles are more abrupt with the new simulations, perhaps because of changes in the initial precipitation rate of new secondary phases.

The model does not appear to be sensitive to small changes in illite content. This insensitivity suggests that this phase is not being dissolved during the experiment and thus does not contribute to the outflow fluid composition. However, major differences were observed for potassium when a small adjustment was made to the thermodynamic data for potassium feldspar. It is, therefore, critical to select the proper thermodynamic data for the key mineral phases that buffer the main chemical constituents in the fluid.

A number of important observations and conclusions can be derived from the tuff dissolution experiment and simulations:

- A good match was obtained between the water compositions for the observed and simulated plug-flow reactions, meeting the model validation criterion specified in Section 7.2.1.

- The simulations are sensitive to a number of parameters, including the initial mineral assemblage, the thermodynamic database used, and (most importantly) the mineral surface area.

- Minor differences in model results obtained using two versions (TOUGHREACT V2.2 (LBNL 1999 [153219]) and V2.3 (LBNL 2001 [153101])) of the TOUGHREACT code result primarily from the temperature-pressure-corrected density values of water used in the mineral surface area calculations incorporated in V2.3 (LBNL 2001 [153101]).

- Differences between the modeled and measured values in pH result from cooling and degassing of the experimental samples after exiting the tuff dissolution column. This illustrates the potential for fluid-chemistry changes during collection in samples obtained from the DST experiment (Section 7.1).

This model validation work satisfies the goals set forth in the TWP (BSC 2002 [160819], Attachment I, Section I-3-4-1), and thus no further validation work associated with the plug-flow experiment is planned.

7.3 SIMULATION OF FRACTURE SEALING EXPERIMENT

The fracture sealing experiment was designed to emulate and evaluate the effects of condensate reflux through a fracture network and into a boiling environment (Figure 7.2-1). Two saw-cut blocks of welded rhyolite ash-flow tuff, measuring 31.7 cm tall, 16.2 cm wide, and 3.2 cm thick,

were separated by 17.7 μm gold shims to create a vertical planar fracture (DTN: LB0101THCPRCPX.001 [154577]). The blocks (SPC 00540498), obtained from the Tptpmn at Alcove 6 in the ESF at Yucca Mountain, contained a small fracture, but do not have any visible lithophysal cavities (DTN: LB0101THCPRCPX.001 [154577]). The mineralogy of the tuff samples was assumed to be similar to the samples used for the tuff dissolution experiment.

The outer surfaces of the blocks were sealed with Dow Corning 1199 silicone, and the vertical sides of the fracture were sealed with an aluminum sheet coated with silicone. Polypropylene endcaps were secured to the assembly with stainless steel bands, with ports at the top and bottom to allow for the introduction of fluid at the top and collection of vapor at the base.

Heating was accomplished through the use of electrical resistance heaters mounted directly on the sides of the blocks. A vertical temperature gradient was established within the block assembly, with a temperature of 80°C at the top and 130°C at the bottom. Temperatures were monitored throughout the experiment with a series of thermocouples located at 2.7, 7.1, 11.5, 15.9, 20.3, 24.7, and 29.1 cm from the base of the blocks, and 0.6 cm from the fracture surface along the centerline of the block (DTN: LB0101THCPRCPX.001 [154577]).

The dimensions of the fracture and the temperature gradient were selected based on relations derived from Phillips (1994 [154459]; 1996 [152005]), Darcy's law, and the cubic law. A hydraulic aperture of 31 μm (DTN: LB0101THCPRCPX.001 [154577]) was calculated using the initial measured air permeability of the fracture and the relation for smooth laminar flow in a channel (permeability = aperture^2/12). The difference between this value and the gold shim thickness (17.7 μm) was attributed to surface roughness and a slight waviness in the ground-flat rock surfaces.

After steady-state chemical conditions were attained in the plug-flow reactor, a portion of the water generated from the reactor was flowed at a rate of 10.8 mL/hr into the top of the fracture (DTN: LB0101THCPRCPX.001 [154577]). After 5 days, the fracture began to seal, as evidenced by a declining outflow rate, leaks in the inlet side of the fracture, and the need for increased pressure to maintain a constant inlet flow rate. After several unsuccessful attempts to plug leaks and the near-zero rate of effluent (condensed vapor) collection, it was concluded that the aperture was effectively sealed.

After cooling, the fracture was opened and examined to determine the location and nature of secondary mineral formation. The precipitate (identified as mainly amorphous silica from SEM x-ray analyses and visual and petrographic examination) was deposited almost exclusively at temperatures exceeding 100°C (Figure 7.3-1). The morphology of the precipitate differed as a function of temperature, as described in Table 7.3-1. Bridging structures of amorphous silica that formed during the experiment in both the saw-cut fracture and a natural fracture (Figure 7.3-2) appear to obstruct fluid flow within the fracture system. Similar precipitate morphologies for secondary opal-A deposited on fracture and borehole surfaces were noted at the Single Heater Test site (CRWMS M&O 1999 [129261], Sections 6.4.3.1 and 6.4.5).

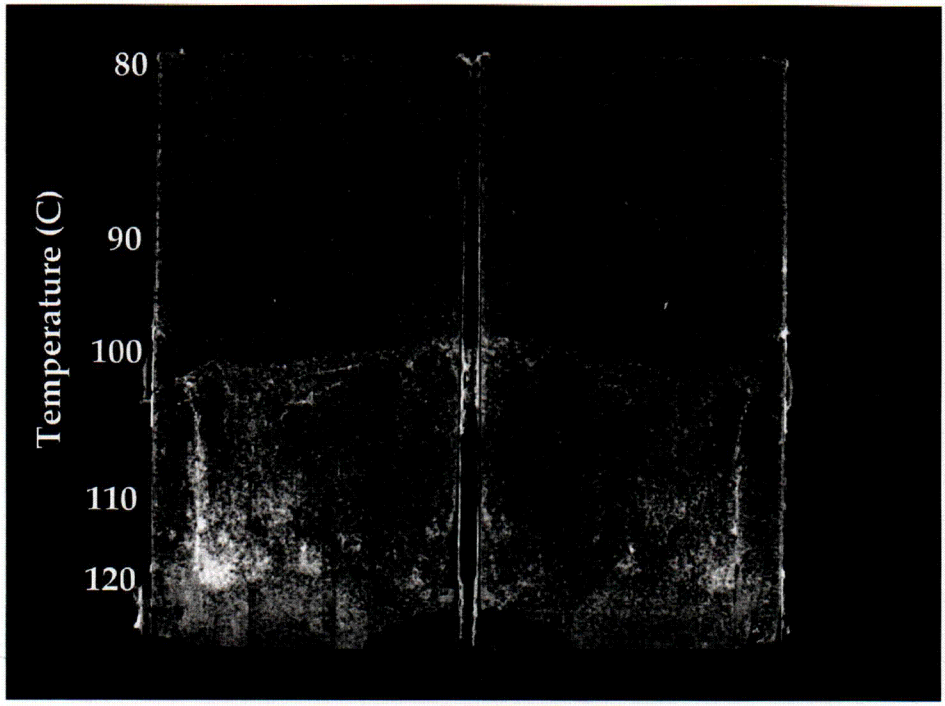

DTN: LB0101THCPRCPX.001 [154577]

NOTE: Enhanced image shows fracture temperature profile and fluorescing precipitate (light shades) under ultraviolet illumination on both fracture faces. Vertical dimension is 0.317 m.

Figure 7.3-1. Opened Fracture Faces at Conclusion of Fracture Sealing Experiment

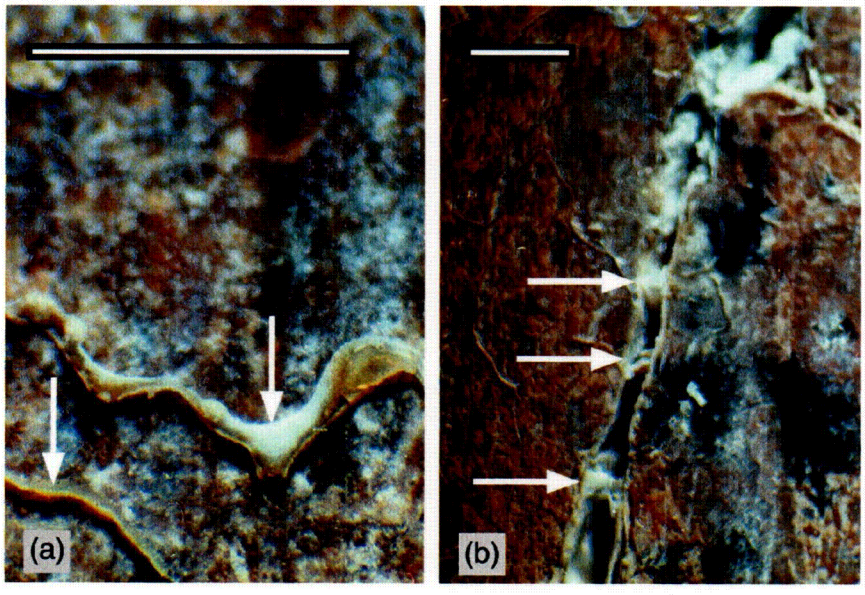

DTN: LB0101THCPRCPX.001 [154577]

NOTE: Scale bars are 0.5 mm.

Figure 7.3-2. Bridging Structures (Identified with Arrows) (a) Extending Outward from Flat Fracture Face; (b) Spanning Aperture in Cross-Cutting Natural Fracture

C141

Table 7.3-1. Characteristics of Fracture Precipitate

Temperature range	Textural characteristics
Sub-boiling	Sparse, fine-grained precipitate
~ 100°C	Solid, well-formed bridging structures Some light wall coating
~ 110°C	Vitreous, wall-coating precipitate with bridging structures
~ 120°C	Very porous, veiny, honeycomb-like bridging structures

Source: Kneafsey et al. 2001 [154460].

Fracture sealing occurred after 5 days, with only a relatively small fraction (1.2–4.7%) of the total fracture porosity filled with solid precipitate (consisting primarily of amorphous silica). These estimates are based on dividing the total volume of dissolved solids (precipitated)—carried by (1) the volume of effluent collected and (2) the volume of water injected into the top of the fracture—by the initial fracture volume (Wang 2003 [161665], SN-LBNL-SCI-190-V2, p. 73). The difference between input and output fluid volumes results from (1) leakage occurring during the later stages of the experiment and (2) filling of matrix porosity within the tuff blocks.

TOUGHREACT V2.4 (LBNL 2001 [160880]) simulations were performed to model fracture sealing, using a mesh configuration with dimensions (in one dimension) identical to those of the tuff fracture experiment. The objectives of these simulations were to validate the geochemical model developed for the THC models presented in this Model Report and test the sensitivity of the simulations to using kinetic versus equilibrium thermodynamic controls for the precipitation and dissolution of amorphous silica (thermodynamic data taken from Attachment V (DTN: LB0101DSTTHCR1.006 [161280]); kinetic data are summarized in Table 6.4-3). Assuming symmetry, only one half of the system was modeled. The mesh design contains two columns of rock blocks and one column of fracture blocks, with each column consisting of 317 elements having a fixed height of 1 mm. The cells of the outermost rock block have fixed temperatures to approximate the experimental temperature gradient (80–130°C). The simulations had a maximum time step of 0.333 s. Fluid with a composition (Table 7.3-2) based on the average composition of the plug-flow reactor effluent (DTN: LB0011THCDISSX.001 [153380]) was injected into the uppermost fracture element. The lowermost fracture element was assigned a very large ($>10^{50}$ m^3) volume to act as a constant pressure and temperature boundary. The initial rock mineralogy was considered to be the same as that used in the plug-flow experiment (the Tptpmn (tsw34) matrix composition reported in Attachment I (DTN: LB991200DSTTHC.003 [161276]). The initial fracture permeability was set to that obtained in the experiment (8.03×10^{-11} m^2: DTN: LB0101THCPRCPX.001 [154577]), whereas the flow rate and fracture width were reduced in half (5.4 mL/h and 15.5 μm, respectively) to account for the assumption of symmetry. To simplify the simulation, the rock matrix blocks were assigned a zero permeability value to force the injected water to flow though and interact only with the fracture elements. Thus, the matrix elements served only as a heat transport mechanism. Different simulations were run for a period of 5.8 days (500,000 s) with amorphous silica controlled by either equilibrium or kinetic conditions. The cubic law was used to specify the relation between porosity and permeability. The results of these simulations are depicted in Figures 7.3-3 (a) and (b).

Table 7.3-2. Initial Water Composition for Fracture Sealing Simulations

Species	Concentration (moles/liter)	Concentration (mg/liter)
Na^+	4.75E-04	10.92
K^+	1.38E-04	5.40
Ca^{2+}	5.64E-06	0.23
Mg^{2+}	1.00E-10	0.00000243
HCO_3^-	3.17E-04	19.34
SiO_2	1.53E-03	92.22
AlO_2^-	1.00E-10	0.00000590
$HFeO_2$	1.00E-10	0.00000889
pH	8.32	

Source: Average of Frac Pump samples from DTN: LB0011THCDISSX.001 [153380].

NOTE: Nominal concentrations (1.00E-10 mol/L) were assigned to species that were below detection in the experimental study. HCO_3^- was estimated assuming a 1:1 molar correspondence with calcite alkalinity. This value should have been 2:1 (2 moles of bicarbonate per mole of calcite) to maintain milliequivalence (see text for discussion).

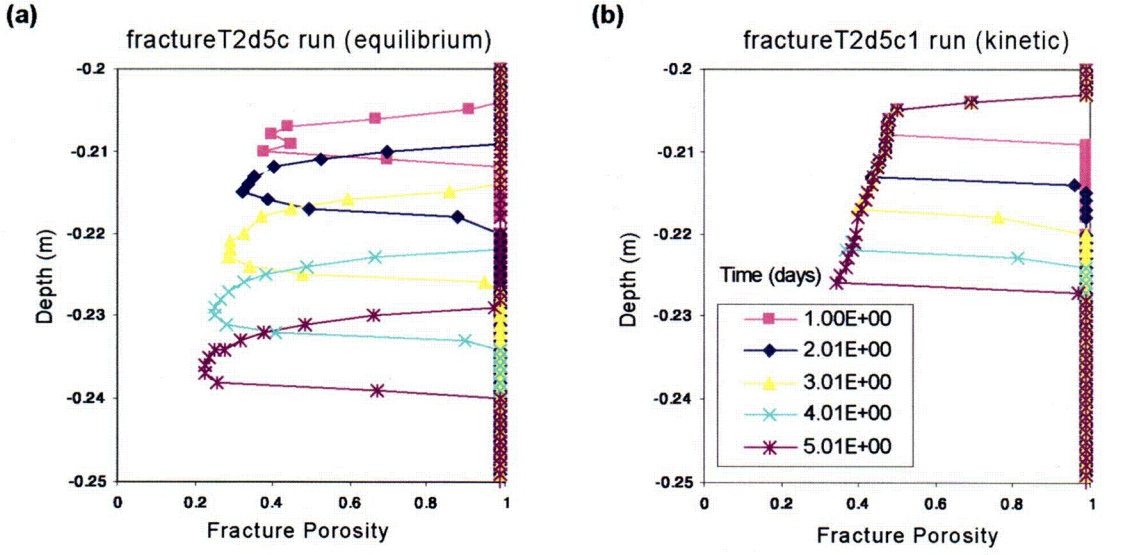

Output-DTN: LB0301FRACSEAL.002

NOTE: Area plotted represents lower portion of two-phase zone (see Figure 7.3-4).

Figure 7.3-3. Porosity vs. Depth over Time for Simulated (a) Equilibrium and (b) Kinetic Control of Amorphous Silica in Fracture Sealing Experiment

C142

7.3.1 Validation Criteria

The criteria for model validation are specified in the *Technical Work Plan for: Performance Assessment Unsaturated Zone* (BSC 2002 [160819], Attachment I, Section I-3-4-1). The model validation criteria applicable for the fracture sealing experiment are that the distribution of precipitated minerals should be qualitatively similar to experimental observations, and that the major solid constituents should be the same. These criteria were deemed reasonable because they capture the two main observed results of the experiments: the location of the precipitate, and its mineralogy. Discussion of uncertainty associated with coupled process (THC) modeling is presented in Section 6.9.

7.3.2 Results of Simulations and Comparison to Measured Data

The simulation results indicated the formation of a nearly isothermal two-phase region (Figure 7.3-4), with an overlying water column below and a vapor zone below. The precipitation of amorphous silica at the base of the two-phase zone accounted for all of the porosity and permeability reduction in the fracture system. A gradual pressure buildup, caused by the reduction of the fracture aperture, occurred at the top of the fracture system, resulting in a downward shift in the base of the boiling zone (and region of silica precipitation) over time. The experimental system experienced a similar phenomena, as reduced permeability led to the need for higher inlet pressure to sustain a constant injection rate, resulting in fluid leaking out along the sides and top of the fracture system.

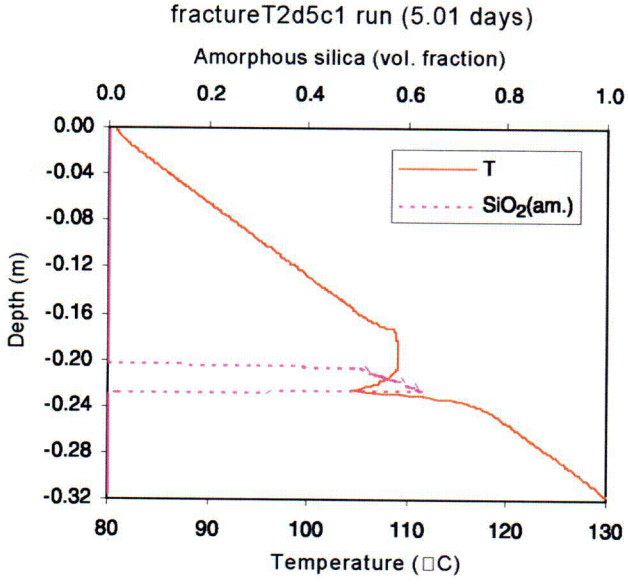

Output-DTN: LB0301FRACSEAL.002

NOTE: Simulation has amorphous silica controlled by kinetic precipitation and dissolution.

Figure 7.3-4. Simulated Temperature Profile and Volume Fraction of Amorphous Silica vs. Depth at 5.01 Days

The thickness and location of the silica precipitation zone were different in the kinetic and equilibrium simulations (Figures 7.3-3 (a and b)). The simulations conducted using equilibrium precipitation and dissolution for amorphous silica showed the effects of both precipitation and dissolution, as the trailing (upper) edge of the silica front underwent dissolution with time. In the kinetic simulations, almost no dissolution of precipitated amorphous silica occurred, resulting in a thicker band of silica that occluded less of the fracture aperture. The maximum porosity and permeability reduction (for a given fracture element) was greater for the equilibrium simulation, with a 79% porosity reduction and a permeability reduction of over 99% over the 5.8-day simulation. The kinetic simulation had maximum porosity and permeability reductions of 66% and 96%, respectively.

Significant permeability reductions occurred within 5 days after initiation of fluid flow for both the experiment and the simulations. The presence of silica precipitate throughout the boiling zone in the experimental fracture system suggests that the kinetic simulation (which retains early-formed precipitate) is a more appropriate match to the experimental results. Some of the differences between the experiment and the simulations may result from variability in the two-dimensional fracture surface in the experiment.

Both of the simulations met the validation criteria relating to the distribution and type of secondary mineral precipitation. Amorphous silica was the dominant secondary mineral phase in both the experiment and simulations. The simulated amorphous silica precipitation was restricted to the lower portion of the two-phase zone, at temperatures of around 105–109°C (Figures 7.3-3 (a and b) and 7.3-4), consistent with the observed pattern of mineralization along the fracture surface in the experiment (Figure 7.3-1). At 5 days, the total fracture-porosity-reduction values resulting from silica precipitation in the equilibrium and kinetic simulations were 2.2 and 3.9 percent, respectively, comparable to the calculated values of 0.9–3.6% total-fracture-porosity reduction resulting from silica mineralization during the experiment (Wang 2003 [161665], SN-LBNL-SCI-190-V2, p. 73). Even though the fracture permeability at the conclusion of the experiment was not measured, the observed near-cessation of fluid flow through the fracture after 5 days indicates a significant reduction in fracture permeability. The minimum simulated permeability values at 5 days of 9.65×10^{-13} m^2 and 3.39×10^{-12} m^2 for the equilibrium and kinetic experiments, respectively, represent permeability reductions of 99% and 96%.

This model validation work satisfies the goals set forth in the TWP (BSC 2002 [160819], Attachment I, Section I-3-4-1), and thus no further validation work associated with the fracture sealing experiment is planned.

8. CONCLUSIONS

This Model Report documents the THC Seepage Model (Sections 4 and 6), the Drift Scale Test (DST) THC Model (Sections 4, 6, and 7.1), and experimental studies to validate various aspects of the models (Sections 7.2 and 7.3). The models describe coupled THC processes at the drift scale to assess (1) the chemistry of water and gas potentially entering drifts and (2) changes in permeability and flow around drifts. The THC Seepage Model was used primarily to predict the composition of waters and gases around and potentially seeping into waste emplacement drifts and the effect of water-rock interaction on flow. Key findings of this model are summarized in Figure 8-1. The DST THC Model was used primarily to validate the THC Seepage Model.

The underlying conceptual and mathematical models (Sections 6.1–6.4) provide the basis for modeling the thermal and hydrological effects of the relevant mineral-water-gas reactions and transport processes in the host rock for 100,000 years. Results are presented to evaluate the sensitivity of the models to different input parameters and conceptualizations. Validation of the models (Section 7) is accomplished through comparison of simulation results to data collected from the DST and to laboratory experiments that explore various specific aspects of the models. Validation of the models was also accomplished through publication in a refereed journal (Xu et al. 2001 [161864]). Model results have been submitted to the Technical Data Management System (TDMS) as output under DTNs listed in Section 9.4 and Attachment X of this Model Report. Applicable acceptance criteria from the YMRP addressed by this report are discussed in Section 4.2 with pointers referring to sections of this report where these criteria are addressed. The barrier capability of the natural system, including host rocks and the capillary barrier effects of drift openings, are considered throughout this report (e.g., Sections 6.8.2 and 6.8.5.2). Potential barrier effects from mineral precipitation during the normal period are also considered (Section 6.8.5.4).

8.1 MODELED COUPLED PROCESSES AND UNCERTAINTY

Simulations of THC processes include coupling among heat, water, and vapor flow, aqueous and gaseous species transport, kinetic and equilibrium mineral-water reactions, and feedback of mineral precipitation/dissolution on porosity, permeability, and capillary pressure for a dual-permeability (fracture-matrix) system. Treatment of CO_2 included gas-water equilibration, gas species diffusion, and advection. Data were incorporated from the calibrated thermal-hydrological property sets, the three-dimensional mineralogical model, the UZ Flow and Transport Model, thermal test geochemical data (fracture and matrix mineralogy, aqueous geochemistry, and gas chemistry), thermodynamic data (minerals, gases, and aqueous species), kinetic data for mineral-water reactions, and transport (diffusion coefficient) data (Section 4.1). The models include a wide range of major and minor aqueous species and minerals (primary and potential secondary phases). The following primary aqueous species are considered: H^+, Ca^{2+}, Mg^{2+}, Na^+, K^+, $SiO_{2(aq)}$, AlO_2^-, $HFeO_{2(aq)}$, SO_4^{2-}, HCO_3^-, Cl^-, NO_3^-, and F^-. Minerals include several silica phases (α-cristobalite, quartz, tridymite, amorphous silica, and opal-CT), calcite, feldspars, smectites, illite, kaolinite, sepiolite, zeolites, fluorite, hematite, goethite, gypsum, and volcanic (rhyolitic) glass. In addition to the calibration of the hydrological properties, some thermodynamic and kinetic data were revised (within their ranges of uncertainty) to yield modeled pore water compositions (under ambient temperatures and infiltration rates) close to the original measured values over long simulation times.

Many uncertainties exist in modeling coupled THC processes (see Section 6.9), because of the large amount of input data needed and the complexity of natural systems as described above and in Sections 4, 6, and 7. Therefore, a quantitative measure of model uncertainty based on the uncertainties of the data themselves is difficult. Model validation provides a better test of whether the system can be described sufficiently well for the intended purposes of the model. Validation was accomplished through analyses of the DST, plug-flow reactor experiments, and fracture sealing experiments performed under temperatures, pressures, and chemical compositions corresponding to the range expected for the repository thermal loading conditions and drift design. As summarized further in this section, results of DST THC simulations captured the important changes in pH, aqueous species concentrations, gas-phase CO_2 concentrations, and mineral deposition at specific locations over time. This provides sufficient validation of the model's capability to predict trends of spatial and temporal variations in water and gas chemistry around emplacement drifts. However, the duration of the heating phase of the DST (approximately 4 years) is short compared to the time over which the repository drifts would be above-boiling (at least one thousand years). Therefore, the DST THC Model and data from the DST cannot be used to directly validate all aspects of THC Seepage Model predictions of water chemistry, gas compositions, and permeability over very long times.

Several simulations were performed to further characterize the effects of natural variability and uncertainty on the THC Seepage Model predictions. These sensitivity analyses address the follow major issues:

1. Different repository host-rock geologic units (Tptpmn and Tptpll)
2. Alternative geochemical systems (base case and extended case, additional minerals and chemical components)
3. Alternative thermodynamic data sets (different equilibrium constants for key minerals)
4. Different treatments of mineral-water reactions (different kinetic rate constants and reactive surface areas; equilibrium vs. kinetic reactions)
5. Spatial heterogeneity in fracture permeability
6. Different infiltration rates and effects of climate change
7. Alternative water vapor pressure models
8. Alternative initial water compositions
9. Different effective CO_2 diffusivities
10. Alternative drift-wall conceptualizations (open vs. closed to liquid flow).

These THC Seepage Model simulations covered a wide range of the most important uncertainties from the standpoint of model validation, bounding analyses, conservatism, their impact on model results, and their propagation to other models. Based on the natural variability in input water composition and the resulting spread in simulation results, the uncertainties in predicted concentrations of aqueous species and of CO_2 gas are estimated to be up to about one order of magnitude (Section 6.9.2), with implications for downstream use examined below in Section 8.4.

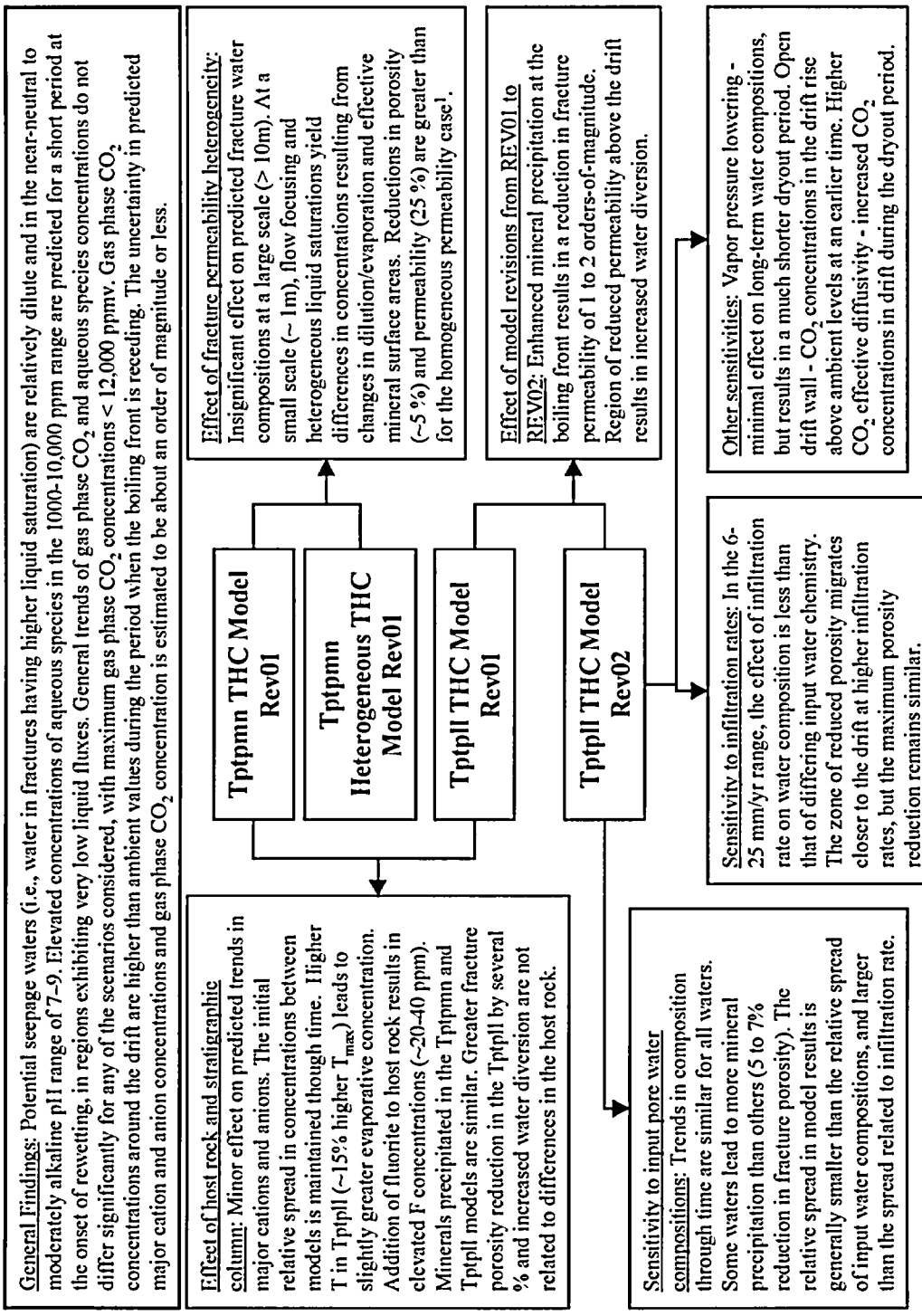

[1]The heterogeneous case was run using REV01 hydrological properties and with TOUGHREACT V2.3 [153101]. The use of REV02 properties and TOUGHREACT V3.0 [161256] resulted in greater reductions in porosity and permeability for the homogeneous permeability case, which would also be expected for the heterogeneous case.

Figure 8-1. Key Findings of the THC Seepage Model

8.2 THC SEEPAGE MODEL RESULTS

The THC Seepage Model was designed to represent waste package heating over time, changes in heat load caused by ventilation, the effective heat transfer within the drift, and THC processes in the unsaturated zone around waste emplacement drifts. Simulations considered an initial heat load of 1.45 kW/m, including a preclosure period of 50 years using two alternative ventilation efficiencies (70% and 86.3%). Model results predict the chemistry of matrix and fracture water at various locations around a drift, the times of rewetting around the drifts, and the net fluxes of water and gas near and across the drift wall for a period of 100,000 years.

The scope of this Model Report includes essentially one design heat load, resulting in temperatures near emplacement drifts that exceed the boiling point of water for several hundred years after repository closure. Temperature is a critical parameter because it strongly affects the extent of water-rock-gas interaction taking place around proposed emplacement drifts. In the cases considered here, increased water-rock-gas interaction resulting from higher temperatures is expected to affect water chemistry and flow to a greater extent than if a lower heat load were considered. The predicted extent of the dryout zone and the time of rewetting vary with the different infiltration rates and water-vapor pressure models considered. Depending on the modeled scenario, the maximum extent of the dryout zone in fractures was predicted to be between 6 and 10 m above drift center, and the predicted time of fracture rewetting at the drift crown varied between 1,200 and 2,000 years in most cases. In one case using REV02 rock properties and neglecting the effect of vapor-pressure lowering caused by capillary suction, rewetting was predicted to occur much later (i.e., between 12,000 and 20,000 years).

Similar trends in water and gas compositions were predicted for modeled cases with heat loading in the Tptpmn and in the Tptpll geologic units. At any point in time, the relative spread in predicted water compositions spatially above the drift, including alternative model conceptualizations and five different input water compositions, was generally one order of magnitude or less (Section 6.9.2). Thus, in a qualitative sense, this spread is small. However, in a quantitative sense, this same spread would be significant for parameters for which small variations in concentrations could have a large impact on the calculated end-brine compositions upon near-complete evaporation of seepage waters. For example, only slight variations in the predicted relative amounts of calcium and bicarbonate could yield different end-brine compositions, and thus lead to different scenarios regarding waste package corrosion. Recognizing this possibility, simulations employed a range of input water compositions likely to yield predicted percolation waters evolving towards a representative range of possible end-brine types (Section 6.2.2.1). Model uncertainties unrelated to input water compositions could still affect predicted percolation water compositions in a way that would also affect conclusions regarding end-brine compositions.

In general, when modeling a geochemical system without aluminum silicate minerals and glass, the predicted pH values were somewhat lower and CO_2 concentrations higher than in simulations including these phases. Clearly, the effect of mineral-water reactions on the geochemistry of waters and gases is strongly influenced by the presence of clays and zeolite minerals and very sensitive to the choice of thermodynamic properties for these minerals. Sodium concentrations under ambient conditions were predicted to increase by a factor of approximately four in 100,000 years (from the dissolution of mostly albite and glass), which could be somewhat greater than

would be expected in the natural system. In this respect, simulations including aluminosilicate minerals could provide an upper limit on effects of water-rock-gas interactions around waste emplacement drifts. In all of the modeled conceptualizations, including five representative input water compositions, relatively dilute and near-neutral to moderately alkaline water compositions were predicted in fractures around drifts, with pH values in the 7–9 range and gas-phase CO_2 concentrations remaining below 12,000 ppmv. General trends of CO_2 gas and aqueous species concentrations around the drifts did not differ significantly for any of the cases. The simulations also exhibited an increase in the CO_2 gas concentrations around the drifts during rewetting, relative to ambient values. Elevated concentrations of aqueous species relative to background values were predicted to occur temporarily at the time of rewetting in fractures, though at very low liquid saturations.

The predicted magnitude of fracture porosity change caused by water-rock interaction around waste emplacement drifts depends strongly on the initial fracture porosity (with the largest relative change for the smallest porosity), and results in large part from mineral precipitation directly at the boiling front due to evaporative concentration. Simulations carried out for REV02 of this Model Report (Section 6.8) considered a more accurate treatment of mineral precipitation at the boiling front than in REV01. For this reason, and because fracture porosity was reduced by a factor of two in the Tptpll unit compared to that used in previous Model Report revisions, a significant fracture porosity change (up to nearly 8%) was predicted compared to the results of REV01 simulations (around 1% or less fracture porosity change). As a result, the REV02 simulations predicted a significant effect of water-gas-rock interactions on flow patterns around the drift, whereas simulations from the previous revision (REV01) of this Model Report did not. REV02 simulations exhibit a thin zone of predominantly amorphous silica deposition several meters above the drift wall that reduces the percolation flux at the drift wall. This zone has a fracture permeability that is one to two orders of magnitude lower than in the surrounding rock fractures, deflecting some of the percolating water around the drift and significantly extending the shadow zone below the drift. Because the silica solubility decreases with declining temperature, the amorphous silica precipitated in fractures does not dissolve significantly into percolating water over 100,000 years.

REV01 simulations incorporated several permeability realizations for the Tptpmn unit THC Seepage Model. Steady-state (ambient temperature), TH, and THC simulations were performed using three heterogeneous fracture permeability realizations with a 4-order-of-magnitude range in permeability. All were run using the mean infiltration climate change scenario for the Tptpmn unit. The heterogeneity in fracture permeability can have varied effects on thermohydrology, including flow focusing and irregularities in the isotherms and liquid saturations. Areas of highest initial liquid saturation, also having lower permeability and generally residing above the drift, tend to show the greatest reduction in fracture permeability as a result of mineral precipitation. The effect of this localized permeability reduction tends to cause some additional flow focusing. The permeability changes (up to 25%) are considerably less than the initial range in permeability. These REV01 simulations used higher fracture porosities than those for REV02 and did not incorporate the more accurate treatment of mineral precipitation at the boiling front implemented in TOUGHREACT V3.0 (LBNL 2002 [161256]). Therefore, the REV01 simulations produced a smaller effect of mineral precipitation on fracture sealing than if REV02 properties and processes were implemented. Spatial differences in water chemistry were not affected significantly by permeability heterogeneities, and because of the strong control of the

mineral assemblage on water chemistry (and not the mineral proportions) this would also be expected to be the case if REV02 properties were used.

8.3 DST THC MODEL RESULTS (VALIDATION)

Validation of the overall approach and data embodied in the Drift Scale THC conceptual model described in this Model Report was accomplished via a comparison of measured gas compositions, water chemistry, and analyses of mineral deposition in the Drift Scale Test (DST) to DST THC Model simulation results. The DST THC Model was not expected to exactly match measurements from the DST, and the validation work combined both sensitivity studies as well as straight comparisons to measured data.

Comparisons between observed and modeled aqueous pH and CO_2 concentrations in the gas phase indicate that a limited set of aqueous species, minerals (calcite, silica phases, fluorite, and gypsum), and gases (H_2O, air, and CO_2) (base case), could describe the general evolution of DST waters with respect to pH, CO_2, and conservative anions. A more complete geochemical system (extended case), including a wide range of aluminosilicates (such as feldspars, clays and zeolites), yielded modeled aqueous silica concentrations closer to those observed, plus information on additional species (i.e., Mg^{2+}, Al^{3+}, and Fe^{3+}). However, predicted pH values for the extended system are slightly higher than those observed, and gas-phase CO_2 concentrations are slightly lower than the measured values.

In particular, simulation results compared to measured gas-phase CO_2 concentrations and the chemistry of waters collected from hydrology boreholes indicate that the model captures the general trend in concentrations in the borehole intervals where comparisons were made. Predicted locations and relative abundances of secondary minerals were consistent with *in situ* sidewall core samples retrieved from zones that had undergone boiling. The main phase was amorphous silica followed by significantly lesser amounts of calcite and gypsum. REV01 TH properties resulted in a better match for the conservative species and fluoride, because of the greater rate of condensate dilution compared to that produced using the REV02 properties. However, REV02 modeled aqueous silica concentrations were more consistent with the measured values, owing to the revised geochemical system (in particular, the addition of opal to the initial mineral assemblage). Analyses of ^{14}C concentrations in CO_2 also corroborated the model results, because of their sensitivity to calcite dissolution and drift air contamination.

The evidence based on numerous field and laboratory measurements, demonstrates that model validation criteria were met for CO_2 concentrations in gas, for several aqueous species concentrations, and for mineral precipitation in fractures. Although some disagreements between modeled and measured values exist, they could generally be attributed to sampling difficulties or the addition of a phase (such as fluorite) in the REV02 mineral assemblage that clearly made the agreement worse than for REV01. These differences, though, highlight the sensitivity of the model to various input parameters. Some heterogeneities in the measured data could not be matched by the model results, as would be expected in the comparison of an idealized model system. Although the model did not include heterogeneity in hydrological properties, and is only a 2-D representation of a 3-D system the agreement to much of the measured data gives confidence in the approach and use of "average" properties.

Confidence in various aspects of the model approach and input data used in the THC Seepage Model is also based on a comparison of modeled and measured water compositions from a laboratory plug-flow dissolution experiment using volcanic tuff from the Tptpmn unit at Yucca Mountain. The model simulations captured the magnitude and change in aqueous species concentrations measured during this experiment at elevated temperatures, and thus the validation criteria were met. A fracture sealing laboratory experiment was also simulated, with the location and amounts of amorphous silica precipitated closely comparable to that observed, also meeting the validation criteria.

The THC responses of the Yucca Mountain Drift Scale Test were independently analyzed by the participants of the DECOVALEX III project, an international research project to develop coupled models and their validation against experiments. The outcome of the analyses by the DECOVALEX participants, generally corroborative of the contents of this Model Report, are to be presented in the GeoProc2003 conference to be held in Stockholm, Sweden, and will be published in a special issue of the *International Journal of Rock Mechanics*.

8.4 UNCERTAINTIES AND RESTRICTIONS FOR DOWNSTREAM USE

Section 1.3 states the general model limitations. Potential uncertainties affecting model results were discussed in a qualitative manner in Section 6.9-1, and addressed more quantitatively in Section 6.9-2. Various alternative conceptualizations and ranges of input data were considered (summarized in Section 8.1; see also Table 6-1). In addition, confidence in the model results was obtained by comparing model results to experimental data from the DST (Section 7.1 and summarized in Section 8.3) and other laboratory experiments (Sections 7.2 and 7.3). Much of the spread in the output compositions from the THC Seepage Model simulations is caused by the natural variability of input water compositions. This spread is up to about one order of magnitude and in many cases lower (for pH, within less than a pH unit; Section 6.9-2). As mentioned in Section 8.2, this margin of uncertainty could be problematic for aqueous species for which small differences in concentrations (by much less than one order of magnitude) could upon evaporation have a large impact on calculated end-brine compositions (e.g., calcium and bicarbonate) because of small changes in their concentration ratios. On the other hand, the input data and model conceptualizations considered in this study all yield similar trends in modeled aqueous species and gas-phase CO_2 concentrations over time. Therefore, it is essential for each downstream user to carefully evaluate the results presented here in light of the level of certainty required.

INTENTIONALLY LEFT BLANK

9. INPUTS AND REFERENCES

The following is a list of the references cited in this document. Column 1 represents the unique six digit numerical identifier (the Document Input Reference System [DIRS] number), which is placed in the text following the reference callout (e.g., BSC 2002 [160819]). The purpose of these numbers is to assist the reader in locating a specific reference. Within the reference list, multiple sources by the same author (e.g., BSC 2002) are sorted alphabetically by title.

9.1 DOCUMENTS CITED

153329 Arnórsson, S. and Stefánsson, A. 1999. "Assessment of Feldspar Solubility Constants in Water in the Range 0° to 350°C at Vapor Saturation Pressures." *American Journal of Science, 299*, (3), 173-209. New Haven, Connecticut: Yale University, Kline Geology Laboratory. TIC: 249258.

101379 Bear, J. 1988. *Dynamics of Fluids in Porous Media.* New York, New York: Dover Publications. TIC: 217568.

155950 BSC (Bechtel SAIC Company) 2001. *FY 01 Supplemental Science and Performance Analyses, Volume 1: Scientific Bases and Analyses.* TDR-MGR-MD-000007 REV 00 ICN 01. Las Vegas, Nevada: Bechtel SAIC Company. ACC: MOL.20010801.0404; MOL.20010712.0062; MOL.20010815.0001.

156065 BSC (Bechtel SAIC Company) 2001. *In-Drift Precipitates/Salts Analysis.* ANL-EBS-MD-000045 REV 00 ICN 03. Las Vegas, Nevada: Bechtel SAIC Company. ACC: MOL.20011212.0252.

164414 BSC (Bechtel SAIC Company) 2001. *Software Baseline Request for LBNL-2000-242, TOUGHREACT V. 2.3.* 10396-2.3-00. Las Vegas, Nevada: Bechtel SAIC Company. ACC: MOL.20020123.0010.

160247 BSC (Bechtel SAIC Company) 2002. *Analysis of Geochemical Data for the Unsaturated Zone.* ANL-NBS-HS-000017 REV 00 ICN 02. Las Vegas, Nevada: Bechtel SAIC Company. ACC: MOL.20020314.0051.

158375 BSC (Bechtel SAIC Company) 2002. *Drift-Scale Coupled Processes (DST and THC Seepage) Models.* MDL-NBS-HS-000001 REV 01 ICN 02. Las Vegas, Nevada: Bechtel SAIC Company. ACC: MOL.20020312.0156.

159124 BSC (Bechtel SAIC Company) 2002. *Geologic Framework Model (GFM2000).* MDL-NBS-GS-000002 REV 01. Las Vegas, Nevada: Bechtel SAIC Company. ACC: MOL.20020530.0078.

159906 BSC (Bechtel SAIC Company) 2002. *Invert Effective Thermal Conductivity Calculation.* 000-00C-WIS0-00100-000-00A. Las Vegas, Nevada: Bechtel SAIC Company. ACC: MOL.20020828.0178.

159527 BSC (Bechtel SAIC Company) 2002. *Repository Design, Repository/PA IED Subsurface Facilities Plan Sht. 1 of 5, Sht. 2 of 5, Sht. 3 of 5, Sht. 4 of 5, and Sht. 5 of 5.* DWG-MGR-MD-000003 REV A. Las Vegas, Nevada: Bechtel SAIC Company. ACC: MOL.20020601.0194.

160819 BSC (Bechtel SAIC Company) 2002. *Technical Work Plan for: Performance Assessment Unsaturated Zone.* TWP-NBS-HS-000003 REV 02. Las Vegas, Nevada: Bechtel SAIC Company. ACC: MOL.20030102.0108.

160771 BSC (Bechtel SAIC Company) 2002. *Thermal Testing Measurements Report.* ANL-NBS-HS-000041 REV 00. Las Vegas, Nevada: Bechtel SAIC Company. ACC: MOL.20021004.0314.

160146 BSC (Bechtel SAIC Company) 2002. *Total System Performance Assessment-License Application Methods and Approach.* TDR-WIS-PA-000006 REV 00. Las Vegas, Nevada: Bechtel SAIC Company. ACC: MOL.20020923.0175.

164454 BSC (Bechtel SAIC Company) 2002. *Users Manual (UM) for TOUGHREACT V3.0.* 10396-UM-3.0-00. Las Vegas, Nevada: Bechtel SAIC Company. ACC: MOL.20030411.0090.

161760 BSC (Bechtel SAIC Company) 2002. *Ventilation Model Report.* ANL-EBS-MD-000030 REV 02. Las Vegas, Nevada: Bechtel SAIC Company. ACC: MOL.20030102.0140.

160975 BSC (Bechtel SAIC Company) 2002. *Ventilation Model.* ANL-EBS-MD-000030 REV 01 ICN 01. Las Vegas, Nevada: Bechtel SAIC Company. ACC: MOL.20021106.0055.

160109 BSC (Bechtel SAIC Company) 2003. *Development of Numerical Grids for UZ Flow and Transport Modeling.* ANL-NBS-HS-000015 REV 01. Las Vegas, Nevada: Bechtel SAIC Company. ACC: DOC.20030404.0005.

161530 BSC (Bechtel SAIC Company) 2003. *Drift-Scale Coupled Processes (DST and TH Seepage) Models.* MDL-NBS-HS-000015 REV 00. Las Vegas, Nevada: Bechtel SAIC Company. URN-1087

161519 BSC (Bechtel SAIC Company) 2003. *Interlocking Drip Shield.* 000-MW0-TED0-00101-000-00A, -00102-000-00A, and -00103-000-00A. 3 Sheets. Las Vegas, Nevada: Bechtel SAIC Company. ACC: ENG.20030205.0001; ENG.20030205.0002; ENG.20030205.0003.

164053 BSC (Bechtel SAIC Company) 2003. *Repository Design Project, RDP/PA IED Typical Waste Package Components Assembly 1 of 9.* 800-IED-WIS0-00201-000-00A. Las Vegas, Nevada: Bechtel SAIC Company. ACC: ENG.20030702.0001.

164052 BSC (Bechtel SAIC Company) 2003. *Repository Design Project, Repository/PA IED Emplacement Drift Committed Materials 1 of 2.* 800-IED-WIS0-00301-000-00A. Las Vegas, Nevada: Bechtel SAIC Company. ACC: ENG.20030627.0003.

162444 BSC (Bechtel SAIC Company) 2003. *Repository Design Project, Repository/PA IED Emplacement Drift Committed Materials.* 800-IED-EBS0-00301-000-00A. Las Vegas, Nevada: Bechtel SAIC Company. ACC: ENG.20030311.0022.

164069 BSC (Bechtel SAIC Company) 2003. *Repository Design Project, Repository/PA IED Emplacement Drift Configuration 1 of 2.* 800-IED-EBS0-00201-000-00A. Las Vegas, Nevada: Bechtel SAIC Company. ACC: ENG.20030630.0002.

161727 BSC (Bechtel SAIC Company) 2003. *Repository Design, Repository/PA IED Subsurface Facilities.* 800-IED-EBS0-00402-000-00B. Las Vegas, Nevada: Bechtel SAIC Company. ACC: MOL.20030109.0146.

161731 BSC (Bechtel SAIC Company) 2003. *Repository Design, Repository/PA IED Subsurface Facilities.* 800-IED-EBS0-00403-000-00B. Las Vegas, Nevada: Bechtel SAIC Company. ACC: MOL.20030109.0147.

100617 Buscheck, T.A. and Nitao, J.J. 1993. "Repository-Heat-Driven Hydrothermal Flow at Yucca Mountain, Part I: Modeling and Analysis." *Nuclear Technology, 104,* (3), 418-448. La Grange Park, Illinois: American Nuclear Society. TIC: 224039.

161770 Canori, G.F. and Leitner, M.M. 2003. *Project Requirements Document.* TER-MGR-MD-000001 REV 01. Las Vegas, Nevada: Bechtel SAIC Company. ACC: DOC.20030404.0003.

105210 Carlos, B.A.; Chipera, S.J.; Bish, D.L.; and Craven, S.J. 1993. "Fracture-Lining Manganese Oxide Minerals in Silicic Tuff, Yucca Mountain, Nevada, U.S.A." *Chemical Geology, 107,* 47-69. Amsterdam, The Netherlands: Elsevier. TIC: 208629.

124275 Carroll, S.; Mroczek, E.; Alai, M.; and Ebert, M. 1998. "Amorphous Silica Precipitation (60 to 120°C): Comparison of Laboratory and Field Rates." *Geochimica et Cosmochimica Acta, 62,* (8), 1379-1396. New York, New York: Elsevier. TIC: 243029.

111115 CRWMS M&O (Civilian Radioactive Waste Management System Management and Operating Contractor) 1998. *Drift Scale Test As-Built Report.* BAB000000-01717-5700-00003 REV 01. Las Vegas, Nevada: CRWMS M&O. ACC: MOL.19990107.0223.

129261 CRWMS M&O 1999. *Single Heater Test Final Report.* BAB000000-01717-5700-00005 REV 00 ICN 1. Las Vegas, Nevada: CRWMS M&O. ACC: MOL.20000103.0634.

123916 CRWMS M&O 2000. *Abstraction of Drift-Scale Coupled Processes.* ANL-NBS-HS-000029 REV 00. Las Vegas, Nevada: CRWMS M&O. ACC: MOL.20000525.0371.

151951 CRWMS M&O 2000. *Engineered Barrier System: Physical and Chemical Environment Model.* ANL-EBS-MD-000033 REV 01. Las Vegas, Nevada: CRWMS M&O. ACC: MOL.20001228.0081.

144454 CRWMS M&O 2000. *Mountain-Scale Coupled Processes (TH) Models.* MDL-NBS-HS-000007 REV 00. Las Vegas, Nevada: CRWMS M&O. ACC: MOL.19990721.0528.

149137 CRWMS M&O 2000. *Repository Subsurface Design Information to Support TSPA-SR.* Input Transmittal PA-SSR-99218.Tc. Las Vegas, Nevada: CRWMS M&O. ACC: MOL.20000424.0690.

151014 CRWMS M&O 2000. *Tabulated In-Drift Geometric and Thermal Properties Used in Drift-Scale Models for TSPA-SR.* CAL-EBS-HS-000002 REV 00. Las Vegas, Nevada: CRWMS M&O. ACC: MOL.20000718.0219.

120903 CRWMS M&O 2000. *Ventilation Model.* ANL-EBS-MD-000030 REV 00. Las Vegas, Nevada: CRWMS M&O. ACC: MOL.20000107.0330.

153814 CRWMS M&O 2001. *Updated CO2 Analysis of Gas Samples Collected from the Drift Scale Test.* Input Transmittal 00423.T. Las Vegas, Nevada: CRWMS M&O. ACC: MOL.20010202.0170.

100439 de Marsily, G. 1986. *Quantitative Hydrogeology: Groundwater Hydrology for Engineers.* San Diego, California: Academic Press. TIC: 208450.

160252 Dobson, P. 2001. Evaluation of Local Altered Hydraulic Characteristics and the Effects of Near Field Thermal and Chemical Alterations (YMP-LBNL-DSM-ELS-PD-1). Scientific Notebook SN-LBNL-SCI-190-V1. ACC: MOL.20010521.0134.

135997 Doughty, C. 1999. "Investigation of Conceptual and Numerical Approaches for Evaluating Moisture, Gas, Chemical, and Heat Transport in Fractured Unsaturated Rock." *Journal of Contaminant Hydrology, 38,* (1-3), 69-106. New York, New York: Elsevier. TIC: 244160.

140067 Drever, J.I. 1997. *The Geochemistry of Natural Waters, Surface and Groundwater Environments.* 3rd Edition. Upper Saddle River, New Jersey: Prentice Hall. TIC: 246732.

117799 Ehrlich, R.; Etris, E.L.; Brumfield, D.; Yuan, L.P.; and Crabtree, S.J. 1991. "Petrography and Reservoir Physics III: Physical Models for Permeability and Formation Factor." *AAPG Bulletin, 75,* (10), 1579-1592. Tulsa, Oklahoma: American Association of Petroleum Geologists. TIC: 246294.

154365 Freeze, G.A.; Brodsky, N.S.; and Swift, P.N. 2001. *The Development of Information Catalogued in REV00 of the YMP FEP Database.* TDR-WIS-MD-000003 REV 00 ICN 01. Las Vegas, Nevada: Bechtel SAIC Company. ACC: MOL.20010301.0237.

160460 Fridriksson, T.; Neuhoff, P.S.; Arnórsson, S.; and Bird, D.K. 2001. "Geological Constraints on the Thermodynamic Properties of the Stilbite—Stellerite Solid Solution in Low-Grade Metabasalts." *Geochimica et Cosmochimica Acta, 65,* (21), 3993-4008. [New York, New York]: Elsevier. TIC: 253460.

144877 Garrels, R.M. and Christ, C.L. 1990. *Solutions, Minerals, and Equilibria.* Boston, Massachusetts: Jones and Barlett Pulishers. TIC: 223483.

160465 Gunnarsson, I. and Arnórsson, S. 2000. "Amorphous Silica Solubility and the Thermodynamic Properties of H{subscript 4}SiO°{subscript 4} in the Range of 0° to 350°C at P{subscript sat}." *Geochimica et Cosmochimica Acta, 64,* (13), 2295-2307. [New York, New York]: Elsevier. TIC: 250506.

160900 Haukwa, C. 2001. Unsaturated Zone Modeling & Synthesis-Intermediate UZ Modeling (YMP-LBNL-GSB-1.6.4). Scientific Notebook SN-LBNL-SCI-085-V2. ACC: MOL.20020204.0074.

106024 Helgeson, H.C.; Kirkham, D.H.; and Flowers, G.C. 1981. "Theoretical Prediction of the Thermodynamic Behavior of Aqueous Electrolytes at High Pressures and Temperatures: IV. Calculation of Activity Coefficients, Osmotic Coefficients, and Apparent Molal and Standard and Relative Partial Molal Properties to 600°C and 5 kb." *American Journal of Science, 281,* (10), 1249-1516. New Haven, Connecticut: Yale University, Kline Geology Laboratory. TIC: 238264.

145636 Kneafsey, T.J. and Pruess, K. 1998. "Laboratory Experiments on Heat-Driven Two-Phase Flows in Natural and Artificial Rock Fractures." *Water Resources Research, 34,* (12), 3349-3367. Washington, D.C.: American Geophysical Union. TIC: 247468.

154460 Kneafsey, T.J.; Apps, J.A.; and Sonnenthal, E.L. 2001. "Tuff Dissolution and Precipitation in a Boiling, Unsaturated Fracture." *"Back to the Future - Managing the Back End of the Nuclear Fuel Cycle to Create a More Secure Energy Future," Proceedings of the 9th International High-Level Radioactive Waste Management Conference (IHLRWM), Las Vegas, Nevada, April 29-May 3, 2001.* La Grange Park, Illinois: American Nuclear Society. TIC: 247873.

128132 Kulik, D.A. and Aja, S.U. 1997. "The Hydrothermal Stability of Illite: Implications of Empirical Correlations and Gibbs Energy Minimization." *Proceedings of the Fifth International Symposium on Hydrothermal Reactions, Gatlinburg, Tennessee, July 20-24, 1997.* Palmer, D.A. and Wesolowski, D.J., eds. Pages 288-292. Oak Ridge, Tennessee: Oak Ridge National Laboratory. TIC: 247217.

100051 Langmuir, D. 1997. *Aqueous Environmental Geochemistry.* Upper Saddle River, New Jersey: Prentice Hall. TIC: 237107.

117091 Lasaga, A.C. 1998. *Kinetic Theory in the Earth Sciences.* Princeton, New Jersey: Princeton University Press. TIC: 246279.

126599 Levy, S.S.; Fabryka-Martin, J.T.; Dixon, P.R.; Liu, B.; Turin, H.J.; and Wolfsberg, A.V. 1997. "Chlorine-36 Investigations of Groundwater Infiltration in the Exploratory Studies Facility at Yucca Mountain, Nevada." *Scientific Basis for Nuclear Waste Management XX, Symposium held December 2-6, 1996, Boston, Massachusetts.* Gray, W.J. and Triay, I.R., eds. *465*, 901-908. Pittsburgh, Pennsylvania: Materials Research Society. TIC: 238884.

123032 Lide, D.R., ed. 1993. *CRC Handbook of Chemistry and Physics.* 74th Edition. Boca Raton, Florida: CRC Press. TIC: 209252.

162470 Liu, H-H.; Haukwa, C.B.; Ahlers, C.F.; Bodvarsson, G.S.; Flint, A.L.; and Guertal, W.B. 2003. "Modeling Flow and Transport in Unsaturated Fractured Rock: An Evaluation of the Continuum Approach." *Journal of Contaminant Hydrology, 62-63,* 173-188. New York, New York: Elsevier. TIC: 254205.

105729 Liu, H.H.; Doughty, C.; and Bodvarsson, G.S. 1998. "An Active Fracture Model for Unsaturated Flow and Transport in Fractured Rocks." *Water Resources Research, 34,* (10), 2633-2646. Washington, D.C.: American Geophysical Union. TIC: 243012.

161130 Mercury, L. and Tardy, Y. 2001. "Negative Pressure of Stretched Liquid Water. Geochemistry of Soil Capillaries." *Geochimica et Cosmochimica Acta, 65,* (20), 3391-3408. [New York, New York]: Elsevier. TIC: 253758.

163274 NRC (U.S. Nuclear Regulatory Commission) 2003. *Yucca Mountain Review Plan, Final Report.* NUREG-1804, Rev. 2. Washington, D.C.: U.S. Nuclear Regulatory Commission, Office of Nuclear Material Safety and Safeguards. TIC: 254568.

154459 Phillips, O.M. 1994. "Liquid Infiltration Through the Boiling-Point Isotherm in a Desiccating Fractured Rock Matrix." *High Level Radioactive Waste Management, Proceedings of the Fifth Annual International Conference, Las Vegas, Nevada, May 22-26, 1994. 4,* 2189-2196. La Grange Park, Illinois: American Nuclear Society. TIC: 210984.

152005 Phillips, O.M. 1996. "Infiltration of a Liquid Finger Down a Fracture into Superheated Rock." *Water Resources Research, 32,* (6), 1665-1670. [Washington, D.C.]: American Geophysical Union. TIC: 239025.

101699 Pokrovskii, V.A. and Helgeson, H.C. 1995. "Thermodynamic Properties of Aqueous Species and the Solubilities of Minerals at High Pressures and Temperatures: The System Al2O3-H2O-NaCl." *American Journal of Science, 295,* 1255-1342. New Haven, Connecticut: Yale University, Kline Geology Laboratory. TIC: 236803.

144794 Pruess, K. 1997. "On Vaporizing Water Flow in Hot Sub-Vertical Rock Fractures." *Transport in Porous Media, 28*, (3), 335-372. Boston, Massachusetts: Kluwer Academic Publishers. TIC: 238922.

144801 Pruess, K.; Tsang, Y.W.; and Wang, J.S.Y. 1984. *Numerical Studies of Fluid and Heat Flow Near High-Level Nuclear Waste Packages Emplaced in Partially Saturated Fractured Tuff.* LBL-18552. Berkeley, California: Lawrence Berkeley Laboratory. TIC: 211033.

100818 Pruess, K.; Wang, J.S.Y.; and Tsang, Y.W. 1990. "On Thermohydrologic Conditions Near High-Level Nuclear Wastes Emplaced in Partially Saturated Fractured Tuff, 1. Simulation Studies with Explicit Consideration of Fracture Effects." *Water Resources Research, 26*, (6), 1235-1248. [Washington, D.C.]: American Geophysical Union. TIC: 221923.

117901 Reed, M.H. 1982. "Calculation of Multicomponent Chemical Equilibria and Reaction Processes in Systems Involving Minerals, Gases and an Aqueous Phase." *Geochimica et Cosmochimica Acta, 46*, (4), 513-528. New York, New York: Pergamon Press. TIC: 224159.

101709 Rimstidt, J.D. 1997. "Quartz Solubility at Low Temperatures." *Geochimica et Cosmochimica Acta, 61*, (13), 2553-2558. New York, New York: Pergamon Press. TIC: 239020.

101708 Rimstidt, J.D. and Barnes, H.L. 1980. "The Kinetics of Silica–Water Reactions." *Geochimica et Cosmochimica Acta, 44*, 1683-1699. [New York, New York]: Pergamon Press. TIC: 219975.

107109 Robie, R.A.; Hemingway, B.S.; and Fisher, J.R. 1979. *Thermodynamic Properties of Minerals and Related Substances at 298.15 K and 1 Bar (10{superscript 5} Pascals) Pressure and at Higher Temperatures.* U.S. Geological Survey Bulletin 1452. Washington, D.C.: U.S. Government Printing Office. TIC: 230505.

154862 Rosenberg, N.D.; Gdowski, G.E.; and Knauss, K.G. 2001. "Evaporative Chemical Evolution of Natural Waters at Yucca Mountain, Nevada." *Applied Geochemistry, 16*, ([9-10]), 1231-1240. [New York, New York]: Pergamon. TIC: 249879.

128146 Slider, H.C. 1976. *Practical Petroleum Reservoir Engineering Methods, An Energy Conservation Science.* Tulsa, Oklahoma: Petroleum Publishing Company. TIC: 247798.

117127 Sonnenthal, E.L. and Bodvarsson, G.S. 1999. "Constraints on the Hydrology of the Unsaturated Zone at Yucca Mountain, NV from Three-Dimensional Models of Chloride and Strontium Geochemistry." *Journal of Contaminant Hydrology, 38*, (1-3), 107-156. New York, New York: Elsevier. TIC: 244160.

160898 Spycher, N. 2001. Drift Scale Modeling (YMP-LBNL-DSM-NS-1). Scientific Notebook SN-LBNL-SCI-141-V1. ACC: MOL.20011017.0003.

101480 Steefel, C.I. and Lasaga, A.C. 1994. "A Coupled Model for Transport of Multiple Chemical Species and Kinetic Precipitation/Dissolution Reactions with Application to Reactive Flow in Single Phase Hydrothermal Systems." *American Journal of Science, 294*, (5), 529-592. New Haven, Connecticut: Yale University, Kline Geology Laboratory. TIC: 235372.

144878 Steefel, C.I. and Lichtner, P.C. 1998. "Multicomponent Reactive Transport in Discrete Fractures: I. Controls on Reaction Front Geometry." *Journal of Hydrology, 209*, 186-199. New York, New York: Elsevier. TIC: 247524.

153578 Stefánsson, A. and Arnórsson, S. 2000. "Feldspar Saturation State in Natural Waters." *Geochimica et Cosmochimica Acta, 64*, (15), 2567-2584. New York, New York: Elsevier. TIC: 249336.

137577 Tsang, Y.W. and Birkholzer, J.T. 1999. "Predictions and Observations of the Thermal-Hydrological Conditions in the Single Heater Test." *Journal of Contaminant Hydrology, 38*, (1-3), 385-425. New York, New York: Elsevier. TIC: 244160.

157427 Vaniman, D.T.; Chipera, S.J.; Bish, D.L.; Carey, J.W.; and Levy, S.S. 2001. "Quantification of Unsaturated-Zone Alteration and Cation Exchange in Zeolitized Tuffs at Yucca Mountain, Nevada, USA." *Geochimica et Cosmochimica Acta, 65*, (20), 3409-3433. [New York, New York]: Elsevier. TIC: 251574.

161665 Wang, J.S. 2003. "Scientific Notebooks Referenced in Model Report N0120/U0110, Drift-Scale Coupled Processes (DST and THC Seepage) Models MDL-NBS-HS-000001 REV 02." Interoffice correspondence from J.S. Wang (BSC) to File, June 6, 2003, with attachments. ACC: MOL.20030611.0079.

163765 Williams, N.H. 2003. "Contract No. DE-AC28-01RW1210 – Transmittal of White Paper, Effects of Neoprene on Water in the Drift Scale Test." Letter from N.H. Williams (BSC) to J.D. Ziegler (DOE/ORD), February 4, 2003, 0129035843, with enclosure. ACC: MOL.20030206.0211.

154279 Wilson, N.S.F.; Cline, J.S.; and Lundberg, S.A.W. 2000. "Paragenesis and Chemical Composition of Secondary Mineralization at Yucca Mountain, Nevada." *Abstracts with Programs - Geological Society of America, 32*, (7), A-260. Boulder, Colorado: Geological Society of America. TIC: 249113.

117170 Xu, T. and Pruess, K. 1998. *Coupled Modeling of Non-Isothermal Multi-Phase Flow, Solute Transport and Reactive Chemistry in Porous and Fractured Media: 1. Model Development and Validation.* LBNL-42050. Berkeley, California: Lawrence Berkeley National Laboratory. TIC: 243735.

156280 Xu, T. and Pruess, K. 2001. "Modeling Multiphase Non-Isothermal Fluid Flow and Reactive Geochemical Transport in Variably Saturated Fractured Rocks: 1. Methodology." *American Journal of Science, 301*, 16-33. [New Haven, Connecticut: Yale University, Kline Geology Laboratory]. TIC: 251482.

101751 Xu, T.; Pruess, K.; and Brimhall, G. 1998. *An Improved Equilibrium-Kinetics Speciation Algorithm for Redox Reactions in Variably Saturated Subsurface Flow Systems*. LBNL-41789. Berkeley, California: Lawrence Berkeley National Laboratory. TIC: 240019.

162124 Xu, T.; Sonnenthal, E.; and Bodvarsson, G. 2003. "A Reaction-Transport Model for Calcite Precipitation and Evaluation of Infiltration Fluxes in Unsaturated Fractured Rock." *Journal of Contaminant Hydrology, 64*, ([1-2]), 113-127. New York, New York: Elsevier. TIC: 254008.

161864 Xu, T.; Sonnenthal, E.; Spycher, N.; Pruess, K.; Brimhall, G.; and Apps, J. 2001. "Modeling Multiphase Non-Isothermal Fluid Flow and Reactive Geochemical Transport in Variably Saturated Fractured Rocks: 2. Applications to Supergene Copper Enrichment and Hydrothermal Flows." *American Journal of Science, 301*, (1), 34-59. New Haven, Connecticut: Yale University, Kline Geology Laboratory. TIC: 253949.

100194 Yang, I.C.; Rattray, G.W.; and Yu, P. 1996. *Interpretation of Chemical and Isotopic Data from Boreholes in the Unsaturated Zone at Yucca Mountain, Nevada*. Water-Resources Investigations Report 96-4058. Denver, Colorado: U.S. Geological Survey. ACC: MOL.19980528.0216.

Software Cited

153217 LBNL (Lawrence Berkeley National Laboratory) 08/29/1999. *Software Code: SOLVEQ/CHILLER*. V1.0. PC w/Windows OS. 10057-1.0-00.

153216 LBNL (Lawrence Berkeley National Laboratory) 09/17/1999. *Software Code: AMESH*. V1.0. DEC and SUN w/Unix OS. 10045-1.0-00.

153219 LBNL (Lawrence Berkeley National Laboratory) 09/21/1999. *Software Code: TOUGHREACT*. V2.2. DEC and SUN w/Unix OS. 10154-2.2-00.

153090 LBNL (Lawrence Berkeley National Laboratory) 09/22/2000. *Software Routine Report: assign.f*. V1.0. SUN w/Unix OS. 10315-1.0-00.

153089 LBNL (Lawrence Berkeley National Laboratory) 09/22/2000. *Software Routine Report: exclude.f*. V1.0. SUN w/Unix OS. 10316-1.0-00.

153087 LBNL (Lawrence Berkeley National Laboratory) 09/22/2000. *Software Routine Report: kswitch*. V1.0. SUN w/Unix OS. 10319-1.0-00.

153091 LBNL (Lawrence Berkeley National Laboratory) 09/22/2000. *Software Routine Report: merggrid2.f*. V1.0. SUN w/Unix OS. 10314-1.0-00.

153092 LBNL (Lawrence Berkeley National Laboratory) 09/22/2000. *Software Routine Report: mk_circ2*. V1.0. SUN w/Unix OS. 10312-1.0-00.

152883 LBNL (Lawrence Berkeley National Laboratory) 09/22/2000. *Software Routine: flipk.* V1.0. SUN w/Unix OS. 10320-1.0-00.

152902 LBNL (Lawrence Berkeley National Laboratory) 09/22/2000. *Software Routine: kreg.* V1.0. SUN w/Unix OS. 10318-1.0-00.

152901 LBNL (Lawrence Berkeley National Laboratory) 09/22/2000. *Software Routine: mk_incon.* V1.0. SUN w/Unix OS. 10350-1.0-00.

152900 LBNL (Lawrence Berkeley National Laboratory) 09/22/2000. *Software Routine: regress.* V1.0. PC w/Windows OS. 10321-1.0-00.

152899 LBNL (Lawrence Berkeley National Laboratory) 09/22/2000. *Software Routine: switch.* V1.0. PC w/Windows OS. 10322-1.0-00.

153068 LBNL (Lawrence Berkeley National Laboratory) 11/03/2000. *Software Routine Report: mk_grav2.f.* V1.0. SUN w/Unix OS. 10379-1.0-00.

153082 LBNL (Lawrence Berkeley National Laboratory) 11/03/2000. *Software Routine Report: mrgdrift.f.* V1.0. SUN w/Unix OS. 10380-1.0-00.

153083 LBNL (Lawrence Berkeley National Laboratory) 11/03/2000. *Software Routine Report: savld_dst2d.f.* V1.0. SUN w/Unix OS. 10381-1.0-00.

153218 LBNL (Lawrence Berkeley National Laboratory) 1999. *Software Code: SUPCRT92.* V1.0. PC w/Windows OS and MAC w/MAC OS. 10058-1.0-00.

153100 LBNL (Lawrence Berkeley National Laboratory) 2000. *Software Code: GSLIB.* V1.0SISIMV1.204. SUN w/Unix OS. 10397-1.0SISIMV1.204-00.

146496 LBNL (Lawrence Berkeley National Laboratory) 2000. *Software Code: TOUGH2.* V1.4. Sun Workstation and DEC/ALPHA. 10007-1.4-01.

153067 LBNL (Lawrence Berkeley National Laboratory) 2000. *Software Routine Report: 2kgridv1a.for.* V1.0. PC w/Windows OS. 10382-1.0-00.

153085 LBNL (Lawrence Berkeley National Laboratory) 2000. *Software Routine Report: avgperm.f.* V1.0. DEC & SUN w/UNIX OS. 10378-1.0-00.

153093 LBNL (Lawrence Berkeley National Laboratory) 2000. *Software Routine: mk_rect2.* V1.0. SUN w/Unix OS. 10313-1.0-00.

153101 LBNL (Lawrence Berkeley National Laboratory) 2001. *Software Code: TOUGHREACT.* V2.3. SUN and DEC w/Unix OS. 10396-2.3-00.

160880 LBNL (Lawrence Berkeley National Laboratory) 2001. *Software Code: TOUGHREACT.* V2.4. SunOS 5.5.1, Dec Alpha TRU64 Unix & OS1 V4.0. 10396-2.4-00.

161127 LBNL (Lawrence Berkeley National Laboratory) 2002. *Software Code: CUTCHEM.* V1.0. DEC ALPHA/OSF1 V5.1, PC /WINDOWS 2000/NT 4.0/98. 10898-1.0-00.

161263 LBNL (Lawrence Berkeley National Laboratory) 2002. *Software Code: DBCONV.* V1.0. PC/Windows 98/NT; DEC-Alpha/OSF1 V5.1; SunOS 5.5.1. 10893-1.0-00.

161258 LBNL (Lawrence Berkeley National Laboratory) 2002. *Software Code: KREG.* V1.1. SUN UltraSparc with Unix SunOS 5.5.1, WINDOWS 2000/NT/98, Dec Alpha with OSF1 V5.1. 10318-1.1-00.

161259 LBNL (Lawrence Berkeley National Laboratory) 2002. *Software Code: KSWITCH.* V1.1. PC with WINDOWS 2000/NT/98, Dec Alpha with OSF1 V5.1, SUN OS 5.5.1. 10319-1.1-00.

161262 LBNL (Lawrence Berkeley National Laboratory) 2002. *Software Code: THERMOCHK.* V1.1. PC/Windows 98/NT/2000; DEC-Alpha/OSF1 V5.1; SunOS 5.5.1. 10895-1.1-00.

161256 LBNL (Lawrence Berkeley National Laboratory) 2002. *Software Code: TOUGHREACT.* V3.0. DEC-Alpha with Unix OSF1 V5.1 and OSF1 V5.0, Sun Solaris 5.5.1, Linux Redhat 7.2. 10396-3.0-00.

161491 LBNL (Lawrence Berkeley National Laboratory) 2003. *Software Code: TOUGH2.* V1.6. PC/MS-DOS under Windows 98, Sun UltraSparc OS 5.5.1, DEC-Alpha OSF1 V4.0. 10007-1.6-01.

9.2 CODES, STANDARDS, REGULATIONS, AND PROCEDURES

156605 10 CFR 63. Energy: Disposal of High-Level Radioactive Wastes in a Geologic Repository at Yucca Mountain, Nevada. Readily available.

AP-2.22Q, Rev. 0, ICN 1. *Classification Criteria and Maintenance of the Monitored Geologic Repository Q-List.* Washington, D.C.: U.S. Department of Energy, Office of Civilian Radioactive Waste Management. ACC: DOC.20030422.0009.

AP-SI.1Q, Rev. 5, ICN 1. *Software Management.* Washington, D.C.: U.S. Department of Energy, Office of Civilian Radioactive Waste Management. ACC: DOC.20030708.0001.

AP-SIII.3Q, Rev. 1, ICN 2. *Submittal and Incorporation of Data to the Technical Data Management System.* Washington, D.C.: U.S. Department of Energy, Office of Civilian Radioactive Waste Management. ACC: MOL.20020701.0177.

AP-SIII.10Q, Rev. 1, ICN 2. *Models.* Washington, D.C.: U.S. Department of Energy, Office of Civilian Radioactive Waste Management. ACC: DOC.20030627.0003.

AP-SV.1Q, Rev. 0, ICN 3. *Control of the Electronic Management of Information.* Washington, D.C.: U.S. Department of Energy, Office of Civilian Radioactive Waste Management. ACC: MOL.20020917.0133.

YMP-LBNL-QIP-6.1 Rev. 8, Mod. 1. *Document Review*. Berkeley, California: Lawrence Berkeley National Laboratory. ACC: MOL.20030724.0162.

YMP-LBNL-QIP-SV.0, Rev. 2, Mod. 1. *Management of YMP-LBNL Electronic Data*. Berkeley, California: Lawrence Berkeley National Laboratory. ACC: MOL.20020717.0319.

9.3 SOURCE DATA, LISTED BY DATA TRACKING NUMBER

160899 GS020408312272.003. Collection and Analysis of Pore Water Samples for the Period from April 2001 to February 2002. Submittal date: 04/24/2002.

153485 LA0009SL831151.001. Fracture Mineralogy of the ESF Single Heater Test Block, Alcove 5. Submittal date: 09/28/2000.

158426 LA0201SL831225.001. Chemical, Textural, and Mineralogical Characteristics of Sidewall Samples from the Drift Scale Test. Submittal date: 01/10/2002.

113495 LA9908JC831321.001. Mineralogic Model "MM3.0" Version 3.0. Submittal date: 08/16/1999.

146447 LA9912SL831151.001. Fracture Mineralogy of Drill Core ESF-HD-TEMP-2. Submittal date: 01/05/2000.

146449 LA9912SL831151.002. Percent Coverage by Fracture-Coating Minerals in Core ESF-HD-TEMP-2. Submittal date: 01/05/2000.

146451 LB000121123142.003. Isotope Data for CO2 Gas Samples Collected From the Hydrology Holes of the ESF Drift Scale Test for the Period August 9, 1999 through November 30, 1999. Submittal date: 01/21/2000.

153460 LB0011CO2DST08.001. Isotope Data for CO2 from Gas Samples Collected from Hydrology Holes in Drift-Scale Test. Submittal date: 12/09/2000.

153470 LB0011DSTFRAC1.001. Drift-Scale Properties Update: 1. Updated Drift-Scale Properties. This is Input Data for AMR U0110 (MDL-NBS-HS-000001 REV01). Submittal date: 12/06/2000.

154759 LB0011DSTTHCR1.001. Tables Showing Geochemical and Drift-Scale Seepage Model Data Which are Presented in AMR U0110/N0120, "Drift-Scale Coupled Processes (DST and THC Seepage) Models REV01". Submittal date: 12/19/2000.

161282 LB0011DSTTHCR1.002. Model Input and Output Files, Excel Spreadsheets and Resultant Figures which are Presented in AMR U0110/N0120, "Drift-Scale Coupled Processes (DST and THC Seepage) Models REV 01". Submittal date: 12/19/2000.

153381 LB0011THCDISSM.001. Comparison Modeling for TPTPMN Tuff Dissolution Experiment: 1. Input Data for AMR U0110 REV01. Submittal date: 12/07/2000.

154578 LB0011THCDISSM.002. Comparison Modeling for TPTPMN Tuff Dissolution Experiment: 2. Output Data for AMR U0110 REV01. Submittal date: 12/07/2000.

153380 LB0011THCDISSX.001. Summary of Results from TPTPMN Tuff Dissolution Experiment. Submittal date: 12/07/2000.

161277 LB0101DSTTHCR1.002. Attachment II - Mineral Initial Volume Fractions for TPTPLL THC Model for AMR N0120/U0110 REV01, "Drift-Scale Coupled Processes (Drift-Scale Test and THC Seepage) Models.". Submittal date: 01/26/2001.

161278 LB0101DSTTHCR1.003. Attachment III - Mineral Reactive Surface Areas: TPTPMN and DST THC Models for AMR N0120/U0110 REV01, "Drift-Scale Coupled Processes (Drift-Scale Test and THC Seepage) Models.". Submittal date: 01/26/2001.

161279 LB0101DSTTHCR1.004. Attachment IV - Mineral Reactive Surface Areas: TPTPLL THC Model for AMR N0120/U0110 REV01, "Drift-Scale Coupled Processes (Drift-Scale Test and THC Seepage) Models.". Submittal date: 01/26/2001.

161676 LB0101DSTTHCR1.005. Attachment V-Thermodynamic Database: TPTPMN THC Backfill and DST THC REV00 Models, for AMR N0120/U0110 REV01 "Drift-Scale Coupled Processes (Drift-Scale Test and THC Seepage) Models.". Submittal date: 01/26/2001.

161280 LB0101DSTTHCR1.006. Attachment VI - Thermodynamic Database: TPTPMN THC (No Backfill) and DST THC REV01 Models for AMR N0120/U0110 REV01, "Drift-Scale Coupled Processes (Drift-Scale Test and THC Seepage) Models.". Submittal date: 01/26/2001.

161281 LB0101DSTTHCR1.007. Attachment VIII - Waste Package Average Heat Transfer: TPTPMN/TPTPLL No-Backfill and THC Models for AMR N0120/U0110 REV01, "Drift-Scale Coupled Processes (Drift-Scale Test and THC Seepage) Models.". Submittal date: 01/26/2001.

153687 LB0101DSTTHGRD.001. 2D Finite Element Mesh Used for DST THC Model Simulations (Input to AMR N0120/U0110 REV. 01). Submittal date: 01/05/2001.

154577 LB0101THCPRCPX.001. Summary of Results from TPTPMN Tuff Precipitation Experiment. Submittal date: 02/13/2001.

159306 LB0102CO2DST98.001. Concentration Data for CO2 from Gas Samples Collected from Hydrology Holes in Drift-scale Test. Submittal date: 02/28/2001.

159525 LB0205REVUZPRP.001. Fracture Properties for UZ Model Layers Developed from Field Data. Submittal date: 05/14/2002.

159672 LB0207REVUZPRP.002. Matrix Properties for UZ Model Layers Developed from Field and Laboratory Data. Submittal date: 07/15/2002.

161638 LB0208ISODSTHP.001. Isotope Data and CO2 Analysis for the Heating Phase of the DST. Submittal date: 08/09/2002.

161243 LB0208UZDSCPMI.002. Drift-Scale Calibrated Property Sets: Mean Infiltration Data Summary. Submittal date: 08/26/2002.

160799 LB0210THRMLPRP.001. Thermal Properties of UZ Model Layers: Data Summary. Submittal date: 10/25/2002.

164433 LB0307KNTDBRTM.001. Kinetic Database for Reactive Transport Modeling. Submittal date: 07/22/2003.

164434 LB0307THMDBRTM.001. Thermodynamic Database for Reactive Transport Modeling. Submittal date: 07/22/2003.

111475 LB990501233129.004. 3-D UZ Model Calibration Grids for AMR U0000, "Development of Numerical Grids of UZ Flow and Transport Modeling". Submittal date: 09/24/1999.

105888 LB990601233124.001. Seepage Data Feed to UZ Drift-Scale Flow Model for TSPA-SR. Submittal date: 06/18/1999.

111476 LB990630123142.003. Fourth, Fifth, and Sixth Quarters TDIF Submission for the Drift Scale Test, September 1998 to May 1999. Submittal date: 06/30/1999.

125604 LB990701233129.002. 3-D Model Calibration Grid for Calculation of Flow Fields Using #3 Perched Water Conceptual Model (Non-Perched Water Model) for AMR U0050, "UZ Flow Models and Submodels". Submittal date: 03/11/2000.

110226 LB990861233129.001. Drift Scale Calibrated 1-D Property Set, FY99. Submittal date: 08/06/1999.

125868 LB991091233129.001. One-Dimensional, Mountain-Scale Calibration for AMR U0035, "Calibrated Properties Model". Submittal date: 10/22/1999.

111480 LB991091233129.006. Thermal Properties and Tortuosity Factor for the UZ Model Layers for AMR U0090, "Analysis of Hydrologic Properties Data". Submittal date: 10/15/1999.

142162 LB991200DSTTHC.002. Model Input and Output Files, Excel Spreadsheets and Resultant Figures Which are Presented in AMR N0120/U0110, "Drift-Scale Coupled Processes (Drift-Scale Test and THC Seepage) Models". Submittal date: 03/11/2000.

161276 LB991200DSTTHC.003. Mineral Initial Volume Fractions: Attachment II of AMR N0120/U0110, "Drift-Scale Coupled Processes (Drift-Scale Test and THC Seepage) Models.". Submittal date: 03/11/2000.

104055 LB997141233129.001. Calibrated Basecase Infiltration 1-D Parameter Set for the UZ Flow and Transport Model, FY99. Submittal date: 07/21/1999.

142884 LL000114004242.090. TSPA-SR Mean Calculations. Submittal date: 01/28/2000.

153288 LL001100931031.008. Aqueous Chemistry of Water Sampled from Boreholes of the Drift Scale Test (DST). Submittal date: 11/10/2000.

153616 LL001200231031.009. Aqueous Chemistry of Water Sampled from Boreholes of the Drift Scale Test (DST). Submittal date: 12/04/2000.

159134 LL020302223142.015. Aqueous Geochemistry of DST Samples Collected from HYD Boreholes. Submittal date: 03/07/2002.

159307 LL020405123142.019. Aqueous Geochemistry of Condensed Fluids Collected During Studies of Introduced Materials. Submittal date: 05/22/2002.

161677 LL020709923142.023. Aqueous Geochemistry of Borehole Waters Collected in the Heating Phase of the DST. Submittal date: 07/26/2002.

144922 LL990702804244.100. Borehole and Pore Water Data. Submittal date: 07/13/1999.

153836 MO0001SEPDSTPC.000. Drift Scale Test (DST) Temperature, Power, Current, and Voltage Data for June 1, 1999 through October 31, 1999. Submittal date: 01/12/2000.

147304 MO0002ABBLSLDS.000. As-Built Borehole Locations and Sensor Locations for the Drift Scale Test Given in Local (DST) Coordinates. Submittal date: 02/01/2000.

150930 MO0005PORWATER.000. Perm-Sample Pore Water Data. Submittal date: 05/04/2000.

153707 MO0007SEPDSTPC.001. Drift Scale Test (DST) Temperature, Power, Current, and Voltage Data for November 1, 1999 through May 31, 2000. Submittal date: 07/13/2000.

153708 MO0012SEPDSTPC.002. Drift Scale Test (DST) Temperature, Power, Current, and Voltage Data for June 1, 2000 through November 30, 2000. Submittal date: 12/19/2000.

153711 MO0101SEPFDDST.000. Field Measured Data of Water Samples from the Drift Scale Test. Submittal date: 01/03/2001.

158321 MO0107SEPDSTPC.003. Drift Scale Test (DST) Temperature, Power, Current, and Voltage Data for December 1, 2000 through May 31, 2001. Submittal date: 07/06/2001.

158320 MO0202SEPDSTTV.001. Drift Scale Test (DST) Temperature, Power, Current, and Voltage Data for June 1, 2001 through January 14, 2002. Submittal date: 02/28/2002.

158910 MO0204SPATHDYN.000. Thermodynamic Data Input Files for Geochemical Calculations. Submittal date: 04/01/2002.

159300 MO0207AL5WATER.001. Water Sampling in Alcove 5 (Results from 2/4/1997 through 4/20/1999). Submittal date: 07/11/2002.

161129 MO0208RESTRDST.002. Restructured Drift Scale Test (DST) Heating Phase Power and Temperature Data. Submittal date: 08/06/2002.

161496 MO0301SEPFEPS1.000. LA FEP List. Submittal date: 01/21/2003.

161756 MO0302SPATHDYN.000. Thermodynamic Data Input Files - Data0.YMP.R2. Submittal date: 02/05/2003.

113644 MO9807DSTSET01.000. Drift Scale Test (DST) Temperature, Power, Current, Voltage Data for November 7, 1997 through May 31, 1998. Submittal date: 07/09/1998.

113662 MO9810DSTSET02.000. Drift Scale Test (DST) Temperature, Power, Current, Voltage Data for June 1 through August 31, 1998. Submittal date: 10/09/1998.

113673 MO9906DSTSET03.000. Drift Scale Test (DST) Temperature, Power, Current, and Voltage Data for September 1, 1998 through May 31, 1999. Submittal date: 06/08/1999.

153364 SN0002T0872799.009. Effective Thermal Conductivity Parameter for the No Backfill Case Implemented in the Drift-Scale Models used in TSPA-SR. Submittal date: 02/10/2000.

159133 SN0203F3903102.001. Drift Scale Test Water Sampling (with Results from 4/17/2001 through 1/14/2002). Submittal date: 03/29/2002.

111485 SN9907T0872799.001. Heat Decay Data and Repository Footprint for Thermal-Hydrologic and Conduction-Only Models for TSPA-SR (Total System Performance Assessment-Site Recommendation). Submittal date: 07/27/1999.

9.4 OUTPUT DATA, LISTED BY DATA TRACKING NUMBER

LB0301FRACSEAL.001. Comparison Modeling for Tptpmn Tuff Fracture Sealing Experiment: Supporting Files. Submittal date: 01/27/2003.

LB0301FRACSEAL.002. Comparison Modeling for Tptpmn Tuff Fracture Sealing Experiment: Data Summary. Submittal date: 01/27/2003.

LB0301PLUGFLOW.001. Comparison Modeling for Tptpmn Tuff Dissolution Experiment: Data Summary Files. Submittal date: 01/13/2003.

LB0302DSCPTHCS.001. Drift-Scale Coupled Processes (THC Seepage) Model: Simulations. Submittal date: 02/11/2003.

LB0302DSCPTHCS.002. Drift-Scale Coupled Processes (THC Seepage) Model: Data Summary. Submittal date: 02/11/2003.

LB0307DSTTHCR2.001. Drift-Scale Coupled Processes (DST Seepage) Model: Simulations. Submittal date: 07/24/2003.

LB0307DSTTHCR2.002. Drift-Scale Coupled Processes (DST Seepage) Model: Data Summary. Submittal date: 07/24/2003.

INTENTIONALLY LEFT BLANK

ATTACHMENT I – MINERAL INITIAL VOLUME FRACTIONS: Tptpmn THC Model REV01, Tptpmn THC Heterogeneous Model REV01 and DST THC Model REV01

(DTN: LB991200DSTTHC.003 [161276])

Unit	Rock Name	Zone	K-feldspar	Albite	Anorthite	Ca-Smectite	Na-Smectite	Mg-Smectite	K-Smectite	Illite	Tridymite
Tcw3	tcwm3	1	0.0946	0.0699	0.0024	0.0407	0.0175	0.0407	0.0175	0.0129	0.0000
	tcwf3	2	0.0946	0.0699	0.0024	0.0407	0.0175	0.0407	0.0175	0.0129	0.0000
Ptn1	ptnm1	3	0.0377	0.0279	0.0009	0.0643	0.0276	0.0643	0.0276	0.0204	0.0000
	ptnf1	4	0.0377	0.0279	0.0009	0.0643	0.0276	0.0643	0.0276	0.0204	0.0000
Ptn2	ptnm2	5	0.0449	0.0332	0.0011	0.0568	0.0244	0.0568	0.0244	0.0180	0.0000
	ptnf2	6	0.0449	0.0332	0.0011	0.0568	0.0244	0.0568	0.0244	0.0180	0.0000
Ptn3	ptnm3	7	0.0156	0.0116	0.0004	0.0095	0.0041	0.0095	0.0041	0.0030	0.0000
	ptnf3	8	0.0156	0.0116	0.0004	0.0095	0.0041	0.0095	0.0041	0.0030	0.0000
Ptn4	ptnm4	9	0.0806	0.0595	0.0020	0.0209	0.0090	0.0209	0.0090	0.0066	0.0000
	ptnf4	10	0.0806	0.0595	0.0020	0.0209	0.0090	0.0209	0.0090	0.0066	0.0000
Ptn5	ptnm5	11	0.0965	0.0712	0.0024	0.0090	0.0039	0.0090	0.0039	0.0029	0.0000
	ptnf5	12	0.0965	0.0712	0.0024	0.0090	0.0039	0.0090	0.0039	0.0029	0.0000
Ptn6	ptnm6	13	0.0855	0.0631	0.0021	0.0329	0.0141	0.0329	0.0141	0.0104	0.0000
	ptnf6	14	0.0855	0.0631	0.0021	0.0329	0.0141	0.0329	0.0141	0.0104	0.0000
Tsw31	tswm1	15	0.2358	0.1741	0.0059	0.0001	0.0001	0.0001	0.0001	0.0000	0.0000
	tswf1	16	0.2358	0.1741	0.0059	0.0001	0.0001	0.0001	0.0001	0.0000	0.0000
Tsw32	tswm2	17	0.4025	0.2973	0.0100	0.0027	0.0012	0.0027	0.0012	0.0009	0.0919
	tswf2	18	0.2435	0.1798	0.0061	0.0174	0.0074	0.0174	0.0074	0.0055	0.0556
Tsw33	tswm3	19	0.3051	0.2253	0.0076	0.0131	0.0056	0.0131	0.0056	0.0042	0.1071
	tswf3	20	0.1846	0.1363	0.0046	0.0237	0.0102	0.0237	0.0102	0.0075	0.0648
Tsw34	tswm4	21	0.3096	0.2286	0.0077	0.0081	0.0035	0.0081	0.0035	0.0026	0.0489
	tswf4	22	0.1873	0.1383	0.0047	0.0207	0.0089	0.0207	0.0089	0.0066	0.0296
Tsw35	tswm5	23	0.3051	0.2253	0.0076	0.0082	0.0035	0.0082	0.0035	0.0026	0.0597
	tswf5	24	0.1846	0.1363	0.0046	0.0207	0.0089	0.0207	0.0089	0.0066	0.0361
Tsw36	tswm6	25	0.3094	0.2285	0.0077	0.0074	0.0032	0.0074	0.0032	0.0024	0.0137
	tswf6	26	0.1872	0.1382	0.0047	0.0202	0.0087	0.0202	0.0087	0.0064	0.0083
Tsw37	tswm7	27	0.3057	0.2257	0.0076	0.0079	0.0034	0.0079	0.0034	0.0025	0.0077
	tswf7	28	0.1849	0.1366	0.0046	0.0205	0.0088	0.0205	0.0088	0.0065	0.0047
Tsw38	tswm8	29	0.0878	0.0648	0.0022	0.0180	0.0077	0.0180	0.0077	0.0057	0.0054
	tswf8	30	0.0878	0.0648	0.0022	0.0180	0.0077	0.0180	0.0077	0.0057	0.0054
Ch2	ch2mz	31	0.0370	0.0273	0.0009	0.0060	0.0026	0.0060	0.0026	0.0019	0.0000
	ch2fz	32	0.0370	0.0273	0.0009	0.0060	0.0026	0.0060	0.0026	0.0019	0.0000

Unit	Rock Name	Zone	Cristobalite	Quartz	Glass	Hematite	Calcite	Stellerite	Heulandite	Mordenite	Clinoptilolite
Tcw3	tcwm3	1	0.1323	0.0037	0.4580	0.0000	0.0000	0.0000	0.0329	0.0110	0.0659
	tcwf3	2	0.1323	0.0037	0.4580	0.0000	0.0000	0.0000	0.0329	0.0110	0.0659
Ptn1	ptnm1	3	0.0000	0.0009	0.7283	0.0000	0.0000	0.0000	0.0000	0.0000	0.0000
	ptnf1	4	0.0000	0.0009	0.7283	0.0000	0.0000	0.0000	0.0000	0.0000	0.0000
Ptn2	ptnm2	5	0.0350	0.0157	0.6895	0.0002	0.0000	0.0000	0.0000	0.0000	0.0000
	ptnf2	6	0.0350	0.0157	0.6895	0.0002	0.0000	0.0000	0.0000	0.0000	0.0000
Ptn3	ptnm3	7	0.0763	0.0009	0.8652	0.0000	0.0000	0.0000	0.0000	0.0000	0.0000
	ptnf3	8	0.0763	0.0009	0.8652	0.0000	0.0000	0.0000	0.0000	0.0000	0.0000
Ptn4	ptnm4	9	0.0524	0.0139	0.7254	0.0000	0.0000	0.0000	0.0000	0.0000	0.0000
	ptnf4	10	0.0524	0.0139	0.7254	0.0000	0.0000	0.0000	0.0000	0.0000	0.0000
Ptn5	ptnm5	11	0.0214	0.0094	0.7679	0.0024	0.0000	0.0000	0.0000	0.0000	0.0000
	ptnf5	12	0.0214	0.0094	0.7679	0.0024	0.0000	0.0000	0.0000	0.0000	0.0000
Ptn6	ptnm6	13	0.0083	0.0142	0.7129	0.0024	0.0070	0.0000	0.0000	0.0000	0.0000
	ptnf6	14	0.0083	0.0142	0.7129	0.0024	0.0070	0.0000	0.0000	0.0000	0.0000
Tsw31	tswm1	15	0.0915	0.0047	0.4550	0.0050	0.0276	0.0000	0.0000	0.0000	0.0000
	tswf1	16	0.0915	0.0047	0.4550	0.0050	0.0276	0.0000	0.0000	0.0000	0.0000
Tsw32	tswm2	17	0.1516	0.0079	0.0152	0.0044	0.0095	0.0011	0.0000	0.0001	0.0000
	tswf2	18	0.0917	0.0048	0.0092	0.0027	0.0257	0.3257	0.0000	0.0001	0.0000
Tsw33	tswm3	19	0.2336	0.0760	0.0000	0.0036	0.0000	0.0000	0.0000	0.0000	0.0000
	tswf3	20	0.1413	0.0460	0.0000	0.0022	0.0200	0.3250	0.0000	0.0000	0.0000
Tsw34	tswm4	21	0.2588	0.1202	0.0000	0.0004	0.0000	0.0000	0.0000	0.0000	0.0000
	tswf4	22	0.1566	0.0727	0.0000	0.0002	0.0200	0.3250	0.0000	0.0000	0.0000
Tsw35	tswm5	23	0.1660	0.2037	0.0000	0.0017	0.0050	0.0000	0.0000	0.0000	0.0000
	tswf5	24	0.1004	0.1232	0.0000	0.0010	0.0230	0.3250	0.0000	0.0000	0.0000
Tsw36	tswm6	25	0.1509	0.2643	0.0000	0.0020	0.0000	0.0000	0.0000	0.0000	0.0000
	tswf6	26	0.0913	0.1599	0.0000	0.0012	0.0200	0.3250	0.0000	0.0000	0.0000
Tsw37	tswm7	27	0.2273	0.2004	0.0000	0.0005	0.0000	0.0000	0.0000	0.0000	0.0000
	tswf7	28	0.1375	0.1212	0.0000	0.0003	0.0200	0.3250	0.0000	0.0000	0.0000
Tsw38	tswm8	29	0.1557	0.0244	0.5629	0.0000	0.0000	0.0000	0.0119	0.0040	0.0238
	tswf8	30	0.1557	0.0244	0.5629	0.0000	0.0000	0.0000	0.0119	0.0040	0.0238
Ch2	ch2mz	31	0.1609	0.0326	0.0000	0.0000	0.0000	0.0000	0.2166	0.0722	0.4333
	ch2fz	32	0.1609	0.0326	0.0000	0.0000	0.0000	0.0000	0.2166	0.0722	0.4333

ATTACHMENT II – MINERAL INITIAL VOLUME FRACTIONS: Tptpll THC Models (REV01 and REV02) and DST THC Model REV02

(DTN: LB0101DSTTHCR1.002 [161277])

Rock	Zone	K-Feldspar	Albite	Anorthite	Ca-Smectite	Na-Smectite	Mg-Smectite	Illite	Tridymite	Cristobalite	Quartz
tcwm1	1	0.36911	0.27257	0.00917	0.00198	0.00085	0.00198	0.00148	0.10285	0.21294	0.00942
tcwf1	2	0.36911	0.27257	0.00917	0.00198	0.00085	0.00198	0.00148	0.10285	0.21294	0.00942
tcwm2	3	0.36911	0.27257	0.00917	0.00198	0.00085	0.00198	0.00148	0.10285	0.21294	0.00942
tcwf2	4	0.36911	0.27257	0.00917	0.00198	0.00085	0.00198	0.00148	0.10285	0.21294	0.00942
tcwm3	5	0.16239	0.11992	0.00403	0.04403	0.01887	0.04403	0.03284	0.00000	0.12577	0.00744
tcwf3	6	0.16239	0.11992	0.00403	0.04403	0.01887	0.04403	0.03284	0.00000	0.12577	0.00744
ptnm1	7	0.05149	0.03802	0.00128	0.02441	0.01046	0.02441	0.01821	0.00015	0.01460	0.00702
ptnf1	8	0.05149	0.03802	0.00128	0.02441	0.01046	0.02441	0.01821	0.00015	0.01460	0.00702
ptnm2	9	0.05148	0.03802	0.00128	0.02441	0.01046	0.02441	0.01821	0.00015	0.01460	0.00702
ptnf2	10	0.05148	0.03802	0.00128	0.02441	0.01046	0.02441	0.01821	0.00015	0.01460	0.00702
ptnm3	11	0.05149	0.03802	0.00128	0.02441	0.01046	0.02441	0.01821	0.00015	0.01460	0.00702
ptnf3	12	0.05149	0.03802	0.00128	0.02441	0.01046	0.02441	0.01821	0.00015	0.01460	0.00702
ptnm4	13	0.05149	0.03802	0.00128	0.02441	0.01046	0.02441	0.01821	0.00015	0.01460	0.00702
ptnf4	14	0.05149	0.03802	0.00128	0.02441	0.01046	0.02441	0.01821	0.00015	0.01460	0.00702
ptnm5	15	0.05136	0.03793	0.00128	0.02435	0.01044	0.02435	0.01817	0.00015	0.01460	0.00702
ptnf5	16	0.05136	0.03793	0.00128	0.02435	0.01044	0.02435	0.01817	0.00015	0.01460	0.00702
ptnm6	17	0.05137	0.03794	0.00128	0.02436	0.01044	0.02436	0.01817	0.00015	0.01457	0.00701
ptnf6	18	0.05137	0.03794	0.00128	0.02436	0.01044	0.02436	0.01817	0.00015	0.01457	0.00701
tswm1	19	0.10362	0.07652	0.00257	0.00213	0.00091	0.00213	0.00159	0.00112	0.01999	0.00118
tswf1	20	0.10362	0.07652	0.00257	0.00213	0.00091	0.00213	0.00159	0.00112	0.01999	0.00118
tswm2	21	0.38312	0.28291	0.00952	0.00343	0.00147	0.00343	0.00256	0.15942	0.13313	0.00473
tswf2	22	0.23179	0.17116	0.00576	0.01767	0.00757	0.01767	0.01318	0.09645	0.08054	0.00286
tswm3	23	0.36306	0.26810	0.00902	0.00777	0.00333	0.00777	0.00580	0.05630	0.23767	0.02695
tswf3	24	0.21965	0.16220	0.00546	0.02029	0.00870	0.02029	0.01514	0.03406	0.14379	0.01630
tswm4	25	0.32265	0.23826	0.00802	0.00517	0.00221	0.00517	0.00385	0.02310	0.35588	0.02526
tswf4	26	0.19520	0.14415	0.00485	0.01872	0.00802	0.01872	0.01396	0.01397	0.21530	0.01529
tswm5	27	0.34968	0.25822	0.00869	0.00686	0.00294	0.00686	0.00512	0.02321	0.18589	0.14046
tswf5	28	0.21155	0.15622	0.00526	0.01974	0.00846	0.01974	0.01473	0.01404	0.11247	0.08498
tswm6	29	0.36268	0.26782	0.00901	0.00327	0.00140	0.00327	0.00244	0.00195	0.16651	0.16845
tswf6	30	0.21942	0.16203	0.00545	0.01757	0.00753	0.01757	0.01311	0.00118	0.10074	0.10191
tswm7	31	0.36322	0.26822	0.00902	0.00328	0.00140	0.00328	0.00244	0.00195	0.16676	0.16870
tswf7	32	0.21975	0.16227	0.00546	0.01758	0.00753	0.01758	0.01311	0.00118	0.10089	0.10206
tswm8	33	0.11030	0.08145	0.00274	0.04279	0.01834	0.04279	0.03192	0.00000	0.09981	0.00790
tswf8	34	0.11030	0.08145	0.00274	0.04279	0.01834	0.04279	0.03192	0.00000	0.09981	0.00790
tswm9	35	0.06105	0.04508	0.00152	0.02739	0.01174	0.02739	0.02044	0.00000	0.06216	0.01481
tswf9	36	0.06105	0.04508	0.00152	0.02739	0.01174	0.02739	0.02044	0.00000	0.06216	0.01481
ch1mv	37	0.07829	0.05781	0.00195	0.00747	0.00320	0.00747	0.00557	0.00586	0.06920	0.03831
ch1fv	38	0.07829	0.05781	0.00195	0.00747	0.00320	0.00747	0.00557	0.00586	0.06920	0.03831

Rock	Zone	Glass	Hematite	Calcite	Stellerite	Heulandite	Mordenite	Clinoptilolite	Kaolinite	Am. Silica	Opal	Fluorite
tcwm1	1	0.00139	0.00000	0.00358	0.00000	0.00083	0.00028	0.00167	0.00000	0.00000	0.00990	0.00000
tcwf1	2	0.00139	0.00000	0.00358	0.00000	0.00083	0.00028	0.00167	0.00000	0.00000	0.00990	0.00000
tcwm2	3	0.00139	0.00000	0.00358	0.00000	0.00083	0.00028	0.00167	0.00000	0.00000	0.00990	0.00000
tcwf2	4	0.00139	0.00000	0.00358	0.00000	0.00083	0.00028	0.00167	0.00000	0.00000	0.00990	0.00000
tcwm3	5	0.43046	0.00000	0.00032	0.00000	0.00000	0.00000	0.00000	0.00000	0.00000	0.00990	0.00000
tcwf3	6	0.43046	0.00000	0.00032	0.00000	0.00000	0.00000	0.00000	0.00000	0.00000	0.00990	0.00000
ptnm1	7	0.78888	0.00000	0.01086	0.00000	0.00008	0.00003	0.00017	0.00000	0.00000	0.00990	0.00000
ptnf1	8	0.78888	0.00000	0.01086	0.00000	0.00008	0.00003	0.00017	0.00000	0.00000	0.00990	0.00000
ptnm2	9	0.78876	0.00015	0.01086	0.00000	0.00008	0.00003	0.00017	0.00000	0.00000	0.00990	0.00000
ptnf2	10	0.78876	0.00015	0.01086	0.00000	0.00008	0.00003	0.00017	0.00000	0.00000	0.00990	0.00000
ptnm3	11	0.78888	0.00000	0.01086	0.00000	0.00008	0.00003	0.00017	0.00000	0.00000	0.00990	0.00000
ptnf3	12	0.78888	0.00000	0.01086	0.00000	0.00008	0.00003	0.00017	0.00000	0.00000	0.00990	0.00000
ptnm4	13	0.78888	0.00000	0.01086	0.00000	0.00008	0.00003	0.00017	0.00000	0.00000	0.00990	0.00000
ptnf4	14	0.78888	0.00000	0.01086	0.00000	0.00008	0.00003	0.00017	0.00000	0.00000	0.00990	0.00000
ptnm5	15	0.78694	0.00239	0.01083	0.00000	0.00008	0.00003	0.00017	0.00000	0.00000	0.00990	0.00000
ptnf5	16	0.78694	0.00239	0.01083	0.00000	0.00008	0.00003	0.00017	0.00000	0.00000	0.00990	0.00000
ptnm6	17	0.78707	0.00228	0.01084	0.00000	0.00008	0.00003	0.00017	0.00000	0.00000	0.00990	0.00000
ptnf6	18	0.78707	0.00228	0.01084	0.00000	0.00008	0.00003	0.00017	0.00000	0.00000	0.00990	0.00000
tswm1	19	0.75630	0.00485	0.01693	0.00000	0.00005	0.00002	0.00009	0.00000	0.00000	0.00990	0.00010
tswf1	20	0.75630	0.00485	0.01693	0.00000	0.00005	0.00002	0.00009	0.00000	0.00000	0.00990	0.00010
tswm2	21	0.00070	0.00439	0.00110	0.00010	0.00000	0.00001	0.00000	0.00000	0.00000	0.00990	0.00010
tswf2	22	0.00042	0.00265	0.02046	0.32181	0.00000	0.00001	0.00000	0.00000	0.00000	0.00990	0.00010
tswm3	23	0.00000	0.00353	0.00067	0.00000	0.00001	0.00000	0.00003	0.00000	0.00000	0.00990	0.00010
tswf3	24	0.00000	0.00214	0.02020	0.32175	0.00001	0.00000	0.00002	0.00000	0.00000	0.00990	0.00010
tswm4	25	0.00000	0.00036	0.00007	0.00000	0.00000	0.00000	0.00000	0.00000	0.00000	0.00990	0.00010
tswf4	26	0.00000	0.00022	0.01984	0.32175	0.00000	0.00000	0.00000	0.00000	0.00000	0.00990	0.00010
tswm5	27	0.00000	0.00162	0.00038	0.00000	0.00002	0.00001	0.00005	0.00000	0.00000	0.00990	0.00010
tswf5	28	0.00000	0.00098	0.02003	0.32175	0.00001	0.00000	0.00003	0.00000	0.00000	0.00990	0.00010
tswm6	29	0.00000	0.00194	0.00007	0.00000	0.00035	0.00012	0.00071	0.00000	0.00000	0.00990	0.00010
tswf6	30	0.00000	0.00118	0.01984	0.32175	0.00021	0.00007	0.00043	0.00000	0.00000	0.00990	0.00010
tswm7	31	0.00000	0.00049	0.00007	0.00000	0.00035	0.00012	0.00071	0.00000	0.00000	0.00990	0.00010
tswf7	32	0.00000	0.00029	0.01984	0.32175	0.00021	0.00007	0.00043	0.00000	0.00000	0.00990	0.00010
tswm8	33	0.49522	0.00000	0.00039	0.00000	0.01691	0.00564	0.03381	0.00000	0.00000	0.00990	0.00010
tswf8	34	0.49522	0.00000	0.00039	0.00000	0.01691	0.00564	0.03381	0.00000	0.00000	0.00990	0.00010
tswm9	35	0.69427	0.00000	0.00005	0.00000	0.00723	0.00241	0.01446	0.00000	0.00000	0.00990	0.00010
tswf9	36	0.69427	0.00000	0.00005	0.00000	0.00723	0.00241	0.01446	0.00000	0.00000	0.00990	0.00010
ch1mv	37	0.50592	0.00000	0.00024	0.00000	0.06265	0.02088	0.12529	0.00000	0.00000	0.00990	0.00000
ch1fv	38	0.50592	0.00000	0.00024	0.00000	0.06265	0.02088	0.12529	0.00000	0.00000	0.00990	0.00000

Rock	Zone	K-Feldspar	Albite	Anorthite	Ca-Smectite	Na-Smectite	Mg-Smectite	Illite	Tridymite	Cristobalite	Quartz
ch2mv	39	0.09836	0.07263	0.00244	0.00691	0.00296	0.00691	0.00515	0.00079	0.05704	0.04824
ch2fv	40	0.09836	0.07263	0.00244	0.00691	0.00296	0.00691	0.00515	0.00079	0.05704	0.04824
ch3mv	41	0.04708	0.03477	0.00117	0.00216	0.00093	0.00216	0.00161	0.00001	0.04663	0.02747
ch3fv	42	0.04708	0.03477	0.00117	0.00216	0.00093	0.00216	0.00161	0.00001	0.04663	0.02747
ch4mz	43	0.04820	0.03559	0.00120	0.00058	0.00025	0.00058	0.00043	0.00000	0.03726	0.02878
ch4fz	44	0.04820	0.03559	0.00120	0.00058	0.00025	0.00058	0.00043	0.00000	0.03726	0.02878
ch5mz	45	0.04551	0.03361	0.00113	0.00046	0.00020	0.00046	0.00035	0.00000	0.02171	0.02707
ch5fz	46	0.04551	0.03361	0.00113	0.00046	0.00020	0.00046	0.00035	0.00000	0.02171	0.02707
ch6mv	47	0.09931	0.07334	0.00247	0.00620	0.00266	0.00620	0.00463	0.00000	0.05861	0.09735
ch6fv	48	0.09931	0.07334	0.00247	0.00620	0.00266	0.00620	0.00463	0.00000	0.05861	0.09735
pp4m	49	0.08283	0.06116	0.00206	0.00829	0.00355	0.00829	0.00619	0.00003	0.06691	0.01512
pp4f	50	0.08283	0.06116	0.00206	0.00829	0.00355	0.00829	0.00619	0.00003	0.06691	0.01512
pp3m	51	0.36843	0.27207	0.00915	0.00332	0.00142	0.00332	0.00248	0.00590	0.07075	0.24829
pp3f	52	0.36843	0.27207	0.00915	0.00332	0.00142	0.00332	0.00248	0.00590	0.07075	0.24829
pp2m	53	0.36843	0.27207	0.00915	0.00332	0.00142	0.00332	0.00248	0.00590	0.07075	0.24829
pp2f	54	0.36843	0.27207	0.00915	0.00332	0.00142	0.00332	0.00248	0.00590	0.07075	0.24829
pp1m	55	0.09931	0.07334	0.00247	0.00620	0.00266	0.00620	0.00463	0.00000	0.05861	0.09735
pp1f	56	0.09931	0.07334	0.00247	0.00620	0.00266	0.00620	0.00463	0.00000	0.05861	0.09735
bf3m4	57	0.36843	0.27207	0.00915	0.00332	0.00142	0.00332	0.00248	0.00590	0.07075	0.24829
bf3f4	58	0.36843	0.27207	0.00915	0.00332	0.00142	0.00332	0.00248	0.00590	0.07075	0.24829

Rock	Zone	Glass	Hematite	Calcite	Stellerite	Heulandite	Mordenite	Clinoptilolite	Kaolinite	Am. Silica	Opal	Fluorite
ch2mv	39	0 60921	0 00000	0.00000	0.00000	0.02384	0 00795	0 04768	0 00000	0.00000	0.00990	0.00000
ch2fv	40	0.60921	0.00000	0.00000	0 00000	0 02384	0 00795	0.04768	0.00000	0.00000	0.00990	0 00000
ch3mv	41	0.73775	0.00000	0.00000	0 00000	0 02651	0.00884	0.05302	0.00000	0.00000	0.00990	0 00000
ch3fv	42	0.73775	0.00000	0.00000	0 00000	0.02651	0.00884	0.05302	0.00000	0 00000	0.00990	0 00000
ch4mz	43	0.73310	0 00000	0 00003	0 00000	0.03123	0.01041	0.06246	0.00000	0.00000	0.00990	0 00000
ch4fz	44	0.73310	0 00000	0 00003	0.00000	0.03123	0.01041	0 06246	0 00000	0 00000	0 00990	0.00000
ch5mz	45	0.77556	0 00000	0 00004	0.00000	0.02520	0 00840	0 05040	0 00000	0 00000	0.00990	0.00000
ch5fz	46	0.77556	0 00000	0 00004	0.00000	0.02520	0.00840	0 05040	0 00000	0 00000	0.00990	0.00000
ch6mv	47	0 32953	0 00000	0 00150	0.00000	0.09249	0 03083	0 18497	0 00000	0 00000	0.00990	0.00000
ch6fv	48	0.32953	0.00000	0 00150	0 00000	0 09249	0.03083	0.18497	0.00000	0.00000	0.00990	0.00000
pp4m	49	0.49175	0.00000	0 00163	0 00000	0 07269	0 02423	0.14538	0.00000	0.00000	0.00990	0.00000
pp4f	50	0.49175	0 00000	0 00163	0 00000	0 07269	0.02423	0.14538	0.00000	0 00000	0 00990	0 00000
pp3m	51	0.00003	0.00474	0 00000	0.00000	0.00005	0.00002	0.00010	0.00000	0 00000	0 00990	0 00000
pp3f	52	0 00003	0 00474	0 00000	0.00000	0.00005	0.00002	0 00010	0 00000	0 00000	0.00990	0.00000
pp2m	53	0 00003	0 00474	0 00000	0.00000	0.00005	0.00002	0 00010	0 00000	0 00000	0.00990	0.00000
pp2f	54	0.00003	0 00474	0 00000	0.00000	0.00005	0.00002	0 00010	0 00000	0 00000	0.00990	0.00000
pp1m	55	0.32953	0.00000	0 00150	0.00000	0.09249	0.03083	0.18497	0 00000	0 00000	0.00990	0.00000
pp1f	56	0 32953	0.00000	0.00150	0.00000	0.09249	0 03083	0 18497	0 00000	0.00000	0.00990	0.00000
bf3m4	57	0 00003	0 00474	0.00000	0.00000	0.00005	0 00002	0 00010	0 00000	0.00000	0.00990	0.00000
bf3f4	58	0 00003	0 00474	0.00000	0.00000	0 00005	0 00002	0 00010	0 00000	0.00000	0.00990	0 00000

ATTACHMENT III – MINERAL REACTIVE SURFACE AREAS: Tptpmn THC Model REV01, Tptpmn THC Heterogeneous Model REV01 and DST THC Model REV01

(DTN: LB0101DSTTHCR1.003 [161278])

Unit	Rock Name	Zone	K-Feldspar	Albite	Anorthite	Ca-Smectite	Na-Smectite	Mg-Smectite	K-Smectite	Illite	Tridymite
Tcw3	tcwm3	1	98.0	98.0	98.0	1516.3	1516.3	1516.3	1516.3	1516.3	98.0
	tcwf3	2	394.8	394.8	394.8	394.8	394.8	394.8	394.8	394.8	394.8
Ptn1	ptnm1	3	7.6	7.6	7.6	2253.3	2253.3	2253.3	2253.3	2253.3	7.6
	ptnf1	4	142.8	142.8	142.8	142.8	142.8	142.8	142.8	142.8	142.8
Ptn2	ptnm2	5	8.6	8.6	8.6	2484.8	2484.8	2484.8	2484.8	2484.8	8.6
	ptnf2	6	184.6	184.6	184.6	184.6	184.6	184.6	184.6	184.6	184.6
Ptn3	ptnm3	7	7.1	7.1	7.1	1721.5	1721.5	1721.5	1721.5	1721.5	7.1
	ptnf3	8	1099.6	1099.6	1099.6	1099.6	1099.6	1099.6	1099.6	1099.6	1099.6
Ptn4	ptnm4	9	9.3	9.3	9.3	2356.2	2356.2	2356.2	2356.2	2356.2	9.3
	ptnf4	10	44.5	44.5	44.5	44.5	44.5	44.5	44.5	44.5	44.5
Ptn5	ptnm5	11	11.0	11.0	11.0	2666.7	2666.7	2666.7	2666.7	2666.7	11.0
	ptnf5	12	276.2	276.2	276.2	276.2	276.2	276.2	276.2	276.2	276.2
Ptn6	ptnm6	13	10.0	10.0	10.0	2666.7	2666.7	2666.7	2666.7	2666.7	10.0
	ptnf6	14	1553.3	1553.3	1553.3	1553.3	1553.3	1553.3	1553.3	1553.3	1553.3
Tsw31	tswm1	15	57.0	57.0	57.0	694.3	694.3	694.3	694.3	694.3	57.0
	tswf1	16	1102.4	1102.4	1102.4	1102.4	1102.4	1102.4	1102.4	1102.4	1102.4
Tsw32	tswm2	17	109.2	109.2	109.2	1317.4	1317.4	1317.4	1317.4	1317.4	109.2
	tswf2	18	530.8	530.8	530.8	530.8	530.8	530.8	530.8	530.8	530.8
Tsw33	tswm3	19	105.6	105.6	105.6	1303.3	1303.3	1303.3	1303.3	1303.3	105.6
	tswf3	20	1056.7	1056.7	1056.7	1056.7	1056.7	1056.7	1056.7	1056.7	1056.7
Tsw34	tswm4	21	89.8	89.8	89.8	1086.6	1086.6	1086.6	1086.6	1086.6	89.8
	tswf4	22	2126.9	2126.9	2126.9	2126.9	2126.9	2126.9	2126.9	2126.9	2126.9
Tsw35	tswm5	23	98.2	98.2	98.2	1195.3	1195.3	1195.3	1195.3	1195.3	98.2
	tswf5	24	1382.3	1382.3	1382.3	1382.3	1382.3	1382.3	1382.3	1382.3	1382.3
Tsw36	tswm6	25	90.8	90.8	90.8	1098.1	1098.1	1098.1	1098.1	1098.1	90.8
	tswf6	26	1289.1	1289.1	1289.1	1289.1	1289.1	1289.1	1289.1	1289.1	1289.1
Tsw37	tswm7	27	82.4	82.4	82.4	996.5	996.5	996.5	996.5	996.5	82.4
	tswf7	28	1289.1	1289.1	1289.1	1289.1	1289.1	1289.1	1289.1	1289.1	1289.1
Tsw38	tswm8	29	40.4	40.4	40.4	526.7	526.7	526.7	526.7	526.7	40.4
	tswf8	30	1746.2	1746.2	1746.2	1746.2	1746.2	1746.2	1746.2	1746.2	1746.2
Ch2	ch2mz	31	44.5	44.5	44.5	2024.7	2024.7	2024.7	2024.7	2024.7	44.5
	ch2fz	32	1570.8	1570.8	1570.8	1570.8	1570.8	1570.8	1570.8	1570.8	1570.8

DTN

Unit	Rock Name	Zone	Cristobalite	Quartz	Glass	Hematite	Calcite	Stellerite	Heulandite	Mordenite	Clinoptilolite
Tcw3	tcwm3	1	98.0	98.0	98.0	128.7	128.7	128.7	128.7	128.7	128.7
	tcwf3	2	394.8	394.8	394.8	394.8	394.8	394.8	394.8	394.8	394.8
Ptn1	ptnm1	3	7.6	7.6	7.6	9.6	9.6	9.6	9.6	9.6	9.6
	ptnf1	4	142.8	142.8	142.8	142.8	142.8	142.8	142.8	142.8	142.8
Ptn2	ptnm2	5	8.6	8.6	8.6	10.5	10.5	10.5	10.5	10.5	10.5
	ptnf2	6	184.6	184.6	184.6	184.6	184.6	184.6	184.6	184.6	184.6
Ptn3	ptnm3	7	7.1	7.1	7.1	7.3	7.3	7.3	7.3	7.3	7.3
	ptnf3	8	1099.6	1099.6	1099.6	1099.6	1099.6	1099.6	1099.6	1099.6	1099.6
Ptn4	ptnm4	9	9.3	9.3	9.3	10.0	10.0	10.0	10.0	10.0	10.0
	ptnf4	10	44.5	44.5	44.5	44.5	44.5	44.5	44.5	44.5	44.5
Ptn5	ptnm5	11	11.0	11.0	11.0	11.3	11.3	11.3	11.3	11.3	11.3
	ptnf5	12	276.2	276.2	276.2	276.2	276.2	276.2	276.2	276.2	276.2
Ptn6	ptnm6	13	10.0	10.0	10.0	11.3	11.3	11.3	11.3	11.3	11.3
	ptnf6	14	1553.3	1553.3	1553.3	1553.3	1553.3	1553.3	1553.3	1553.3	1553.3
Tsw31	tswm1	15	57.0	57.0	57.0	59.0	59.0	59.0	59.0	59.0	59.0
	tswf1	16	1102.4	1102.4	1102.4	1102.4	1102.4	1102.4	1102.4	1102.4	1102.4
Tsw32	tswm2	17	109.2	109.2	109.2	111.9	111.9	111.9	111.9	111.9	111.9
	tswf2	18	530.8	530.8	530.8	530.8	530.8	530.8	530.8	530.8	530.8
Tsw33	tswm3	19	105.6	105.6	105.6	110.7	110.7	110.7	110.7	110.7	110.7
	tswf3	20	1056.7	1056.7	1056.7	1056.7	1056.7	1056.7	1056.7	1056.7	1056.7
Tsw34	tswm4	21	89.8	89.8	89.8	92.3	92.3	92.3	92.3	92.3	92.3
	tswf4	22	2126.9	2126.9	2126.9	2126.9	2126.9	2126.9	2126.9	2126.9	2126.9
Tsw35	tswm5	23	98.2	98.2	98.2	101.5	101.5	101.5	101.5	101.5	101.5
	tswf5	24	1382.3	1382.3	1382.3	1382.3	1382.3	1382.3	1382.3	1382.3	1382.3
Tsw36	tswm6	25	90.8	90.8	90.8	93.2	93.2	93.2	93.2	93.2	93.2
	tswf6	26	1289.1	1289.1	1289.1	1289.1	1289.1	1289.1	1289.1	1289.1	1289.1
Tsw37	tswm7	27	82.4	82.4	82.4	84.6	84.6	84.6	84.6	84.6	84.6
	tswf7	28	1289.1	1289.1	1289.1	1289.1	1289.1	1289.1	1289.1	1289.1	1289.1
Tsw38	tswm8	29	40.4	40.4	40.4	44.7	44.7	44.7	44.7	44.7	44.7
	tswf8	30	1746.2	1746.2	1746.2	1746.2	1746.2	1746.2	1746.2	1746.2	1746.2
Ch2	ch2mz	31	44.5	44.5	44.5	171.9	171.9	171.9	171.9	171.9	171.9
	ch2fz	32	1570.8	1570.8	1570.8	1570.8	1570.8	1570.8	1570.8	1570.8	1570.8

ATTACHMENT IV – MINERAL REACTIVE SURFACE AREAS: Tptpll THC Models (REV01 and REV02) and DST THC Model REV02

(DTN: LB0101DSTTHCR1.004 [161279])

Rock	Zone	K-Feldspar	Albite	Anorthite	Ca-Smectite	Na-Smectite	Mg-Smectite	Illite	Tridymite	Cristobalite	Quartz
tcwm1	1	110.5	110.5	110.5	1516.3	1516.3	1516.3	1516.3	110.5	110.5	110.5
tcwf1	2	394.8	394.8	394.8	394.8	394.8	394.8	394.8	394.8	394.8	394.8
tcwm2	3	110.5	110.5	110.5	1516.3	1516.3	1516.3	1516.3	110.5	110.5	110.5
tcwf2	4	394.8	394.8	394.8	394.8	394.8	394.8	394.8	394.8	394.8	394.8
tcwm3	5	110.5	110.5	110.5	1516.3	1516.3	1516.3	1516.3	110.5	110.5	110.5
tcwf3	6	394.8	394.8	394.8	394.8	394.8	394.8	394.8	394.8	394.8	394.8
ptnm1	7	8.7	8.7	8.7	2253.3	2253.3	2253.3	2253.3	8.7	8.7	8.7
ptnf1	8	142.8	142.8	142.8	142.8	142.8	142.8	142.8	142.8	142.8	142.8
ptnm2	9	9.6	9.6	9.6	2484.8	2484.8	2484.8	2484.8	9.6	9.6	9.6
ptnf2	10	184.6	184.6	184.6	184.6	184.6	184.6	184.6	184.6	184.6	184.6
ptnm3	11	6.7	6.7	6.7	1721.5	1721.5	1721.5	1721.5	6.7	6.7	6.7
ptnf3	12	1099.6	1099.6	1099.6	1099.6	1099.6	1099.6	1099.6	1099.6	1099.6	1099.6
ptnm4	13	9.1	9.1	9.1	2356.2	2356.2	2356.2	2356.2	9.1	9.1	9.1
ptnf4	14	44.5	44.5	44.5	44.5	44.5	44.5	44.5	44.5	44.5	44.5
ptnm5	15	10.3	10.3	10.3	2666.7	2666.7	2666.7	2666.7	10.3	10.3	10.3
ptnf5	16	276.2	276.2	276.2	276.2	276.2	276.2	276.2	276.2	276.2	276.2
ptnm6	17	10.3	10.3	10.3	2666.7	2666.7	2666.7	2666.7	10.3	10.3	10.3
ptnf6	18	1553.3	1553.3	1553.3	1553.3	1553.3	1553.3	1553.3	1553.3	1553.3	1553.3
tswm1	19	57.2	57.2	57.2	694.3	694.3	694.3	694.3	57.2	57.2	57.2
tswf1	20	1102.4	1102.4	1102.4	1102.4	1102.4	1102.4	1102.4	1102.4	1102.4	1102.4
tswm2	21	110.0	110.0	110.0	1317.4	1317.4	1317.4	1317.4	110.0	110.0	110.0
tswf2	22	530.8	530.8	530.8	530.8	530.8	530.8	530.8	530.8	530.8	530.8
tswm3	23	107.4	107.4	107.4	1303.3	1303.3	1303.3	1303.3	107.4	107.4	107.4
tswf3	24	1056.7	1056.7	1056.7	1056.7	1056.7	1056.7	1056.7	1056.7	1056.7	1056.7
tswm4	25	90.7	90.7	90.7	1086.6	1086.6	1086.6	1086.6	90.7	90.7	90.7
tswf4	26	2126.9	2126.9	2126.9	2126.9	2126.9	2126.9	2126.9	2126.9	2126.9	2126.9
tswm5	27	99.0	99.0	99.0	1195.3	1195.3	1195.3	1195.3	99.0	99.0	99.0
tswf5	28	844.7	844.7	844.7	844.7	844.7	844.7	844.7	844.7	844.7	844.7
tswm6	29	92.0	92.0	92.0	1098.1	1098.1	1098.1	1098.1	92.0	92.0	92.0
tswf6	30	1289.1	1289.1	1289.1	1289.1	1289.1	1289.1	1289.1	1289.1	1289.1	1289.1
tswm7	31	83.6	83.6	83.6	996.5	996.5	996.5	996.5	83.6	83.6	83.6
tswf7	32	1289.1	1289.1	1289.1	1289.1	1289.1	1289.1	1289.1	1289.1	1289.1	1289.1
tswm8	33	36.0	36.0	36.0	526.7	526.7	526.7	526.7	36.0	36.0	36.0
tswf8	34	1746.2	1746.2	1746.2	1746.2	1746.2	1746.2	1746.2	1746.2	1746.2	1746.2
tswm9	35	36.0	36.0	36.0	526.7	526.7	526.7	526.7	36.0	36.0	36.0
tswf9	36	1007.4	1007.4	1007.4	1007.4	1007.4	1007.4	1007.4	1007.4	1007.4	1007.4
ch1mv	37	152.6	152.6	152.6	2024.7	2024.7	2024.7	2024.7	152.6	152.6	152.6
ch1fv	38	683.0	683.0	683.0	683.0	683.0	683.0	683.0	683.0	683.0	683.0

Rock	Zone	Glass	Hematite	Calcite	Stellerite	Heulandite	Mordenite	Clinoptilolite	Kaolinite	Am. Silica	Opal	Fluorite
tcwm1	1	110.5	128.7	128.7	128.7	128.7	128.7	128.7	1516.3	1516.3	1516.3	128.7
tcwf1	2	394.8	394.8	394.8	394.8	394.8	394.8	394.8	394.8	394.8	394.8	394.8
tcwm2	3	110.5	128.7	128.7	128.7	128.7	128.7	128.7	1516.3	1516.3	1516.3	128.7
tcwf2	4	394.8	394.8	394.8	394.8	394.8	394.8	394.8	394.8	394.8	394.8	394.8
tcwm3	5	110.5	128.7	128.7	128.7	128.7	128.7	128.7	1516.3	1516.3	1516.3	128.7
tcwf3	6	394.8	394.8	394.8	394.8	394.8	394.8	394.8	394.8	394.8	394.8	394.8
ptnm1	7	8.7	9.6	9.6	9.6	9.6	9.6	9.6	2253.3	2253.3	2253.3	9.6
ptnf1	8	142.8	142.8	142.8	142.8	142.8	142.8	142.8	142.8	142.8	142.8	142.8
ptnm2	9	9.6	10.5	10.5	10.5	10.5	10.5	10.5	2484.8	2484.8	2484.8	10.5
ptnf2	10	184.6	184.6	184.6	184.6	184.6	184.6	184.6	184.6	184.6	184.6	184.6
ptnm3	11	6.7	7.3	7.3	7.3	7.3	7.3	7.3	1721.5	1721.5	1721.5	7.3
ptnf3	12	1099.6	1099.6	1099.6	1099.6	1099.6	1099.6	1099.6	1099.6	1099.6	1099.6	1099.6
ptnm4	13	9.1	10.0	10.0	10.0	10.0	10.0	10.0	2356.2	2356.2	2356.2	10.0
ptnf4	14	44.5	44.5	44.5	44.5	44.5	44.5	44.5	44.5	44.5	44.5	44.5
ptnm5	15	10.3	11.3	11.3	11.3	11.3	11.3	11.3	2666.7	2666.7	2666.7	11.3
ptnf5	16	276.2	276.2	276.2	276.2	276.2	276.2	276.2	276.2	276.2	276.2	276.2
ptnm6	17	10.3	11.3	11.3	11.3	11.3	11.3	11.3	2666.7	2666.7	2666.7	11.3
ptnf6	18	1553.3	1553.3	1553.3	1553.3	1553.3	1553.3	1553.3	1553.3	1553.3	1553.3	1553.3
tswm1	19	57.2	59.0	59.0	59.0	59.0	59.0	59.0	694.3	694.3	694.3	59.0
tswf1	20	1102.4	1102.4	1102.4	1102.4	1102.4	1102.4	1102.4	1102.4	1102.4	1102.4	1102.4
tswm2	21	110.0	111.9	111.9	111.9	111.9	111.9	111.9	1317.4	1317.4	1317.4	111.9
tswf2	22	530.8	530.8	530.8	530.8	530.8	530.8	530.8	530.8	530.8	530.8	530.8
tswm3	23	107.4	110.7	110.7	110.7	110.7	110.7	110.7	1303.3	1303.3	1303.3	110.7
tswf3	24	1056.7	1056.7	1056.7	1056.7	1056.7	1056.7	1056.7	1056.7	1056.7	1056.7	1056.7
tswm4	25	90.7	92.3	92.3	92.3	92.3	92.3	92.3	1086.6	1086.6	1086.6	92.3
tswf4	26	2126.9	2126.9	2126.9	2126.9	2126.9	2126.9	2126.9	2126.9	2126.9	2126.9	2126.9
tswm5	27	99.0	101.5	101.5	101.5	101.5	101.5	101.5	1195.3	1195.3	1195.3	101.5
tswf5	28	844.7	844.7	844.7	844.7	844.7	844.7	844.7	844.7	844.7	844.7	844.7
tswm6	29	92.0	93.2	93.2	93.2	93.2	93.2	93.2	1098.1	1098.1	1098.1	93.2
tswf6	30	1289.1	1289.1	1289.1	1289.1	1289.1	1289.1	1289.1	1289.1	1289.1	1289.1	1289.1
tswm7	31	83.6	84.6	84.6	84.6	84.6	84.6	84.6	996.5	996.5	996.5	84.6
tswf7	32	1289.1	1289.1	1289.1	1289.1	1289.1	1289.1	1289.1	1289.1	1289.1	1289.1	1289.1
tswm8	33	36.0	44.7	44.7	44.7	44.7	44.7	44.7	526.7	526.7	526.7	44.7
tswf8	34	1746.2	1746.2	1746.2	1746.2	1746.2	1746.2	1746.2	1746.2	1746.2	1746.2	1746.2
tswm9	35	36.0	44.7	44.7	44.7	44.7	44.7	44.7	526.7	526.7	526.7	44.7
tswf9	36	1007.4	1007.4	1007.4	1007.4	1007.4	1007.4	1007.4	1007.4	1007.4	1007.4	1007.4
ch1mv	37	152.6	171.9	171.9	171.9	171.9	171.9	171.9	2024.7	2024.7	2024.7	171.9
ch1fv	38	683.0	683.0	683.0	683.0	683.0	683.0	683.0	683.0	683.0	683.0	683.0

Rock	Zone	K-Feldspar	Albite	Anorthite	Ca-Smectite	Na-Smectite	Mg-Smectite	Illite	Tridymite	Cristobalite	Quartz
ch2mv	39	152.6	152.6	152.6	2024.7	2024.7	2024.7	2024.7	152.6	152.6	152.6
ch2fv	40	758.9	758.9	758.9	758.9	758.9	758.9	758.9	758.9	758.9	758.9
ch3mv	41	152.6	152.6	152.6	2024.7	2024.7	2024.7	2024.7	152.6	152.6	152.6
ch3fv	42	758.9	758.9	758.9	758.9	758.9	758.9	758.9	758.9	758.9	758.9
ch4mz	43	152.6	152.6	152.6	2024.7	2024.7	2024.7	2024.7	152.6	152.6	152.6
ch4fz	44	1570.8	1570.8	1570.8	1570.8	1570.8	1570.8	1570.8	1570.8	1570.8	1570.8
ch5mz	45	152.6	152.6	152.6	2024.7	2024.7	2024.7	2024.7	152.6	152.6	152.6
ch5fz	46	1570.8	1570.8	1570.8	1570.8	1570.8	1570.8	1570.8	1570.8	1570.8	1570.8
ch6mv	47	152.6	152.6	152.6	2024.7	2024.7	2024.7	2024.7	152.6	152.6	152.6
ch6fv	48	1016.4	1016.4	1016.4	1016.4	1016.4	1016.4	1016.4	1016.4	1016.4	1016.4
pp4m	49	152.6	152.6	152.6	2024.7	2024.7	2024.7	2024.7	152.6	152.6	152.6
pp4f	50	1570.8	1570.8	1570.8	1570.8	1570.8	1570.8	1570.8	1570.8	1570.8	1570.8
pp3m	51	152.6	152.6	152.6	2024.7	2024.7	2024.7	2024.7	152.6	152.6	152.6
pp3f	52	871.1	871.1	871.1	871.1	871.1	871.1	871.1	871.1	871.1	871.1
pp2m	53	152.6	152.6	152.6	2024.7	2024.7	2024.7	2024.7	152.6	152.6	152.6
pp2f	54	871.1	871.1	871.1	871.1	871.1	871.1	871.1	871.1	871.1	871.1
pp1m	55	152.6	152.6	152.6	2024.7	2024.7	2024.7	2024.7	152.6	152.6	152.6
pp1f	56	1570.8	1570.8	1570.8	1570.8	1570.8	1570.8	1570.8	1570.8	1570.8	1570.8
bf3m4	57	152.6	152.6	152.6	2024.7	2024.7	2024.7	2024.7	152.6	152.6	152.6
bf3f4	58	2228.3	2228.3	2228.3	2228.3	2228.3	2228.3	2228.3	2228.3	2228.3	2228.3

Rock	Zone	Glass	Hematite	Calcite	Stellerite	Heulandite	Mordenite	Clinoptilolite	Kaolinite	Am. Silica	Opal	Fluorite
ch2mv	39	152.6	171.9	171.9	171.9	171.9	171.9	171.9	2024.7	2024.7	2024.7	171.9
ch2fv	40	758.9	758.9	758.9	758.9	758.9	758.9	758.9	758.9	758.9	758.9	758.9
ch3mv	41	152.6	171.9	171.9	171.9	171.9	171.9	171.9	2024.7	2024.7	2024.7	171.9
ch3fv	42	758.9	758.9	758.9	758.9	758.9	758.9	758.9	758.9	758.9	758.9	758.9
ch4mz	43	152.6	171.9	171.9	171.9	171.9	171.9	171.9	2024.7	2024.7	2024.7	171.9
ch4fz	44	1570.8	1570.8	1570.8	1570.8	1570.8	1570.8	1570.8	1570.8	1570.8	1570.8	1570.8
ch5mz	45	152.6	171.9	171.9	171.9	171.9	171.9	171.9	2024.7	2024.7	2024.7	171.9
ch5fz	46	1570.8	1570.8	1570.8	1570.8	1570.8	1570.8	1570.8	1570.8	1570.8	1570.8	1570.8
ch6mv	47	152.6	171.9	171.9	171.9	171.9	171.9	171.9	2024.7	2024.7	2024.7	171.9
ch6fv	48	1016.4	1016.4	1016.4	1016.4	1016.4	1016.4	1016.4	1016.4	1016.4	1016.4	1016.4
pp4m	49	152.6	171.9	171.9	171.9	171.9	171.9	171.9	2024.7	2024.7	2024.7	171.9
pp4f	50	1570.8	1570.8	1570.8	1570.8	1570.8	1570.8	1570.8	1570.8	1570.8	1570.8	1570.8
pp3m	51	152.6	171.9	171.9	171.9	171.9	171.9	171.9	2024.7	2024.7	2024.7	171.9
pp3f	52	871.1	871.1	871.1	871.1	871.1	871.1	871.1	871.1	871.1	871.1	871.1
pp2m	53	152.6	171.9	171.9	171.9	171.9	171.9	171.9	2024.7	2024.7	2024.7	171.9
pp2f	54	871.1	871.1	871.1	871.1	871.1	871.1	871.1	871.1	871.1	871.1	871.1
pp1m	55	152.6	171.9	171.9	171.9	171.9	171.9	171.9	2024.7	2024.7	2024.7	171.9
pp1f	56	1570.8	1570.8	1570.8	1570.8	1570.8	1570.8	1570.8	1570.8	1570.8	1570.8	1570.8
bf3m4	57	152.6	171.9	171.9	171.9	171.9	171.9	171.9	2024.7	2024.7	2024.7	171.9
bf3f4	58	2228.3	2228.3	2228.3	2228.3	2228.3	2228.3	2228.3	2228.3	2228.3	2228.3	2228.3

ATTACHMENT V – THERMODYNAMIC DATABASE: REV01 THC Models

(DTN: LB0101DSTTHCR1.006 [161280])

Mineral	Molecular Weight (g/mol)	Molar Volume (cm^3/mol)	Reaction Stoichiometry[1]	log (K)					
				0 (°C)	25 (°C)	60 (°C)	100 (°C)	150 (°C)	200 (°C)
albite-low	262.223	100.07	(1)alo2-, (1)na+, (3)sio2(aq)	-21.694	-20.177	-18.362	-16 684	-15.094	-13 986
anorthite	278.207	100.79	(2)alo2-, (1)ca+2, (2)sio2(aq)	-21.229	-20.484	-19.64	-18.96	-18.514	-18 485
calcite	100.087	36.934	(1)ca+2, (-1)h+, (1)hco3-	2.226	1.849	1.333	0.774	0.1	-0.584
SiO2(amor.)	60.084	29	(1)sio2(aq)	-2.871	-2.663	-2.423	-2.205	-1.99	-1.82
cristobalite-a	60.084	25.74	(1)sio2(aq)	-3.63	-3 332	-2.99	-2.678	-2.371	-2.129
fluorite	78 075	24.542	(1)ca+2, (2)f-	-10.31	-10.037	-9 907	-9.967	-10.265	-10.784
goethite	88 854	20.82	(1)hfeo2	-12.78	-11.483	-10.202	-9.208	-8.407	-7.92
glass1	56 588	23 978	(-0.0362)h2o, (0.15)alo2-, (0 0021)ca+2,(0.0654)h+, (0.0042)k+,(0.0003)mg+2, (0.0756)na+,(0.7608)sio2(aq), (0.007)hfeo2	-4 55	-4 39	-4 2	-4 01	-3.83	-3.71
glass	60 084	29	(1)sio2(aq)	-2.871	-2.663	-2.423	-2.205	-1.99	-1.82
gypsum	172.172	74.69	(2)h2o, (1)ca+2, (1)so4-2	-4 533	-4 482	-4 609	-4 903	-5.41	-6.127
hematite	159 692	30.274	(-1)h2o, (2)hfeo2	-26.439	-23.927	-21.485	-19 661	-18 293	-17.573
illite	378 963	135 08	(0.44)h2o, (2.06)alo2-, (1.12)h+,(0.5)k+, (0.22)mg+2,(3 72)sio2(aq)	-45.354	-41.926	-38.294	-34.994	-31.867	-29.606
k-spar	278.332	108 741	(1)alo2-, (1)k+, (3)sio2(aq)	-23.77	-21.82	-19.53	-17.44	-15.46	-14.06
kaolinite	258.16	99.52	(1)h2o, (2)alo2-, (2)h+,(2)sio2(aq)	-43.073	-39 895	-36.336	-33 181	-30.212	-28.082
quartz	60 084	22.688	(1)sio2(aq)	-4 079	-3.739	-3.349	-2.992	-2.642	-2.365
opal_proxy	60.084	29.000	(1)sio2(aq)	-3 501	-3.005	-2.627	-2.358	-2.118	-1.926
tridymite	60.084	26.586	(1)sio2(aq)	-3 872	-3.567	-3.193	-2.821	-2.394	-1.984
smectite-ca	365.394	132 51	(0.52)h2o, (1.77)alo2-, (0.145)ca+2,(0 96)h+, (0.26)mg+2,(3 97)sio2(aq)	-39.970	-36.970	-33.600	-30.610	-27.750	-25.670
smectite-na	366 25	132.51	(0.52)h2o, (1.77)alo2-, (0 96)h+,(0.26)mg+2, (0.29)na+,(3 97)sio2(aq)	-40 080	-36.980	-33 500	-30.380	-27.400	-25.210
smectite-mg	363 107	132.51	(0.52)h2o, (1.77)alo2-, (0.96)h+,(0.405)mg+2, (3.97)sio2(aq)	-40.030	-37.060	-33 730	-30.770	-27.940	-25.880
steller/10	281.733	133 1	(2.8)h2o, (0 79)alo2-, (0.39)ca+2,(0 01)na+, (2.81)sio2(aq)	-17.910	-16 400	-14 670	-13.100	-11.560	-10.420
heuland/10	279 347	126.64	(2.6)h2o, (0 8)alo2-, (0.33)ca+2,(0 04)k+, (0.1)na+,(2.8)sio2(aq)	-17.900	-16 350	-14 580	-12.970	-11.400	-10.230
mordeni/10	269 631	127.35	(2.2)h2o, (0.6)alo2-, (0.15)ca+2,(0 09)k+, (0.21)na+,(3)sio2(aq)	-16 150	-14 660	-12 950	-11.390	-9.840	-8 670
clinopt/10	277.66	126.41	(2.6)h2o, (0 68)alo2-, (0.28)ca+2,(0.08)k+, (0.04)na+,(2.92)sio2(aq)	-17.040	-15 500	-13 740	-12.130	-10.560	-9 350

Gaseous Species	Molecular Weight (g/mol)	Molecular Diameter (m)	Reaction Stoichiometry	0 (°C)	25 (°C)	60 (°C)	100 (°C)	150 (°C)	200 (°C)
CO2(g)	44.01	2.50E-10	(-1)h2o, (1)h+, (1)hco3-	-7.677	-7.818	-8.053	-8.36	-8.77	-9.217

NOTES: [1] Negative number in parenthesis indicate the species is on the left side of equation Minerals names or abbreviations above are those used in the database and may not exactly match names used in the text of the report Names ending by /10 indicate the stoichiometry, molecular weight, molar volume, and log(K) values for those minerals were divided by 10 compared to original data. Glass phases, glass1 and glass, were used with the extended-case and base-case geochemical systems, respectively.
Data in this Attachment are associated with input file thermok2 07 dat

Aqueous Species	r_{ej}	Charge	Reaction Stoichiometry[1]	log (K)					
				0 (°C)	25 (°C)	60 (°C)	100 (°C)	150 (°C)	200 (°C)
CO2(aq)	0.231	0	(-1)h2o, (1)h+, (1)hco3-	-6.58	-6.345	-6.268	-6.388	-6.724	-7.197
CO3-2	2.81	-2	(-1)h+, (1)hco3-	10.624	10.329	10.13	10.084	10.2	10.465
OH-	1.4	-1	(1)h2o, (-1)h+	14.94	13.995	13.027	12.255	11.631	11.284
Al(OH)2+	2.31	1	(1)alo2-, (2)h+	-13.66	-12.29	-10.83	-9.6	-8.53	-7.823
$HAlO_2$	0	0	(1)alo2-, (1)h+	-7.08	-6.45	-5.846	-5.409	-5.121	-5.035
Al+3	3.33	3	(-2)h2o, (1)alo2-, (4)h+	-25.8	-22.88	-19.57	-16.58	-13.68	-11.41
AlOH+2	2.8	2	(-1)h2o, (1)alo2-, (3)h+	-20.07	-17.93	-15.57	-13.52	-11.62	-10.24
CaCl+	2.31	1	(1)ca+2, (1)cl-	0.673	0.696	0.589	0.357	-0.04	-0.533
CaCl2(aq)	0	0	(1)ca+2, (2)cl-	0.452	0.644	0.629	0.381	-0.159	-0.911
CaCO3(aq)	0	0	(1)ca+2, (-1)h+, (1)hco3-	7.502	7.002	6.452	5.964	5.468	5.018
CaHCO3+	2.31	1	(1)ca+2, (1)hco3-	-1.095	-1.047	-1.159	-1.418	-1.859	-2.4
CaSO4(aq)	0	0	(1)ca+2, (1)so4-2	-2.071	-2.111	-2.265	-2.511	-2.91	-3.433
CaF+	2.31	1	(1)ca+2, (1)f-	-0.655	-0.682	-0.862	-1.17	-1.649	-2.215
CaOH+	2.31	1	(1)h2o, (-1)h+, (1)ca+2	14.085	12.833	11.416	10.142	8.904	7.931
HSiO3-	1.81	-1	(1)h2o, (-1)h+, (1)sio2(aq)	10.323	9.953	9.468	9.084	8.85	8.839
HCl(aq)	0.2	0	(1)cl-, (1)h+	0.661	0.67	0.689	0.62	0.41	0.092
KCl(aq)	0	0	(1)cl-, (1)k+	1.71	1.495	1.216	0.924	0.575	0.215
KHSO4(aq)	0	0	(1)h+, (1)k+, (1)so4-2	-0.435	-0.814	-1.479	-2.294	-3.341	-4.431
KSO4-	1.81	-1	(1)k+, (1)so4-2	-0.885	-0.88	-0.99	-1.194	-1.52	-1.919
HF(aq)	0.2	0	(1)h+, (1)f-	-2.985	-3.168	-3.474	-3.848	-4.338	-4.859
MgCl+	2.31	1	(1)cl-, (1)mg+2	0.049	0.135	0.055	-0.182	-0.607	-1.139
MgCO3(aq)	0	0	(-1)h+, (1)hco3-, (1)mg+2	7.74	7.35	6.926	6.563	6.204	5.872
MgHCO3+	2.31	1	(1)hco3-, (1)mg+2	-1.08	-1.036	-1.164	-1.436	-1.88	-2.415
MgSO4(aq)	0	0	(1)mg+2, (1)so4-2	-2.139	-2.412	-2.837	-3.347	-4.073	-4.955
MgF+	2.31	1	(1)mg+2, (1)f-	-1.387	-1.352	-1.478	-1.739	-2.168	-2.688
MgOH+	2.31	1	(1)h2o, (-1)h+, (1)mg+2	12.674	11.682	10.502	9.399	8.291	7.398
NaOH(aq)	0	0	(1)h2o, (-1)h+, (1)na+	15.645	14.795	13.8	12.885	11.971	11.221
NaCO3-	1.81	-1	(-1)h+, (1)hco3-, (1)na+	9.815	9.814	10.075	10.649	11.568	12.632
NaHCO3(aq)	0	0	(1)hco3-, (1)na+	-0.373	-0.154	0.11	0.411	0.793	1.213
NaHSiO3	0	0	(1)h2o, (-1)h+, (1)na+,(1)sio2(aq)	8.414	8.304	8.053	7.829	7.684	7.658
NaF(aq)	0	0	(1)na+, (1)f-	1.082	0.998	0.833	0.624	0.338	0.011
NaSO4-	1.81	-1	(1)na+, (1)so4-2	-0.677	-0.700	-0.842	-1.063	-1.389	-1.772
FeO2-	1.81	-1	(-1)h+, (1)hfeo2	10.231	9.602	8.839	8.111	7.38	6.821
FeO+	2.31	1	(-1)h2o, (1)h+, (1)hfeo2	-7.324	-6.368	-5.372	-4.561	-3.865	-3.393

Primary Aqueous Species:	r_{ej}	Charge	Molecular Weight (g/mol)
H2O	0	0	18.015
AlO2-	1.81	-1	58.98
Ca+2	2.87	2	40.078
Cl-	1.81	-1	35.453
H+	3.08	1	1.008
HCO3-	2.1	-1	61.017
K+	2.27	1	39.098
Mg+2	2.54	2	24.305
Na+	1.91	1	22.99
SiO2(aq)	0.08	0	60.084
SO4-2	3.15	-2	96.064
F-	1.33	-1	18.998
HFeO2	0	0	88.854

ATTACHMENT VI – THERMODYNAMIC DATABASE: REV02 THC Models

(DTN: LB0307THMDBRTM.001 [164434])

Mineral	Molecular Weight (g/mol)	Molar Volume (cm^3/mol)	Reaction Stoichiometry[1]	log (K)							
				0 (°C)	25 (°C)	60 (°C)	100 (°C)	150 (°C)	200 (°C)	250 (°C)	300 (°C)
albite-low	262.223	100.070	(1)alo2-, (1)na+, (3)sio2(aq)	-21.697	-20.179	-18.365	-16.686	-15.096	-13.987	-13.293	-12.963
anorthite	278.207	100.790	(2)alo2-, (1)ca+2, (2)sio2(aq)	-21.229	-20.484	-19.640	-18.960	-18.514	-18.485	-18.839	-19.547
calcite	100.087	36.934	(1)ca+2, (-1)h+, (1)hco3-	2.226	1.849	1.333	0.774	0.100	-0.584	-1.326	-2.215
clinopt/10	277.660	126.410	(2.6)h2o, (0.68)alo2-, (0.28)ca+2, (0.08)k+, (0.04)na+,(2.92)sio2(aq)	-20.216	-18.475	-16.703	-15.136	-13.577	-12.339	-11.395	-10.816
clpt/10-r02	277.660	126.410	(2.6)h2o, (0.68)alo2-, (0.28)ca+2, (0.08)k+, (0.04)na+,(2.92)sio2(aq)	-17.760	-16.020	-14.250	-12.680	-11.120	-9.880	-8.940	-8.360
cristoba-a	60.084	25.740	(1)sio2(aq)	-3.542	-3.192	-2.867	-2.589	-2.306	-2.071	-1.877	-1.742
fluorite	78.075	24.542	(1)ca+2, (2)f-	-10.310	-10.037	-9.907	-9.967	-10.265	-10.784	-11.555	-12.703
gypsum	172.172	74.690	(2)h2o, (1)ca+2, (1)so4-2	-4.533	-4.482	-4.609	-4.904	-5.410	-6.058	-6.874	-7.971
halite	58.442	27.015	(1)na+, (1)cl-	1.492	1.586	1.618	1.578	1.450	1.242	0.936	0.468
hematite	159.688	30.274	(-1)h2o, (2)hfeo2(aq)	-26.438	-23.927	-21.486	-19.661	-18.293	-17.573	-17.272	-17.248
heuland/10	279.347	126.640	(2.6)h2o, (0.8)alo2-, (0.33)ca+2, (0.04)k+, (0.1)na+, (2.8)sio2(aq)	-21.097	-19.348	-17.565	-15.992	-14.437	-13.217	-12.306	-11.779
heul/10-r02	279.347	126.640	(2.6)h2o, (0.8)alo2-, (0.33)ca+2, (0.04)k+, (0.1)na+, (2.8)sio2(aq)	-18.620	-16.870	-15.090	-13.510	-11.960	-10.740	-9.830	-9.300
illite	378.963	135.080	(0.44)h2o, (2.06)alo2-, (1.12)h+,(0.5)k+, (0.22)mg+2, (3.72)sio2(aq)	-45.566	-42.016	-38.333	-35.129	-32.064	-29.760	-28.120	-27.254
kaolinite	258.160	99.520	(1)h2o, (2)alo2-, (2)h+, (2)sio2(aq)	-43.234	-39.917	-36.348	-33.216	-30.252	-28.074	-26.558	-25.754
microcline-b	278.332	108.741	(1)alo2-, (1)k+, (3)sio2(aq)	-23.770	-21.820	-19.530	-17.440	-15.470	-14.080	-13.170	-12.670
morden/10	269.631	127.350	(2.2)h2o, (0.6)alo2-, (0.15)ca+2, (0.09)k+, (0.21)na+, (3)sio2(aq)	-19.244	-17.542	-15.820	-14.298	-12.776	-11.558	-10.617	-10.021
mord/10-r02	269.631	127.350	(2.2)h2o, (0.6)alo2-, (0.15)ca+2, (0.09)k+, (0.21)na+, (3)sio2(aq)	-16.950	-15.250	-13.530	-12.010	-10.480	-9.270	-8.330	-7.730
opal-proxy	60.084	29.000	(1)sio2(aq)	-3.501	-3.005	-2.627	-2.358	-2.118	-1.926	-1.765	-1.632
quartz	60.084	22.688	(1)sio2(aq)	-4.153	-3.743	-3.348	-3.006	-2.661	-2.376	-2.142	-1.976
sepiolite	323.913	142.830	(-4)h+, (5.5)h2o, (2)mg+2, (3)sio2(aq)	17.631	15.992	13.961	12.164	10.536	9.352	8.397	7.457
sio2(amor.)	60.084	29.000	(1)sio2(aq)	-2.954	-2.670	-2.422	-2.213	-1.998	-1.815	-1.663	-1.562
smect-ca-cal	365.394	132.510	(0.52)h2o, (1.77)alo2-, (0.145)ca+2, (0.96)h+, (0.26)mg+2, (3.97)sio2(aq)	-40.190	-36.970	-33.660	-30.790	-28.010	-25.900	-24.370	-23.550
smect-na-cal	366.250	132.510	(0.52)h2o, (1.77)alo2-, (0.96)h+, (0.26)mg+2, (0.29)na+, (3.97)sio2(aq)	-40.290	-36.980	-33.560	-30.560	-27.660	-25.440	-23.820	-22.900
smect-mg-cal	363.107	132.510	(0.52)h2o, (1.77)alo2-, (0.96)h+, (0.405)mg+2, (3.97)sio2(aq)	-40.240	-37.060	-33.790	-30.950	-28.200	-26.110	-24.600	-23.790

Mineral	Molecular Weight (g/mol)	Molar Volume (cm^3/mol)	Reaction Stoichiometry[1]	log (K) 0 (°C)	25 (°C)	60 (°C)	100 (°C)	150 (°C)	200 (°C)	250 (°C)	300 (°C)
steller/10	281.733	133.1	(2.8)h2o, (0.79)alo2-, (0.39)ca+2,(0.01)na+, (2.81)sio2(aq)	-21.144	-19.432	-17.691	-16.156	-14.636	-13.444	-12.553	-12.041
stell/10-r02	281.733	133.1	(2.8)h2o, (0.79)alo2-, (0.39)ca+2,(0.01)na+, (2.81)sio2(aq)	-18.37	-16.88	-15.4	-14.12	-12.86	-11.89	-11.2	-10.87
sylvite	74.551	37.524	(1)k+, (1)cl-	0.525	0.846	1.122	1.285	1.330	1.238	1.013	0.604
tridymite	60.084	26.586	(1)sio2(aq)	-3.946	-3.572	-3.193	-2.834	-2.413	-1.995	-1.587	-1.203
hydglassfe3	48.466	20.536	(-0.0006)h+, (0.5981)sio2(aq), (0.1180)alo2-, (0.0556)na+, (0.0594)k+, (0.016)ca+2, (0.0002)mg+2, (0.0055)hfeo2(aq), (0.0783)h2o	1.646	1.462	1.209	0.978	0.759	0.584	0.415	0.211
mgso4	120.369	45.250	(1)mg+2, (1)so4-2	6.237	4.882	3.1	1.263	-0.811	-2.748	-4.677	-6.787
nano3	84.995	50.000	(1)na+, (1)no3-	-0.811	-0.206	0.403	0.88	1.275	1.518	1.651	1.665
k2so4 (arcanite)	174.260	65.500	(2)k, (1)so4-2	-2.273	-1.801	-1.469	-1.365	-1.488	-1.826	-2.365	-3.19
na2so4 (thenardite)	142.043	53.330	(2)na+, (1)so4-2	-0.35	-0.309	-0.438	-0.705	-1.15	-1.716	-2.473	-3.548

Gaseous Species	Molecular Weight (g/mol)	Molecular Diameter (m)	Reaction Stoichiometry	0 (°C)	25 (°C)	60 (°C)	100 (°C)	150 (°C)	200 (°C)	250 (°C)	300 (°C)
co2(g)	44.01	2.50E-10	(-1)h2o, (1)h+, (1)hco3-	-7.677	-7.814	-8.053	-8.357	-8.769	-9.217	-9.720	-10.339

NOTES: [1] Negative number in parenthesis indicate the species is on the left side of equation.
Minerals names or abbreviations above are those used in the database and may not exactly match names used in the text of the report. Names ending by /10 indicate the stoichiometry, molecular weight, molar volume, and log(K) values for those minerals were divided by 10 compared to original data. Glass phases glass1 and glass were used with the extended-case and base-case geochemical systems, respectively.
Data in this Attachment are associated with input file thermok1.01.dat.

Aqueous Species	Molecular Weight (g/mol)	r_{ej}	Charge	Reaction Stoichiometry[1]	0 (°C)	25 (°C)	60 (°C)	100 (°C)	150 (°C)	200 (°C)	250 (°C)	300 (°C)
Al+3	26.982	3.33	3	(-2)h2o, (1)alo2-, (4)h+	-25.795	-22.883	-19.571	-16.582	-13.676	-11.409	-9.598	-8.167
Al(OH)2+	60.996	2.31	1	(1)alo2-, (2)h+	-13.655	-12.289	-10.825	-9.600	-8.530	-7.823	-7.396	-7.238
AlOH+2	43.989	2.8	2	(-1)h2o, (1)alo2-, (3)h+	-20.068	-17.926	-15.567	-13.519	-11.625	-10.242	-9.232	-8.547
CO2(aq)	44.010	0	0	(-1)h2o, (1)h+, (1)hco3-	-6.580	-6.345	-6.268	-6.388	-6.724	-7.197	-7.787	-8.528
CO3-2	60.009	2.81	-2	(-1)h+, (1)hco3-	10.624	10.329	10.130	10.084	10.200	10.465	10.871	11.464
CaCO3(aq)	100.087	0	0	(1)ca+2, (-1)h+, (1)hco3-	7.505	7.002	6.455	5.975	5.492	5.057	4.589	3.978
CaCl+	75.531	2.31	1	(1)ca+2, (1)cl-	0.356	0.293	0.094	-0.215	-0.682	-1.227	-1.870	-2.677
CaCl2(aq)	110.983	0	0	(1)ca+2, (2)cl-	0.456	0.644	0.634	0.400	-0.118	-0.844	-1.802	-3.116
CaF+	59.076	2.31	1	(1)ca+2, (1)f-	-0.655	-0.682	-0.862	-1.171	-1.650	-2.217	-2.888	-3.728
CaHCO3+	101.095	2.31	1	(1)ca+2, (1)hco3-	-1.094	-1.047	-1.158	-1.413	-1.848	-2.383	-3.027	-3.840
CaHSiO3+	117.170	2.31	1	(-1)h+, (1)ca+2, (1)h2o, (1)sio2(aq)	8.778	8.575	8.115	7.596	7.043	6.588	6.200	5.837
CaOH+	57.085	2.31	1	(-1)h+, (1)ca+2, (1)h2o	14.085	12.833	11.416	10.142	8.903	7.928	7.126	6.434
CaSO4(aq)	136.142	0	0	(1)ca+2, (1)so4-2	-2.071	-2.111	-2.265	-2.511	-2.910	-3.433	-4.144	-5.188
Fe+3	55.845	3.46	3	(3)h+, (1)hfeo2(aq), (-2)h2o	-14.305	-12.018	-9.602	-7.594	-5.807	-4.521	-3.530	-2.696
FeCl+2	91.298	2.8	2	(1)cl-, (3)h+, (-2)h2o, (1)hfeo2	-15.770	-13.498	-11.217	-9.449	-8.047	-7.230	-6.813	-6.721
FeF+2	74.843	2.8	2	(1)f-, (3)h+, (-2)h2o, (1)hfeo2(aq)	-20.032	-18.018	-16.038	-14.546	-13.418	-12.827	-12.608	-12.697
FeF2+	93.842	2.31	1	(2)f-, (3)h+, (-2)h2o, (1)hfeo2(aq)	-22.323	-20.368	-18.459	-17.037	-16.011	-15.569	-15.590	-16.086
FeO+	71.844	2.31	1	(1)h+, (-1)h2o, (1)hfeo2(aq)	-7.324	-6.368	-5.372	-4.561	-3.865	-3.393	-3.060	-2.807
FeO2-	87.844	1.81	-1	(-1)h+, (1)hfeo2(aq)	10.231	9.602	8.839	8.111	7.381	6.822	6.430	6.249
FeOH+2	72.852	2.8	2	(2)h+, (-1)h2o, (1)hfeo2(aq)	-11.409	-9.813	-8.174	-6.853	-5.727	-4.964	-4.415	-3.979
FeSO4+	151.909	2.31	1	(1)so4-2, (3)h+, (-2)h2o, (1)hfeo2(aq)	-15.846	-13.946	-12.089	-10.700	-9.681	-9.213	-9.179	-9.602
HAlO2	59.988	0	0	(1)alo2-, (1)h+	-7.080	-6.450	-5.846	-5.409	-5.119	-5.035	-5.120	-5.384
HF	20.006	0	0	(1)f-, (1)h+	-2.985	-3.168	-3.474	-3.848	-4.338	-4.859	-5.437	-6.135
HF2-	39.005	1.81	-1	(1)h+, (2)f-	-2.238	-2.551	-2.960	-3.385	-3.880	-4.374	-4.915	-5.578
HNO3(aq)	63.013	0	0	(1)h+, (1)no3-	1.540	1.303	0.952	0.556	0.074	-0.412	-0.936	-1.579
HSiO3-	77.092	1.81	-1	(-1)h+, (1)h2o, (1)sio2(aq)	9.811	9.585	9.241	8.960	8.802	8.833	9.035	9.433
KCl(aq)	74.551	0	0	(1)cl-, (1)k+	2.840	2.536	2.141	1.731	1.255	0.785	0.278	-0.344
KHSO4(aq)	136.170	0	0	(1)h+, (1)k+, (1)so4-2	2.039	1.495	0.595	-0.476	-1.817	-3.172	-4.601	-6.242
KOH(aq)	56.106	0	0	(-1)h+, (1)h2o, (1)k+	15.498	14.439	13.314	12.378	11.552	10.978	10.570	10.267
KSO4-	135.162	1.81	-1	(1)k+, (1)so4-2	-0.886	-0.880	-0.991	-1.195	-1.521	-1.921	-2.419	-3.090
MgCO3(aq)	84.314	0	0	(-1)h+, (1)hco3-, (1)mg+2	7.742	7.350	6.929	6.574	6.228	5.911	5.543	5.019
MgCl+	59.758	2.31	1	(1)cl-, (1)mg+2	0.097	0.135	0.041	-0.173	-0.537	-0.992	-1.550	-2.276
MgF+	43.303	2.31	1	(1)f-, (1)mg+2	-1.387	-1.352	-1.478	-1.739	-2.169	-2.691	-3.321	-4.125
MgHCO3+	85.322	2.31	1	(1)hco3-, (1)mg+2	-1.077	-1.036	-1.160	-1.423	-1.852	-2.369	-2.984	-3.758
MgHSiO3+	101.397	2.31	1	(-1)h+, (1)h2o, (1)mg+2, (1)sio2(aq)	8.454	8.325	7.943	7.501	7.036	6.666	6.358	6.072
MgOH+	41.312	2.31	1	(-1)h+, (1)h2o, (1)mg+2	12.674	11.683	10.502	9.399	8.291	7.392	6.634	5.967
MgSO4(aq)	120.369	0	0	(1)mg+2, (1)so4-2	-2.184	-2.230	-2.393	-2.641	-3.031	-3.539	-4.236	-5.271
NaCO3-	82.999	1.81	-1	(-1)h+, (1)hco3-, (1)na+	9.725	9.815	9.917	10.012	10.104	10.177	10.236	10.285
NaCl(aq)	58.442	0	0	(1)cl-, (1)na+	0.829	0.777	0.651	0.473	0.214	-0.093	-0.478	-1.013
NaF(aq)	41.988	0	0	(1)f-, (1)na+	1.082	0.998	0.833	0.623	0.338	0.010	-0.397	-0.957

Aqueous Species	Molecular Weight (g/mol)	r_{ej}	Charge	Reaction Stoichiometry[1]	0 (°C)	25 (°C)	60 (°C)	100 (°C)	150 (°C)	200 (°C)	250 (°C)	300 (°C)
NaHCO3(aq)	84.007	0	0	(1)hco3-, (1)na+	-0.398	-0.154	0.075	0.244	0.358	0.374	0.277	0.004
NaHSiO3(aq)	100.081	0	0	(-1)h+, (1)h2o, (1)na+, (1)sio2(aq)	7.603	7.754	7.780	7.795	7.873	8.014	8.190	8.365
NaOH(aq)	39.997	0	0	(-1)h+, (1)h2o, (1)na+	15.132	14.205	13.210	12.377	11.642	11.130	10.762	10.480
NaSO4-	119.053	1.81	-1	(1)na+, (1)so4-2	-0.677	-0.700	-0.842	-1.063	-1.389	-1.772	-2.242	-2.873
OH-	17.007	1.4	-1	(-1)h+, (1)h2o	14.940	13.995	13.027	12.255	11.631	11.284	11.168	11.300
SiF6-2	142.076	3	-2	(-2)h2o, (1)sio2(aq), (4)h+, (6)f-	-27.654	-26.275	-25.220	-24.654	-24.534	-24.919	-25.819	-27.436

Primary Aqueous Species	Molecular Weight (g/mol)	r_{ej}	Charge
H2O	18.015	0.00	0
AlO2-	58.980	1.81	-1
Ca+2	40.078	2.87	2
Cl-	35.453	1.81	-1
F-	18.998	1.33	-1
H+	1.008	3.08	1
HCO3-	61.017	2.10	-1
HFeO2(aq)	88.852	0.00	0
K+	39.098	2.27	1
Mg+2	24.305	2.54	2
Na+	22.990	1.91	1
NO3-	62.005	2.81	-1
SiO2(aq)	60.084	0.00	0
SO4-2	96.064	3.15	-2

ATTACHMENT VII – WASTE PACKAGE AVERAGE HEAT TRANSFER: All REV01 THC Seepage Models

(DTN: LB0101DSTTHCR1.007 [161281])

Time (years)	Total Heat (no ventilation) (W/meter)	Model Heat Load (W/meter)
0.01	1450.000	435.000
0.02	1448.649	434.595
0.03	1447.802	434.341
0.04	1446.966	434.090
0.05	1446.126	433.838
0.06	1445.292	433.587
0.07	1444.468	433.340
0.08	1443.617	433.085
0.09	1442.813	432.844
0.1	1441.979	432.594
0.15	1437.970	431.391
0.2	1434.003	430.201
0.25	1430.183	429.055
0.3	1426.428	427.928
0.35	1422.757	426.827
0.4	1419.171	425.751
0.45	1415.657	424.697
0.5	1412.230	423.669
0.55	1408.866	422.660
0.6	1405.590	421.677
0.65	1402.353	420.706
0.7	1399.207	419.762
0.75	1396.090	418.827
0.8	1393.072	417.922
0.85	1390.093	417.028
0.9	1387.169	416.151
0.95	1384.277	415.283
1.0	1381.471	414.441
1.5	1355.408	406.623
2.0	1332.834	399.850
2.5	1312.844	393.853
3.0	1294.686	388.406
3.5	1278.327	383.498
4.0	1263.118	378.935
4.5	1248.692	374.608
5.0	1235.091	370.527
5.5	1220.694	366.208
6.0	1207.008	362.102
6.5	1194.297	358.289
7.0	1182.135	354.641

Data from DTN: SN9907T0872799.001 [111485] multiplied by 1450/1540.413 (Total Heat) to reflect a design change at the time of REV01 work.

NOTE: Point at 50.001 years was interpolated between original data points at 50 and 55 years. From 0 to 50 years: Model Heat Load = Total Heat x 0.3 (70% heat removal)

Time (years)	Total Heat (no ventilation) (W/meter)	Model Heat Load (W/meter)
7.5	1169.685	350.905
8.0	1157.754	347.326
8.5	1146.156	343.847
9.0	1134.992	340.498
9.5	1123.659	337.098
10	1112.692	333.808
15	1011.525	303.458
20	925.760	277.728
25	848.670	254.601
30	781.226	234.368
35	721.996	216.599
40	668.553	200.566
45	620.521	186.156
50	578.485	173.545
50.001	578.477	578.477
55	540.350	540.350
60	506.148	506.148
65	475.148	475.148
70	448.192	448.192
75	422.908	422.908
80	400.854	400.854
85	380.461	380.461
90	362.592	362.592
95	345.744	345.744
100	331.164	331.164
150	238.417	238.417
200	196.608	196.608
250	172.037	172.037
300	155.179	155.179
350	142.089	142.089
400	131.355	131.355
450	122.099	122.099
500	114.135	114.135
550	106.970	106.970
600	100.772	100.772
650	95.156	95.156
700	89.938	89.938
750	85.321	85.321
800	80.938	80.938
850	76.894	76.894

Data from DTN: SN9907T0872799.001 [111485] multiplied by 1450/1540.413 (Total Heat) to reflect a design change at the time of REV01 work.

NOTE: Point at 50.001 years was interpolated between original data points at 50 and 55 years. From 0 to 50 years: Model Heat Load = Total Heat x 0.3 (70% heat removal)

Time (years)	Total Heat (no ventilation) (W/meter)	Model Heat Load (W/meter)
900	73.190	73.190
950	69.859	69.859
1000	66.992	66.992
1500	46.231	46.231
2000	36.450	36.450
2500	31.644	31.644
3000	28.693	28.693
3500	26.993	26.993
4000	25.815	25.815
4500	24.684	24.684
5000	23.772	23.772
5500	22.783	22.783
6000	22.211	22.211
6500	21.355	21.355
7000	20.624	20.624
7500	20.091	20.091
8000	19.347	19.347
8500	18.777	18.777
9000	18.174	18.174
9500	17.630	17.630
10000	17.079	17.079
15000	12.774	12.774
20000	10.009	10.009
25000	8.089	8.089
30000	6.615	6.615
35000	5.561	5.561
40000	4.774	4.774
45000	4.148	4.148
50000	3.641	3.641
55000	3.180	3.180
60000	2.862	2.862
65000	2.514	2.514
70000	2.282	2.282
75000	2.063	2.063
80000	1.869	1.869
85000	1.710	1.710
90000	1.593	1.593
95000	1.470	1.470
100000	1.372	1.372

Data from DTN: SN9907T0872799.001 [111485] multiplied by 1450/1540.413 (Total Heat) to reflect a design change at the time of REV01 work.

NOTE: Point at 50.001 years was interpolated between original data points at 50 and 55 years. From 0 to 50 years: Model Heat Load = Total Heat x 0.3 (70% heat removal)

INTENTIONALLY LEFT BLANK

ATTACHMENT VIII – WASTE PACKAGE AVERAGE HEAT TRANSFER: Tptpll THC Model REV02

Time (years)	Total Heat (no ventilation) (W/meter)	Model Heat Load (W/meter)
0	1450.000	198.650
1	1400.000	191.800
2	1360.000	186.320
3	1320.000	180.840
4	1290.000	176.730
5	1260.000	172.620
6	1230.000	168.510
7	1210.000	165.770
8	1180.000	161.660
9	1160.000	158.920
10	1140.000	156.180
11	1110.000	152.070
12	1090.000	149.330
13	1070.000	146.590
14	1050.000	143.850
15	1030.000	141.110
16	1010.000	138.370
17	995.000	136.315
18	978.000	133.986
19	961.000	131.657
20	946.000	129.602
21	929.000	127.273
22	912.000	124.944
23	897.000	122.889
24	882.000	120.834
25	868.000	118.916
26	854.000	116.998
27	840.000	115.080
28	826.000	113.162
29	813.000	111.381
30	801.000	109.737
31	787.000	107.819
32	775.000	106.175
33	762.000	104.394
34	751.000	102.887
35	740.000	101.380
36	728.000	99.736
37	716.000	98.092
38	706.000	96.722
39	695.000	95.215
40	685.000	93.845
41	675.000	92.475

Time (years)	Total Heat (no ventilation) (W/meter)	Model Heat Load (W/meter)
42	665.000	91.105
43	655.000	89.735
44	646.000	88.502
45	636.000	87.132
46	627.000	85.899
47	618.000	84.666
48	609.000	83.433
49	601.000	82.337
50	593.000	81.241
50.001	593.000	593.000
51	585.000	585.000
52	577.000	577.000
53	569.000	569.000
54	561.000	561.000
55	554.000	554.000
56	547.000	547.000
57	539.000	539.000
58	532.000	532.000
59	526.000	526.000
60	519.000	519.000
61	512.000	512.000
62	506.000	506.000
63	500.000	500.000
64	494.000	494.000
65	488.000	488.000
66	482.000	482.000
67	476.000	476.000
68	470.000	470.000
69	465.000	465.000
70	460.000	460.000
71	454.000	454.000
72	449.000	449.000
73	444.000	444.000
74	439.000	439.000
75	434.000	434.000
76	430.000	430.000
77	425.000	425.000
78	420.000	420.000
79	416.000	416.000
80	412.000	412.000
81	407.000	407.000
82	403.000	403.000
83	399.000	399.000
84	395.000	395.000
85	391.000	391.000
86	387.000	387.000
87	383.000	383.000

Time (years)	Total Heat (no ventilation) (W/meter)	Model Heat Load (W/meter)
88	379.000	379.000
89	376.000	376.000
90	372.000	372.000
91	369.000	369.000
92	365.000	365.000
93	362.000	362.000
94	359.000	359.000
95	355.000	355.000
96	352.000	352.000
97	349.000	349.000
98	346.000	346.000
99	343.000	343.000
100	340.000	340.000
110	315.000	315.000
120	294.000	294.000
140	259.000	259.000
150	245.000	245.000
160	235.000	235.000
170	225.000	225.000
180	216.000	216.000
190	208.000	208.000
200	201.000	201.000
250	176.000	176.000
300	159.000	159.000
350	145.000	145.000
400	134.000	134.000
450	125.000	125.000
500	117.000	117.000
550	110.000	110.000
600	103.000	103.000
650	97.300	97.300
700	92.100	92.100
750	87.200	87.200
800	82.800	82.800
850	78.800	78.800
900	75.000	75.000
950	71.600	71.600
1000	68.400	68.400
1500	47.300	47.300
2000	37.200	37.200
2500	32.100	32.100
3000	29.300	29.300
3500	27.500	27.500
4000	26.200	26.200
4500	25.200	25.200
5000	24.200	24.200
5500	23.400	23.400

Time (years)	Total Heat (no ventilation) (W/meter)	Model Heat Load (W/meter)
6000	22.600	22.600
6500	21.800	21.800
7000	21.100	21.100
7500	20.500	20.500
8000	19.800	19.800
8500	19.200	19.200
9000	18.600	18.600
9500	18.000	18.000
10000	17.500	17.500
15000	13.200	13.200
20000	10.200	10.200
25000	8.210	8.210
30000	6.760	6.760
35000	5.680	5.680
40000	4.850	4.850
45000	4.190	4.190
50000	3.680	3.680
55000	3.250	3.250
60000	2.880	2.880
65000	2.580	2.580
70000	2.330	2.330
75000	2.110	2.110
80000	1.910	1.910
85000	1.750	1.750
90000	1.640	1.640
95000	1.520	1.520
100000	1.400	1.400

Source: BSC (2002 [159527], Sheet 5 of 5) (see Section 4.1.7)

NOTE: Point at 50.001 years was interpolated between original data points at 50 and 55 years. From 0 to 50 years: Model Heat Load = Total Heat x (1-0.863) [86.3% heat removal]

ATTACHMENT IX – EFFECTIVE THERMAL CONDUCTIVITY FOR IN-DRIFT OPEN SPACES: Tptpmn and Tptpll THC Models

Pre-closure

Time		Factor
(sec)	(year)	
3.15360E+03	0.0	0.395
3.15360E+07	1.0	0.777
4.73040E+07	1.5	0.825
6.30720E+07	2	0.856
9.46080E+07	3	0.898
1.26144E+08	4	0.921
1.57680E+08	5	0.939
1.89216E+08	6	0.955
2.20752E+08	7	0.966
2.52288E+08	8	0.975
2.83824E+08	9	0.982
3.15360E+08	10	0.988
3.46896E+08	11	0.993
3.78432E+08	12	0.997
4.73040E+08	15	1
6.30720E+08	20	0.993
7.88400E+08	25	0.977
8.19936E+08	26	0.974
8.51472E+08	27	0.97
9.46080E+08	30	0.958
1.10376E+09	35	0.936
1.26144E+09	40	0.915
1.57680E+09	50	0.879

DTN: SN0002T0872799.009 [153364]

NOTE: $K_{thermal}$ is calculated as Max. $K_{thermal}$ x Factor

Maximum $K_{thermal}$ (W/m-K) = 10.568

Post-closure (No Backfill)

Time		Factor	
(sec)	(year)	Inner	Outer
1.57680E+09	50	0.879	0.879
1.608336E+09	51	0.844	0.829
1.639872E+09	52	0.892	0.878
1.734480E+09	55	0.951	0.944
1.892160E+09	60	0.988	0.986
2.049840E+09	65	1	1
2.207520E+09	70	0.995	0.998
2.365200E+09	75	0.985	0.99
2.396736E+09	76	0.983	0.988
2.428272E+09	77	0.981	0.986
2.522880E+09	80	0.973	0.98
2.838240E+09	90	0.954	0.963
3.153600E+09	100	0.932	0.943
3.185136E+09	101	0.929	0.941
3.311280E+09	105	0.918	0.929
3.468960E+09	110	0.905	0.917
3.784320E+09	120	0.882	0.896
4.099680E+09	130	0.872	0.886
4.415040E+09	140	0.864	0.879
5.045760E+09	160	0.852	0.869
5.676480E+09	180	0.839	0.857
6.307200E+09	200	0.83	0.849
6.937920E+09	220	0.818	0.838
7.884000E+09	250	0.798	0.818
9.460800E+09	300	0.763	0.784
1.103760E+10	350	0.736	0.758
1.261440E+10	400	0.707	0.729
1.419120E+10	450	0.689	0.711
1.576800E+10	500	0.677	0.7
1.734480E+10	550	0.672	0.694
1.892160E+10	600	0.667	0.69
2.207520E+10	700	0.656	0.68
2.522880E+10	800	0.646	0.67
2.838240E+10	900	0.637	0.661

DTN: SN0002T0872799.009 [153364]

NOTE: $K_{thermal}$ is calculated as Max. $K_{thermal}$ x Factor

Maximum $K_{thermal}$ (W/m-K) Inner=2.298, Outer=14.407

Post-closure (No Backfill) (Cont.)

Time		Factor	
(sec)	(year)	Inner	Outer
3.153600E+10	1000	0.627	0.651
3.468960E+10	1100	0.619	0.643
3.784320E+10	1200	0.611	0.635
4.099680E+10	1300	0.602	0.626
4.415040E+10	1400	0.592	0.616
4.730400E+10	1500	0.582	0.605
5.045760E+10	1600	0.574	0.597
5.676480E+10	1800	0.559	0.583
6.307200E+10	2000	0.543	0.566
6.937920E+10	2200	0.533	0.555
7.884000E+10	2500	0.519	0.541
9.460800E+10	3000	0.503	0.523
1.103760E+11	3500	0.491	0.51
1.261440E+11	4000	0.48	0.499
1.419120E+11	4500	0.472	0.491
1.576800E+11	5000	0.465	0.484
1.892160E+11	6000	0.453	0.471
2.207520E+11	7000	0.444	0.461
2.522880E+11	8000	0.436	0.452
3.153600E+11	10000	0.422	0.438
4.730400E+11	15000	0.395	0.411
6.307200E+11	20000	0.378	0.393
9.460800E+11	30000	0.354	0.367
1.261440E+12	40000	0.341	0.354
1.576800E+12	50000	0.333	0.346
1.892160E+12	60000	0.326	0.339
2.522880E+12	80000	0.318	0.33
3.153600E+12	100000	0.314	0.325

DTN: SN0002T0872799.009 [153364]
NOTE: $K_{thermal}$ is calculated as Max. $K_{thermal}$ x Factor
Maximum $K_{thermal}$ (W/m-K) Inner=2.298, Outer=14.407

INTENTIONALLY LEFT BLANK

ATTACHMENT X – LIST OF MODEL INPUT AND OUTPUT FILES

X.1. REV01 INPUT AND OUTPUT FILES

These files were submitted with REV01 of this Model Report to the TDMS under DTN: LB0011DSTTHCR1.002 [161282].

1. Input and output files of simulations with the reactive transport model TOUGHREACT V2.3 (LBNL 2001 [153101]). For each simulation, these files were concatenated into one file using the Unix *tar* utility then compressed using the Unix *gzip* utility. Resulting concatenated/compressed files have the extension *.tar.gz*.

2. Summary Excel spreadsheets of seepage models output data at three locations adjacent to the drift wall (crown, side, and base).

3. Spreadsheets containing calculations have been included as part of several DTNs in order to document the embedded calculations and supplement the Scientific Notebooks. READ.ME files are also included which outline the use of calculations in each spreadsheet. The calculations can be observed by clicking on the spreadsheet cells or selecting the "Tools\Options\View\Formulas" option in MS Excel. In addition, the cell references in the equations show all cells used as input to the calculation executed in the spreadsheet. The formulae in the submitted spreadsheets use the standard functions of MS Excel 97.

DST THC Model REV01 Input and Output File Folders (Simulations in Section 7.1.8.1)

dst00_amr1	Base Case CC Kin
dst00_amr2	Extended CC Kin
dst00_amr3	Base Case CC Eq
dst00_amr4	Extended CC Eq
dst00_amr5	Extended An Full
dst00_amr6	Base Case No CC

More complete descriptions can be found in Section 7.1.8.1.

Tptpmn THC Model REV01 Input and Output File Folders (Simulations in Table 6.5-4)

th6_3_r (_, _a, _b, _c, _d)
th6_16_25_7 (_, _a, _b, _c, _d)
thc6_16_25_9 (_, _a, _b, _c, _d)
thc6_16_25_9_amb (_, _a, _b, _c, _d)
thc6_16_25_10 (_, _a, _b, _c, _d)
thc6_16_25_10_amb (_, _a, _b, _c, _d)

Tptpmn Heterogeneous THC Model REV01 Input and Output File Folders (Simulations in Table 6.6-1)

ds00ss_het1
ds00th_het1(_, _a, _b, _c)
ds00amb1_het1 (_, _a, _b, _c, _d)
ds00amb2_het1 (_, _a, _b, _c, _d)
ds00thc1_het1 (_, _a, _b, _c, _d)
ds00thc2_het1 (_, _a, _b, _c, _d)
ds00ss_het2
ds00th_het2 (_, _a, _b, _c)
ds00thc1_het2 (_, _a, _b, _c, _d)
ds00thc2_het2 (_, _a, _b, _c, _d)
ds00ss_het3
ds00th_het3 (_, _a, _b, _c)
ds00thc1_het3 (_, _a, _b, _c, _d)
ds00thc2_het3 (_, _a, _b, _c, _d)

Tptpll THC Model REV01 Input and Output File Folders (Simulations in Table 6.7-3)

th6_16_25_g4 (_, _a, _b, _c, _d)
thc6_16_25_2g4 (_, _a, _b, _c, _d)
thc6_16_25_2g4_amb (_, _a, _b, _c, _d)
thc6_16_25_g4 (_, _a, _b, _c, _d)
thc6_16_25_g4_amb (_, _a, _b, _c, _d)

X.2. REV02 INPUT AND OUTPUT FILES

The following types of files were submitted for REV02 of this Model Report to the TDMS under DTN: LB0307DSTTHCR2.001 and LB0302DSCPTHCS.001.

1. Input and output files of simulations with the reactive transport code TOUGHREACT V3.0 (LBNL 2002 [161256]). For each simulation, these files were concatenated into one file using the Unix *tar* utility then compressed using the Unix *gzip* utility. Resulting concatenated/compressed files have the extension *.tar.gz*.

2. Summary Excel spreadsheets of seepage models output data at three locations adjacent to the drift wall (crown, side, and base).

3. Spreadsheets containing calculations have been included as part of several DTNs in order to document the embedded calculations and supplement the Scientific Notebooks. READ.ME files are also included which outline the use of calculations in each spreadsheet. The calculations can be observed by clicking on the spreadsheet cells or selecting the "Tools\Options\View\Formulas" option in MS Excel. In addition, the cell references in the equations show all cells used as input to the calculation executed in the spreadsheet. The formulae in the submitted spreadsheets use the standard functions of MS Excel 97.

DST THC Model REV02 Input and Output File Folders (Simulations in Section 7.1.8.2)
(DTN: LB0307DSTTHCR2.001)
dstrev2_th12
dstrev2_th13
dstrev2_thc7
dstrev2_thc8
dstrev2_thc9

More complete descriptions can be found in Section 7.1.

Tptpll THC Model REV02 Input and Output File Folders (Simulations listed in Table 6.8-4)

(DTN: LB0307DSTTHCR2.001)
th6_1.45kw (_, _a, _b, _c)
thc6_w0e3 (_, _a, _b2, _b, bb, _c, _d)
thc6_w0a (_b, _c, _d)
thc6_w0b (_, _a, _b, _bb, _c, _d)
thc25_w0 (_, _a, _b, _c, _d)
thc6_w0_q
thc6_w0_q1
thc6_w0amb
thc6_w0amb1
thc6_w4amb1
thc6_w5amb1
thc6_w6amb1

(DTN: LB0302DSCPTHCS.001)
thc6_w0 (_, _a, _b, _bb, _c, _d)
thc6_w4 (_, _a, _b, _bb, _c, _d)
thc6_w5 (_, _a, _b, _bb, _c, _d)
thc6_w6 (_, _a, _b, _bb, _c, _d)
thc6_w7 (_, _a, _b, _bb, _c, _d)

X.3. CONTENTS OF *.tar.gz* FILES (NOTE: SOME FILE NAMES ARE LOWERCASE IN TOUGHREACT V3.0 (LBNL 2002 [161256]) AND UPPERCASE IN EARLIER VERSIONS)

flow.inp	Rock thermal and hydrological properties, run flags and other specifications (input)
flow.out	Thermal and hydrological results (gas/liquid saturation, T, P, air mass fraction, etc.) (output)
GENER	Infiltration rates, heat load, and effective thermal conductivity (input)
INCON	Initial thermal and hydrological conditions (T, P, liquid saturation, etc.) (input)
MESH	Input numerical mesh (input)

SAVE	Thermal and hydrological conditions (T, P, liquid saturation, etc.) to use for restarting a run (output, same format as INCON file)
TABLE	Miscellaneous output data
VERS	Miscellaneous output data
LINEQ	Miscellaneous output data
CHEMICAL.INP	Water chemistry, mineralogy, and CO_2 partial pressure data (input)
CHEMICAL.OUT	Echo of data read in CHEMICAL.INP
SOLUTE.INP	Run flags and other data relating to reactive transport (input)
SOLUTE.OUT	Echo of data read in SOLUTE.INP
thermk1.01.dat	Thermodynamic database for REV02 (input). Note: The solid KNO3 in this file is actually NaNO3.
TEC_CONC.DAT	Calculated concentrations of aqueous species (moles/liter) at each grid node (two records for each node - first record for fractures and second record for matrix) (output)
TEC_MIN.DAT	Calculated volume fraction change for minerals at each grid node (two records for each node - first record for fractures and second record for matrix) (output)
TEC_GAS.DAT	Calculated CO_2 volume fraction at each grid node (two records for each node - first record for fractures and second record for matrix) (output)
TIME.DAT	Chemical data at selected grid nodes (output)
chdump.dat	Chemical speciation of initial water (output) and nodes with convergence problems
inchem	Chemistry data at all grid nodes to use for restarting a run (input)
savechem	Chemistry data at all grid nodes to use for restarting a run (output, same format as INCHEM file)
ITER.DAT	Iteration information (output)
runlog.dat (run_log.dat)	Miscellaneous run-time information. Note: mass balances may not be printed out correctly in this file for runs that have been restarted (i.e., starting at times different than zero).
mbalance.out	Mass balance information for chemical species Note: mass balances may not be accurate for runs that have been restarted (i.e., starting at times different than zero). Also, mass balances do not reflect mass loss by transport into large boundary grid blocks.
GASOBS.DAT	optional tabular flow output for individual grid blocks

X.4. SUMMARY SPREADSHEETS OF THC SEEPAGE MODELS OUTPUT DATA (ALSO USED FOR PLOTTING TIME PROFILES AND TABULATING STANDARD DEVIATION)

The data in these files were extracted from output files FLOW.OUT, TEC_CONC.DAT, TEC_MIN.DAT, and TEC_GAS.DAT for each simulation and submitted to the TDMS under DTN: LB0011DSTTHCR1.001 [154759], LB0302DSCPTHCS.002, and LB0307DSTTHCR2.002.

Tptpmn THC Model REV01 (TOUGHREACT V2.3 (LBNL 2001 [153101])):
(DTN: LB0011DSTTHCR1.001 [154759])

th6_7.xls	TH, 6/16/25 mm/year infiltration

thc6_9base.xls	THC, base-case, 6/16/25 mm/year infiltration
thc6_9base_amb.xls	THC, no heat load, base-case, 6/16/25 mm/year infiltration
thc6_10ext.xls	THC, extended-case, 6/16/25 mm/year infiltration
thc6_10ext_amb.xls	THC, no heat load, extended-case, 6/16/25 mm/year infiltration

Tptpll THC Model REV01 (TOUGHREACT V2.3 (LBNL 2001 [153101])):
(DTN: LB0011DSTTHCR1.001 [154759])

th6_g4.xls	TH, 6/16/25 mm/year infiltration
thc6_2g4base.xls	THC, base-case, 6/16/25 mm/year infiltration
thc6_2g4base_amb.xls	THC, no heat load, base-case, 6/16/25 mm/year infiltration
thc6_2g4ext.xls	THC, extended-case, 6/16/25 mm/year infiltration
thc6_2g4ext_amb.xls	THC, no heat load, extended-case, 6/16/25 mm/year infiltration

Tptpll THC Model REV02 (TOUGHREACT V3.0 (LBNL 2002 [161256]))
(extended-case only, simulations details listed in Table 6.8-4)

(DTN: LB0302DSCPTHCS.002)

thc6_w0_r.xls	THC, Water W0, 6/16/25 mm/year (track wet nodes)
thc6_w0_drift_r.xls	THC, Water W0, 6/16/25 mm/year (drift wall only)
thc6_w4_r.xls	THC, Water W4, 6/16/25 mm/year (track wet nodes)
thc6_w4_drift_r.xls	THC, Water W4, 6/16/25 mm/year (drift wall only)
thc6_w5_r.xls	THC, Water W5, 6/16/25 mm/year (track wet nodes)
thc6_w5_drift_r.xls	THC, Water W5, 6/16/25 mm/year (drift wall only)
thc6_w6_r.xls	THC, Water W6, 6/16/25 mm/year (track wet nodes)
thc6_w6_drift_r.xls	THC, Water W6, 6/16/25 mm/year (drift wall only)
thc6_w7_r.xls	THC, Water W7, 6/16/25 mm/year (track wet nodes)
thc6_w7_drift_r.xls	THC, Water W7, 6/16/25 mm/year (drift wall only)

(DTN: LB0307DSTTHCR2.002)

th6_1.45kw.xls	TH, 6/16/25 mm/year
thc25_w0.xls	THC, Water W0, 25 mm/year (track wet nodes)
thc25_w0_drift.xls	THC, Water W0, 25 mm/year (drift wall only)
thc6_w0e3.xls	THC, Water W0, 6/16/25 mm/year, EOS3 (track wet nodes)
thc6_w0e3_drift.xls	THC, Water W0, 6/16/25 mm/year, EOS3 (drift wall only)
thc6_w0b.xls	THC, Water W0, 6/16/25 mm/year, D_{CO2} change (track wet nodes)
thc6_w0b_drift.xls	THC, Water W0, 6/16/25 mm/year, D_{CO2} change (drift wall only)
thc6_w0a.xls	THC, Water W0, 6 mm/year (track wet nodes)
thc6_w0a_drift.xls	THC, Water W0, 6 mm/year (drift wall only)
thc6_w0_amb1.xls	THC, Water W0, no heat load, 6/16/25 mm/year (drift wall only)
wo_4_5_6_7.xls	THC, Water W0, W4, W5, W6, and W7, 6/15/25 mm/year, track wet nodes (concentrations of data from files listed above under DTN: LB0302DSCPTHCS.002)
hisat_top-w04567.xls	Filtered data from w0-4-5-6-7.xls, used to tabulate standard deviations in Table 6.9-2.

X.5. PLUG FLOW REACTOR EXPERIMENT, REV01 (SECTION 7.3)

Input and output files for this section were submitted to the TDMS as DTN: LB0011THCDISSM.001 [153381] and DTN: LB0011THCDISSM.002 [154578], respectively. The input files (for DTN: LB0011THCDISSM.001 [153381]) consist of SOLVEQ/CHILLER V1.0 (LBNL 1999 [153217]) files used to calculate the initial water composition for the simulations, along with the input files for two TOUGHREACT V2.2 (LBNL 1999 [153219]) simulations and three TOUGHREACT V2.3 (LBNL 2001 [153101]) simulations. The output files (for DTN: LB0011THCDISSM.002 [154578]) consist of the output files for the TOUGHREACT V2.2 (LBNL 1999 [153219]) and V2.3 (LBNL 2001 [153101]) simulations, and SOLVEQ/CHILLER V1.0 (LBNL 1999 [153217]) files used to correct for degassing and cooling. The files for each of the DTNs were grouped into folders (one for each simulation, plus additional folders for the SOLVEQ/CHILLER runs), and these were compressed using the Windows *Winzip* V7.0 utility. A Word 97 document (LB0011THCDISSM.00# notes.doc) describing the information contained in each DTN file was included in the compressed master file for each DTN.

A common model mesh was used for all of the simulations. The mesh was generated using the file *plugmesh* and TOUGH2 V1.4 (LBNL 2000 [146496]), resulting in the output file *plugmesh.mes*. This file was edited and incorporated in the FLOW.INP file used in each simulation.

Each of the TOUGHREACT simulations is grouped in a distinct folder. These are as follows:

simulation1input	TOUGHREACT V2.2 (LBNL 1999 [153219]), 60 μm diameter grain size surface area model, potassium feldspar as microcline
simulation2input	TOUGHREACT V2.2 (LBNL 1999 [153219]), 120 μm diameter grain size surface area model, potassium feldspar as microcline

X.5.1 PLUG FLOW SIMULATIONS, REV02 (SECTION 7.2)

Output data were compiled and graphically represented in the file plugflow_data.xls in the new Output-DTN: LB0301PLUGFLOW.001. Alkalinity data (represented as mg/L calcite) were corrected as described in Wang 2003 ([161665], SN-LBNL-SCI-190-V2, p. 85) to account for an error in conversion from moles of bicarbonate to moles of calcium carbonate (two moles of bicarbonate per mole of carbonate are needed to achieve the proper milliequivalence). This correction results in a closer match between experimental and simulated alkalinity values. Experimental data for all collection times (not just after 11 days) are portrayed in the updated plots
(Figures 7.2-3a through 7.2-3f).

X.5.2 FRACTURE SEALING SIMULATIONS, REV 02 (SECTION 7.3)

The following types of files were submitted for REV02 of this Model Report to the TDMS under Output-DTN: LB0301FRACSEAL.001.

Input files of simulations with the reactive transport model TOUGHREACT V2.4 (LBNL 2001 [160880]). Each simulation contains the input files CHEMICAL.INP, FLOW.INP, and SOLUTE.INP.

Output files of simulations with the reactive transport model TOUGHREACT V2.4 (LBNL 2001 [160880]). Each simulation contains the output files CHEMICAL.OUT, FLOW.OUT, SOLUTE.OUT, TEC_CONC.DAT, TEC_GAS.DAT, and TEC_MIN.DAT.

Data summary files with graphs were submitted to the TDMS under Output-DTN: LB0301FRACSEAL.002. Data from the TEC_MIN.DAT output files were compiled, edited, and graphically represented in the files T2d5cmin.xls and T2d5c1min.xls.

INTENTIONALLY LEFT BLANK

ATTACHMENT XI – REV02 PARAMETERS FOR FRACTURE PERMEABILITY MODIFICATION

Rock Unit	a-parameter	b-parameter
tcw11	1.5385E-02	1.0870
tcw12	1.2696E-03	0.5236
tcw13	3.4483E-03	0.3584
ptn21	9.2000E-03	1.4925
ptn22	7.0922E-03	2.1739
ptn23	1.2000E-03	1.7544
ptn24	2.9412E-02	2.1739
ptn25	5.0459E-03	1.9231
ptn26	8.7079E-04	1.0309
tsw31	1.2953E-03	0.4608
tsw32	2.5857E-03	0.8929
tsw33	1.3063E-03	1.2346
tsw34	6.2777E-04	0.2315
tsw35	9.9174E-04	0.3165
tsw3[67]	1.0561E-03	0.2488
tsw38	8.2459E-04	0.2294
tsw39	1.4576E-03	1.0417
ch1Ze	1.4545E-03	25.0000
ch1Vl	2.0333E-03	10.0000
ch[23456]Vl	1.7907E-03	7.1429
ch[2345]Ze	8.6047E-04	7.1429
ch6	1.4545E-03	25.0000
pp4	8.6047E-04	7.1429
pp3	1.5902E-03	5.0000
pp2	1.5902E-03	5.0000
pp1	8.6047E-04	7.1429
bf3	1.5902E-03	5.0000
bf2	8.6047E-04	7.1429
tr3	1.5902E-03	5.0000
tr2	8.6047E-04	7.1429

NOTE: The calculation and use of the *a* and *b* parameters are presented in Section 6.4.4.2. Parameter *a* (b_g) is calculated using Equation 6.4-20. Parameter *b* is the inverse of the fracture frequency (derived from DTN: LB0205REVUZPRP.001 [159525]).

INTENTIONALLY LEFT BLANK